1988

Axisymmetric wave propagation in a finite linear elastic cylinder

Brian D. Johnson
University of Central Florida

AXISYMMETRIC WAVE PROPAGATION IN A FINITE LINEAR ELASTIC CYLINDER

BY

BRIAN D. JOHNSON
B.S., University of Idaho, 1983

THESIS

Submitted in partial fulfillment of the requirements
for the degree of Master of Science in Engineering
in the Graduate Studies Program
of the College of Engineering
University of Central Florida
Orlando, Florida

Spring Term
1988

UNIVERSITY OF CENTRAL FLORIDA

OFFICE OF GRADUATE STUDIES

THESIS APPROVAL

DATE: March 16, 1988

I HEREBY RECOMMEND THAT THE THESIS PREPARED UNDER MY SUPERVISION

BY Brian D. Johnson

ENTITLED "Axisymmetric Wave Propagation in a Finite Linear Elastic Cylinder"

BE ACCEPTED IN PARTIAL FULFILLMENT OF THE REQUIREMENTS OF THE

DEGREE OF Master of Science in Engineering

FROM THE COLLEGE OF Engineering

W. F. Carroll
Supervisor of Thesis

RECOMMENDATION CONCURRED IN:

Bruce E. Mathews
Coordinator of Degree Program

COMMITTEE ON FINAL EXAMINATION

Louis M. Trefonas
Dean of Graduate Studies

ABSTRACT

This work addresses the linear elastic analysis of axisymmetric wave propagation in a finite elastic cylinder. The waves are generated by the Fast Triaxial Device (FTRXD), which fails soil specimens at very rapid rates. The very short duration of the triaxial tests requires the consideration of wave phenomena in the analysis of the test results.

The soil specimens are modeled as linear elastic cylinders which are compressed in the axial direction. The resulting axisymmetric waves are analyzed with the wave equations which are cast in finite difference form, allowing the solution of displacements and stresses throughout the cylinder as a function of time. The validity of the axisymmetric (two-dimensional) analysis is verified by comparing its results to the exact solution of Pochhammer's equations, and by verifying the proper solution of boundary conditions.

A one-dimensional wave analysis of the FTRXD has been completed by Carroll and has proven to closely predict the FTRXD results found in the laboratory. The one-dimensional and two-dimensional analysis results are compared in an effort to identify the FTRXD loading rates, the specimen properties, or the specimen geometries for which the one-dimensional analysis may not be adequate.

Of the variety of parameters considered, only Poisson's ratio is found to have a significant impact when comparing the one-dimensional and two-dimensional analysis results. Also, some significant wave phenomena not apparent in a one-dimensional analysis are observed in the

two-dimensional analysis at very high loading rates. But these loading rates are not presently attained in the actual FTRXD testing. Furthermore, for most of the parameters considered, much of the largest differences between the two analyses can be attributed to a difference in time scales used in the two analyses.

Thus, at least in the linear elastic range, the one-dimensional anlysis appears to adequately predict FTRXD results for present loading rates. Further consideration should be given to the non-linear, two-dimensional analysis and to an appropriate time scale on which the one-dimensional and two-dimensional analyses should be compared.

two-dimensional analysis at very high loading rates. But these loading rates are not presently attained in the actual FTRXD testing. Furthermore, for most of the parameters considered, much of the largest differences between the two analyses can be attributed to a difference in time scales used in the two analyses.

Thus, at least in the linear elastic range, the one-dimensional anlysis appears to adequately predict FTRXD results for present loading rates. Further consideration should be given to the non-linear, two-dimensional analysis and to an appropriate time scale on which the one-dimensional and two-dimensional analyses should be compared.

ACKNOWLEDGEMENTS

The author would like to thank the following individuals in the preparation of this report:

Dr. William F. Carroll for his guidance and direction.

My wife, Debra, for her support, encouragement, and endless patience.

TABLE OF CONTENTS

APPENDIX

LIST OF TABLES

LIST OF FIGURES

LIST OF SYMBOLS

A	Constant acceleration of upper pedestal
A_o	Initial acceleration of upper pedestal with hyperbolic velocity input
C_d	Dilatational wave velocity
C_o	Rod wave velocity
C_t	Shear wave velocity
dr	Radial increment of finite difference mesh
dt	Time increment of finite difference mesh
dz	Axial increment of finite difference mesh
E	Young's modulus of elasticity
H	Height of specimen
i	Radial position coordinate
IMAX	Number of radial increments in finite difference mesh
j	Axial position coordinate
JMAX	Number of axial increments in finite difference mesh
k	Time coordinate
KMAX	Number of time increments in finite difference mesh
L	Wavelength of harmonic disturbance
r	Radial position
R	Radius of specimen
t	Time
U	Radial displacement

V	Constant velocity of upper pedestal
V_o	Limiting velocity of upper pedestal with hyperbolic velocity input
W	Axial displacement
z	Axial position
α	dr/dz
β	$(C_t/C_d)^2$
δr	Radial increment
$\delta\theta$	Circumferential increment
δz	Axial increment
ε_1	Radial strain
ε_2	Circumferential strain
ε_3	Axial strain
nu	Poisson's ratio
rho	Mass density of specimen
σ_1	Radial stress
σ_2	Circumferential stress
σ_3	Axial stress
τ	Shear stress

CHAPTER 1

INTRODUCTION

In static mechanics, displacements imposed at one point in an object are assumed to occur simultaneously at each point throughout the object. There is some finite time, however, required for the effects of a disturbance imposed at one point to propagate through the body and be observed at other points. Such considerations involve the study of wave motion in solids.

This study addresses axisymmetric waves in an elastic cylinder. Extensive studies have already been carried out in this field, with the governing equations first derived by Pochhammer in 1876 and then independently by Chree in 1889 [1]. The problem considered here is of soil specimens which undergo triaxial shear testing and are failed at rapid rates under transient loads. As the speed of the tests is increased, the pressure wave that propagates through the specimen begins to affect the stresses that can be measured at the end or surface of the specimen, and thus obscures the true stress-strain curve of the material. Thus, the wave phenomena need to be considered when analyzing the results of such triaxial tests.

The Testing Device

The Fast Triaxial Device (FTRXD) brings soil samples to failure under very rapid transient loading. The device is composed of a specimen chamber, which includes the non-movable base, upper and lower

load cells, and the specimen itself. Above the specimen chamber is the loading chamber containing high pressure nitrogen gas used to drive the loading ram, or upper pedestal, (refer to Figure 1).

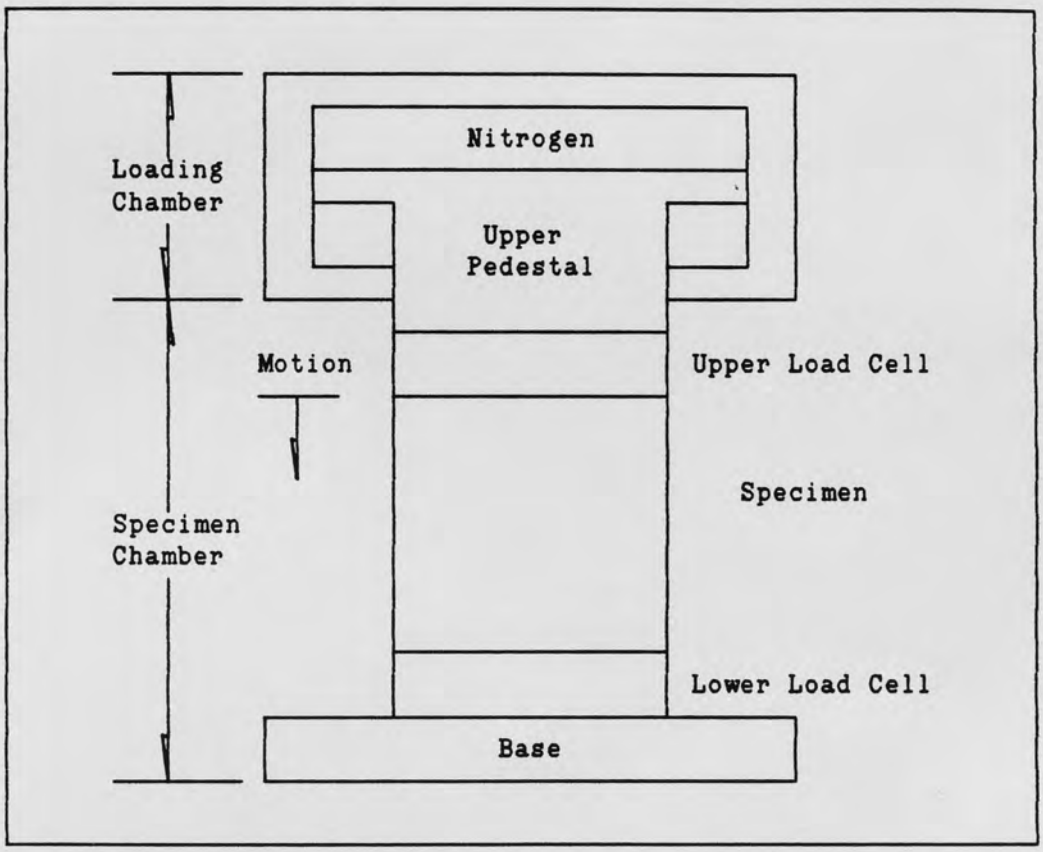

Figure 1. The Fast Triaxial Device.

The soil specimens tested are right circular cylinders 0.75 inches in diameter and 1.5 inches long. In very basic terms, the specimens are loaded in the axial direction by the downward motion of the upper pedestal. The rate of loading of the specimen is controlled by the pressure of the nitrogen. One way to control the loading rate is to first prevent the motion of the upper pedestal by use of a shear pin. By

increasing the pressure of the nitrogen, the shear pin will eventually fail and the upper pedestal will move downward. Faster loading rates are obtained by using stronger shear pins which require higher pressures to fail them.

Ideally, the stress-strain characteristics of the specimen would be measured at the middle of the specimen where there are minimal end constraint effects. Actually measuring the stress and strain at the middle, however, is virtually impossible. Instead, stresses are measured at the top and bottom of the specimen, and the gross strain of the specimen is calculated. Gross strain is the displacement of the top of the specimen divided by the initial specimen length. These values of stress and strain are assumed to be representative of the actual soil characteristics.

The load cells placed at the top and bottom of the specimens allow the measurement of load versus time during the test. The device also records the displacement of the upper pedestal as a function of time. By knowing the cross-sectional area of the specimen and its original height, stress-time, strain-time and stress-strain curves can be generated from the data.

A more detailed description of the FTRXD and testing methods can be found in Carroll [2].

Wave Phenomena

The wave motion may be analyzed in one of two ways. A one-dimensional wave analysis considers the waves travelling only up and down the specimen in the axial direction, accounting for longitudinal

inertia in the specimen. A two-dimensional analysis accounts for the effects of radial waves, as well as the axial waves, incorporating longitudinal and radial inertia as well as shear stress effects.

Due to the downward motion of the upper pedestal, a stress wave is generated, and the wavefront begins propagating through the medium. In the one-dimensional analysis, the wavefront travels at C_o, the rod wave velocity. When the stress wave reaches the bottom of the specimen, it is reflected and travels back up the specimen. These reflections continue as the wavefront propagates up and down the specimen during the triaxial test.

In the two-dimensional analysis, there are two wave velocities to consider. The dilatational wave velocity, C_d, is the faster of the two wave velocities and represents the limiting speed at which energy can propagate in the elastic medium. Shear waves, travelling at C_s, propagate more slowly and lag behind the dilatational waves.

In the triaxial tests, the reflections occurring in the two-dimensional wave analysis are much more complicated than those in the one-dimensional analysis. Not only are there two wavefronts to account for, but reflections occur at the sides of the specimen as well as at the top and bottom. Furthermore, when either a dilatational or shear wave is incident upon a boundary, four waves may be generated: a reflected dilatational and shear wave, and a refracted dilatational and shear wave. Only reflected waves are considered in these analyses.

The wave reflections and interactions occurring in the radial direction of the cylindrical specimen cause dispersion of the wavefront. This can lead to a significant portion of the energy

associated with the wave lagging behind the theoretical wavefront assumed to be travelling at the dilatational wave speed. Thus, in the two-dimensional wave analysis, it is difficult to visualize the varied reflections of the wavefront, let alone the actual position of a well defined wavefront at any given time.

One-Dimensional Wave Analysis

The one-dimensional wave analyses of FTRXD results have already been considered. The soil samples were modeled as initially linear elastic and then non-linear inelastic cylinders which deform only in the axial direction. That is, the specimens were assumed to undergo no deformation in the radial or circumferential direction.

The displacements and resulting stesses and strains were found by approximating the derivatives in the equations of motion with finite differences. The specimens were divided into a fine mesh in the axial direction, and displacements were calculated as a function of axial position and time. Time itself was also considered only at discrete intervals, so that a two-dimensional mesh is considered: axial position versus time.

A thorough summary of the linear and non-linear, one-dimensional analysis of the FTRXD is found in Carroll [2].

Statement of the Problem

It was found that the one-dimensional analysis did indeed approximate the FTRXD results found in the laboratory. Questions remain, however, regarding the validity of the one-dimensional wave analysis when factors such as the loading rate, the specimen height-

to-diameter ratio, or the height of the specimen change. If changing such factors affects the accuracy of the one-dimensional analysis, are there cases for which a two-dimensional wave analysis might be required in order to obtain meaningful results in the laboratory?

In the two-dimensional wave analysis presented in this study, the specimen is assumed to be a linear elastic cylinder that undergoes axisymmetric deformations; that is, the specimen can undergo axial and radial displacements, but all displacements in the circumferential direction are assumed to be zero. The specimen, therefore, is divided into a three-dimensional mesh: axial position versus radial position versus time. Finite difference approximations are used to calculate displacements, strains and stresses.

An advantage of this analysis over the one-dimensional analyis is that it accounts for radial displacements, radial inertia, and shear stress and their effects on axial stresses. This two-dimensional analysis, however, addresses only the linear stress-strain behavior observed at smaller values of strain. The analysis might be expanded in the future to also address the non-linear behavior observed in the laboratory at larger values of strain.

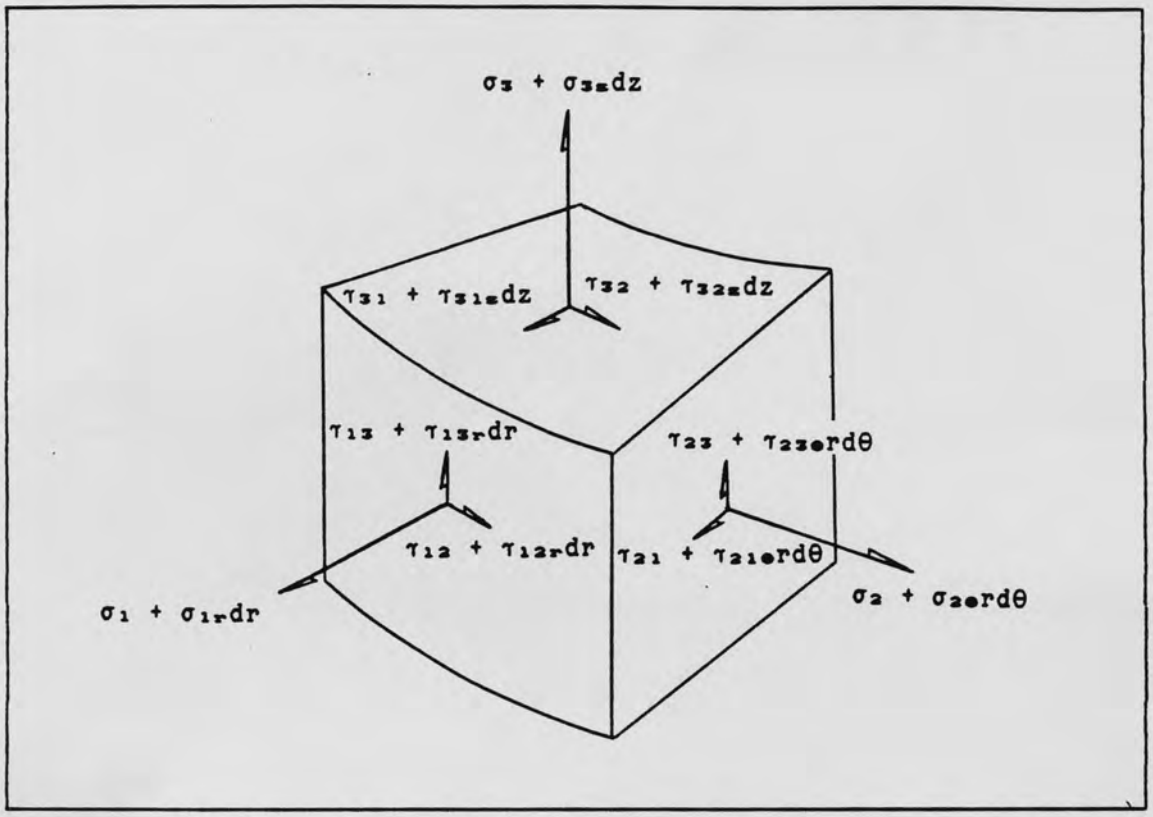

Figure 2. Incremental Volume and Stresses Acting.

Now apply Newton's Second Law to the incremental volume. For a specimen of mass density, rho, the mass, m, of the incremental volume is given by:

$$m = \rho(r)(\delta r)(\delta\theta)(\delta z) \qquad (1)$$

Let the displacements in the r, θ, and z directions be equal to U, V, and W, respectively. Also, assume body forces, such as gravitational forces equal to zero. For each of the three directions, sum the forces and equate to the mass of the incremental volume times its acceleration. Neglect second order terms and simplify to obtain:

$$\sigma_{zz} + \tau_{rz\theta}/r + \tau_{rz}/r + \tau_{rz,r} = \text{rho}W_{tt} \quad (2a)$$

$$\tau_{rz,z} + \tau_{r\theta\theta}/r + (\sigma_r - \sigma_\theta)/r + \sigma_{r,r} = \text{rho}U_{tt} \quad (2b)$$

$$\sigma_{\theta\theta}/r + \tau_{\theta z,z} + 2\tau_{r\theta}/r + \tau_{r\theta,r} = \text{rho}V_{tt} \quad (2c)$$

With the loading and resulting displacements assumed to be axisymmetric, V = 0 everywhere, and all stresses are independent of θ. This reduces the number of equations to only two:

$$\sigma_{zz} + \tau_{rz}/r + \tau_{rz,r} = \text{rho}W_{tt} \quad (3a)$$

$$\tau_{rz,z} + (\sigma_r - \sigma_\theta)/r + \sigma_{r,r} = \text{rho}U_{tt} \quad (3b)$$

Using the constitutive relations, the stresses in equations 3a and 3b can be written as functions of the strains ε_r, ε_θ, and ε_z. In cylindrical coordinates, the appropriate equations are [9]:

$$\begin{bmatrix} \sigma_r \\ \sigma_\theta \\ \sigma_z \end{bmatrix} = E' \begin{bmatrix} 1\text{-nu} & \text{nu} & \text{nu} \\ \text{nu} & 1\text{-nu} & \text{nu} \\ \text{nu} & \text{nu} & 1\text{-nu} \end{bmatrix} \begin{bmatrix} \varepsilon_r \\ \varepsilon_\theta \\ \varepsilon_z \end{bmatrix} \quad (4a)\ (4b)\ (4c)$$

where:

$E' = E/((1+nu)(1-2nu))$

E = Young's Modulus of Elasticity

nu = Poisson's ratio

Also, shear strain is given by $U_{z} + W_{r}$, such that:

$$\tau_{rz} = (E/(2(1+nu)))(U_{z} + W_{r}) \quad (4d)$$

After noting V = 0 and that strains are independent of θ, the strains ε_1, ε_2, and ε_3, can be written as functions of displacements [9]:

$$\varepsilon_1 = U_r \tag{5a}$$

$$\varepsilon_2 = U/r \tag{5b}$$

$$\varepsilon_3 = W_z \tag{5c}$$

Substituting equations 5 into equations 4 and then equations 4 into equations 3 and rearranging, the following relationships are obtained:

$$\rho W_{tt} = E'(\nu U_{rz} + \nu U_z/r + (1-\nu)W_{zz} + (E/(2(1+\nu)))(U_{rz} + W_{rr} + U_z/r + W_r/r) \tag{6a}$$

$$\rho U_{tt} = (E/(2(1+\nu)))(U_{zz} + W_{rz}) + (E'/r)((1-2\nu)U_r + U/r) + E'((1-\nu)U_{rr} + \nu(U_r/r - U/r^2 + W_{rz})) \tag{6b}$$

Combine like terms, divide through by rho, and note that [4, 10]:

$$E'(1-\nu)/\rho = C_d^2 \tag{7a}$$

$$E/(2(1+\nu)\rho) = C_t^2 \tag{7b}$$

$$E'/(2\rho) = C_d^2 - C_t^2 \tag{7c}$$

where:

C_d = dilitational wave speed

C_t = shear wave speed.

Rearranging equations 6a and 6b and substituting equations 7a, 7b, and 7c, the axisymmetric wave equations are obtained in their standard form [7]:

$$\begin{bmatrix} W_{tt} \\ U_{tt} \end{bmatrix} = \begin{bmatrix} (W_{zz} + U_{rz} + U_z/r) & (W_{rr} + W_r/r - U_{rz} - U_z/r) \\ (U_{rr} + U_r/r - U/r^2 + W_{rz}) & (U_{zz} - W_{rz}) \end{bmatrix} \begin{bmatrix} C_d^2 \\ C_t^2 \end{bmatrix} \quad (8a) \quad (8b)$$

A good check on the validity of the wave equations, shown above for the two-dimensional case, is that they reduce to the well known one-dimensional wave equation when only axial displacements are considered. In such cases, U = 0 everywhere, and all terms are independent of r. As such, equations 8a and 8b become:

$$W_{tt} = C_d^2 W_{zz} \quad (9)$$

But, as noted in Kolsky [1],

$$(C_d/C_o)^2 = (1-nu)/((1+nu)(1-2nu)) \quad (10)$$

where:

C_o = rod wave speed

$$C_o^2 = E/rho \quad (11)$$

For the one-dimensional case, nu = 0 and $C_d = C_o$. Thus the wave equations do indeed reduce to the one-dimensional wave equation [11]:

$$W_{tt} = C_o^2 W_{zz} \quad (12)$$

where equation 11 gives C_o, regardless of Poisson's ratio.

Equation 12 will be used to carry out one-dimensional wave analyses, the results of which will be compared to those of two-dimensional wave analyses. Such comparisons should lead to an

understanding of the loading conditions or specimen geometries for which the two-dimensional analysis provides significantly more accurate results than the one-dimensional analysis.

CHAPTER 3

FINITE DIFFERENCING

The solution to the wave equations for waves propagating in an unbounded medium is well documented, and an exact solution exists [1, 3]. However, waves propagating in a bounded medium undergo refraction and reflection at the boundaries. As such, the integrals for the solution of the wave equations are complicated. For an elastic cylinder, an exact solution has been obtained only for waves in a semi-infinite rod at points far removed from the end of it.

It is necessary, therefore, in the problem at hand to solve the wave equations numerically. By casting the wave equations in finite difference form, the partial differential equations are transformed into a system of algebraic equations best solved using a computer.

To apply the finite difference method, consider the plane ABCD in an elastic cylinder of height H and radius R shown in Figure 3. Plane ABCD is divided into a fine mesh, each unit of the mesh having axial length dz and radial length dr. The number of radial increments and axial increments are defined by IMAX and JMAX, respectively, such that:

$$IMAX = R/dr$$

$$JMAX = H/dz$$

Time, as well, is divided into increments, dt. For a test of duration T

the number of time increments in the test is given by KMAX. Thus:

KMAX = T/dt

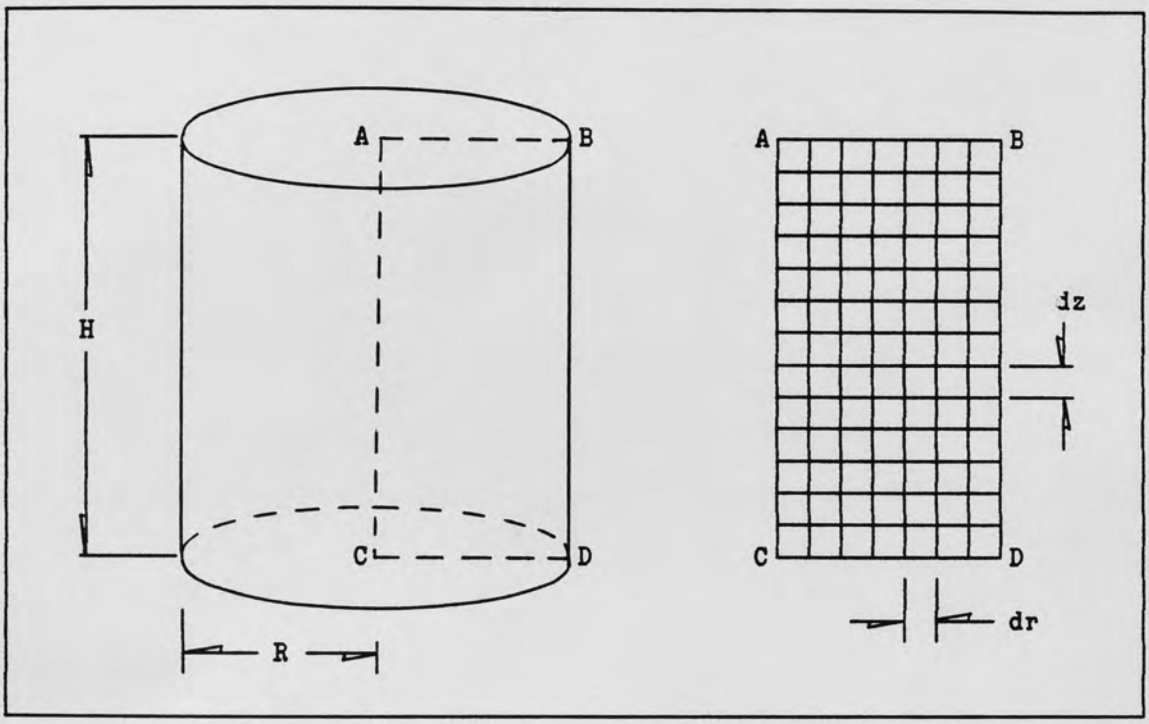

Figure 3. Elastic Cylinder and Plane of Interest Divided into the Finite Difference Mesh.

Hence, a three dimensional mesh exists: radial position versus axial position versus time. Writing the wave equations in finite difference form and solving gives the radial and axial displacements, U and W, respectively, at each point throughout the mesh. A given point in this mesh is defined by specifying its coordinates (i,j,k) where:

i = radial coordinate

= 1,2,3 . . . . ,IMAX+1

j = axial coordinate

= 1,2,3 . . . . ,JMAX+1

k = time coordinate

= 1,2,3 . . . . ,KMAX+1

The coordinates of a point are included when referring to a quantity measured at that point. For example,

U(i,j,k) = radial displacement at point (i,j,k)

U_r(i,j,k) = partial derivative of radial displacement with respect to radial position, evaluated at point (i,j,k)

With the mesh established, the finite difference approximations may be written. Different types of approximations can be made for a given derivative; central, forward, or backward differences can be written at a given point, yielding different results due to different biasing effects. When possible, central differences are used, since they are more accurate than comparable order forward or backward differences. However, some derivatives on the boundaries of the mesh can only be found using forward or backward differences. Three point approximations are used throughout the finite difference mesh in order to maintain comparable accuracies.

The following are approximations for partial derivatives, all evaluated at point (i,j,k) [12]. As such, the (i,j,k) is omitted from the left-hand terms for brevity.

Central Difference Approximations

$$U_r = (U(i+1,j,k) - U(i-1,j,k))/(2dr) \quad (13a)$$

$$U_{rr} = (U(i+1,j,k) - 2U(i,j,k) + U(i-1,j,k))/dr^2 \quad (13b)$$

$$U_z = (U(i,j+1,k) - U(i,j-1,k))/(2dz) \quad (13c)$$

$$U_{zz} = (U(i,j+1,k) - 2U(i,j,k) + U(i,j-1,k))/dz^2 \quad (13d)$$

$$U_{tt} = (U(i,j,k+1) - 2U(i,j,k) + U(i,j,k-1))/dt^2 \quad (13e)$$

$$U_{rz} = (U(i+1,j+1,k) - U(i+1,j-1,k) - U(i-1,j+1,k) + U(i-1,j-1,k))/(4drdz) \quad (13f)$$

Backward Difference Approximations

$$U_r = (3U(i,j,k) - 4U(i-1,j,k) + U(i-2,j,k))/(2dr) \quad (13g)$$

$$U_{rr} = (U(i,j,k) - 2U(i-1,j,k) + U(i-2,j,k))/dr^2 \quad (13h)$$

$$U_z = (3U(i,j,k) - 4U(i,j-1,k) + U(i,j-2,k))/(2dz) \quad (13i)$$

$$U_{rz} = (3(U(i,j+1,k) - U(i,j-1,k)) - 4(U(i-1,j+1,k) - U(i-1,j-1,k)) + (U(i-2,j+1,k) - U(i-2,j-1,k)))/(4dzdr) \quad (13j)$$

Forward Difference Approximations

$$U_r = (-3U(i,j,k) + 4U(i+1,j,k) - U(i+2,j,k))/(2dr) \quad (13k)$$

$$U_{rr} = (U(i,j,k) - 2U(i+1,j,k) + U(i+2,j,k))/dr^2 \quad (13l)$$

$$U_z = (-3U(i,j,k) + 4U(i,j+1,k) - U(i,j+2,k))/(2dz) \quad (13m)$$

$$U_{rz} = (-3(U(i,j+1,k) - U(i,j-1,k) + 4(U(i+1,j+1,k) - U(i+1,j-1,k)) - (U(i+2,j+1,k) - U(i+2,j-1,k)))/(4drdz) \quad (13n)$$

Similar approximations can be written for partial derivatives of axial displacements, W.

Substituting the appropriate central differences into the one-dimensional and two-dimensional wave equations (equations 8a, 8b, and 12), multiplying through by dt^2, and solving for displacements at the new time interval yields:

Two-Dimensional Wave Equations

$$W(i,j,k+1) = -W(i,j,k-1) + 2W(i,j,k) \tag{14a}$$
$$+ (C_s dt/dz)^2 (W(i,j+1,k) - 2W(i,j,k) + W(i,j-1,k))$$
$$+ (C_s dt)^2/(4drdz)(U(i+1,j+1,k) - U(i+1,j-1,k)$$
$$- U(i-1,j+1,k) + U(i-1,j-1,k))$$
$$+ (C_s dt)^2/(2rdz)(U(i,j+1,k) - U(i,j-1,k))$$
$$+ (C_t dt/dr)^2 (W(i+1,j,k) - 2W(i,j,k) + W(i-1,j,k))$$
$$+ (C_t dt)^2/(2rdr)(W(i+1,j,k) - W(i-1,j,k))$$
$$- (C_t dt)^2/(2rdz)(U(i,j+1,k) - U(i,j-1,k))$$
$$- (C_t dt)^2/(4drdz)(U(i+1,j+1,k) - U(i+1,j-1,k)$$
$$- U(i-1,j+1,k) + U(i-1,j-1,k))$$

$$U(i,j,k+1) = -U(i,j,k-1) + 2U(i,j,k) \tag{14b}$$
$$+ (C_s dt/dr)^2 (U(i+1,j,k) - 2U(i,j,k) + U(i-1,j,k))$$
$$+ (C_s dt)^2/(2rdr)(U(i+1,j,k) - U(i-1,j,k))$$
$$- (C_s dt/r)^2 U(i,j,k) + (C_s dt)^2/(4drdz)(W(i+1,j+1,k)$$
$$- W(i+1,j-1,k) - W(i-1,j+1,k) + W(i-1,j-1,k))$$
$$+ (C_t dt/dz)^2 (U(i,j+1,k) - 2U(i,j,k) + U(i,j-1,k))$$
$$- (C_t dt)^2/(4drdz)(W(i+1,j+1,k) - W(i+1,j-1,k)$$
$$- W(i-1,j+1,k) + W(i-1,j-1,k))$$

One-Dimensional Wave Equation

$$W(i,j,k+1) = -W(i,j,k-1) + 2(1 - (C_o dt/dz)^2)W(i,j,k) \tag{15}$$
$$+ (C_o dt/dz)^2 (W(i,j+1,k) - W(i,j-1,k))$$

Before proceeding further, consideration of the stability of the solutions to the wave equations is required.

Stability Analysis

The length of the time increments in relation to the axial and radial increments is important in determining the stability of the numerical solution to the two-dimensional wave equations. Bertholf [6] applied von Neumann stability criteria to each of the two-dimensional wave equations to obtain limiting values for the ratio, dt/dr. Bertholf's equations can be written in terms of the wave velocities and Poisson's ratio:

$$dt/dr \leq ((C_d/\alpha)^2 + .25nu(C_d^2-C_t^2)/\alpha + C_t^2)^{-1/2} \quad (16a)$$

$$dt/dr \leq (.25(C_d^2-C_t^2)/(nu\alpha) + (C_t/\alpha)^2 + 1.25C_d^2)^{-1/2} \quad (16b)$$

where:

$$\alpha = dr/dz \quad (17)$$

Note also that:

$$nu = (1 - 2\beta)/(2 - 2\beta) \quad (18)$$

where:

$$\beta = (C_t/C_d)^2 \quad (19)$$

For simplicity, the code discussed later assumes that the radial and axial increments are of equal length, such that $\alpha = 1$. Therefore, subsequent discussion of stability will refer to the ratio of dt/dz.

For various values of nu and C_d, equations 18 and 19 may be solved for C_t. Then substituting values into equations 16a and 16b, Table 1 may be generated.

TABLE 1

STABILITY ANALYSIS FOR
DETERMINING THE PROPER TIME INCREMENT

C_d (fps)	nu	Limiting dt/dz (Equation 16b)
1000	0.1	1/1756
	0.2	1/1551
	0.3	1/1460
1100	0.1	1/1932
	0.2	1/1706
	0.3	1/1606
1200	0.1	1/2107
	0.2	1/1801
	0.3	1/1752

These particular values of C_d and nu cover a wide range of possible soil characteristics. From Table 1, it is apparent that the most severely limiting case is when Cd = 1200 fps and nu = 0.1, in which case:

$$dt/dz \leq 1/2107$$

If the axial and time increments are set such that it takes two time increments for the dilitational wave to travel one axial increment, then

$$2(dt)C_d = dz$$

Or:

$$dt/dz = 1/(2C_d)$$

Considering the most limiting case, with C_d = 1200 fps, yields:

$$dt/dz = 1/2400$$

It is clear that this indeed is smaller than the most limiting case in Table 1. Therefore, initially the chosen ratio for dt/dz appears adequate.

The validity of this stability requirement is supported by considering what happens if the time increment above is doubled in the two-dimensional analysis, such that,

$$dt/dz = 1/C_d$$

Making this substitution into the two-dimensional wave equation finite difference algorithm causes the numerical results to be erratic and unreasonable, making clear the need for the smaller time increments.

The larger time increment is ideal, however, for stability of the one-dimensional wave analysis [13]. Although it would be easier to use comparable time increments when comparing the one-dimensional and two-dimensional wave anyalyses, the most efficient use of computer time is achieved by using the longest time increments which yield a stable solution.

In summary, a stable solution is obtained in the two-dimensional analysis when:

$$dt/dz = 1/(2C_d) \qquad (20)$$

A stable solution and the most efficient use of computer time is achieved in the one-dimensional analysis when:

$$dt/dz = 1/C_o \tag{21}$$

Return now to the wave equations in finite difference form, and note that:

$$r = (i-1)dr \tag{22}$$

Substituting equations 20, 21, and 22 into equations 14a, 14b, and 15 and regrouping terms gives:

Two-Dimensional Wave Equations

$$\begin{aligned} W(i,j,k+1) = {} & -W(i,j,k-1) + (1.5-\beta/2)W(i,j,k) \\ & + .25(\beta+\beta/(2(i-1)))W(i+1,j,k) \\ & + .25(\beta-\beta/(2(i-1)))W(i-1,j,k) \\ & + .25(W(i,j+1,k) + W(i,j-1,k)) \\ & + ((1-\beta)/(8(i-1)))(U(i,j+1,k) - U(i,j-1,k)) \\ & + ((1-\beta)/16)(U(i+1,j+1,k) - U(i+1,j-1,k) \\ & - U(i-1,j+1,k) + U(i-1,j-1,k)) \end{aligned} \tag{23a}$$

$$\begin{aligned} U(i,j,k+1) = {} & -U(i,j,k-1) + .25\beta(U(i,j+1,k) + U(i,j-1,k)) \\ & + .25((1+1/(2(i-1)))U(i+1,j,k) \\ & + (1-1/(2(i-1)))U(i-1,j,k)) \\ & + (1.5 - \beta/2 - 1/(4(i-1)^2))U(i,j,k) \\ & + ((1-\beta)/16)(W(i+1,j+1,k) - W(1+1,j-1,k) \\ & - W(i-1,j+1,k) + W(i-1,j-1,k)) \end{aligned} \tag{23b}$$

One Dimensional Wave Equation

$$W(i,j,k+1) = -W(i,j,k-1) + W(i,j+1,k) + W(i,j-1,k) \tag{24}$$

These are the wave equations in their finite difference form. Note that although the general two-dimensional wave equations can be reduced to the one-dimensional wave equation as shown earlier, this does not occur with the equations in their finite difference form. This is due to the different time increments used in deriving the one-dimensional and two-dimensional wave equations in finite difference form.

CHAPTER 4

ESTABLISHING THE CODE

The purpose of the code is to calculate axial stresses as a function of dimensionless time at the top, middle, and bottom of the specimen using the one-dimensional and two-dimensional wave analyses, and then to analyze and compare the results. Dimensionless time, TD, is equal to the number of times the wavefront has traversed the length of the specimen. The equation is:

$$TD = Ct/H$$

where:

C = governing wave speed
  = C_d for two-dimensional analysis
  = C_o for one-dimensional analysis

t = time

H = specimen height

The code contains three general segments: 1) calculation of displacements, 2) calculation of strains, and 3) calculation of stresses. The methods used for the calculations in the two-dimensional analysis are described below, and are followed by the methods used in the one-dimensional analysis.

Displacements

With the wave equations and the finite difference mesh established, a method for solving the displacements at each mesh point is needed. Consider the plane ABCD, shown earlier in Figure 3, at a given time interval in the three dimensional finite difference grid.

The mesh points in this plane can be divided into two general categories: those on the perimeter, and all others, called interior mesh points. The displacements on the perimeter are solved as a function of various boundary conditions, and are discussed in detail later.

The wave equations are used to solve for displacements at time t + dt at interior mesh points as a function of displacements at nearby mesh points at times t and t - dt. For instance, as shown in Figure 4, to solve for the unknown displacements at mesh point (i,j,k+1), displacements from ten other mesh points at earlier times must be known.

By systematically centering point (i,j,k) of this grid system on all interior mesh points at a given time interval, t, of the finite difference mesh, the displacements at all interior mesh points at the next time interval, t + dt, can be found. The process is to first center the grid on point (2,2,k) and increment radially outward for increasing values of i. Once the displacements are found for all interior mesh points for j=2, the process is repeated for j=3, and then j=4, and so on, working toward the bottom of the specimen, finishing with j=jmax.

The process is repeated again at the next time interval, always solving for displacements at the following time interval. In this way,

the finite difference grid is 'marched' forward in time, ultimately solving for displacements throughout the finite difference mesh. In order to solve for all displacements at a given time interval, however, the displacements at earlier times must be known not only at the interior mesh points, but also at the perimeter mesh points.

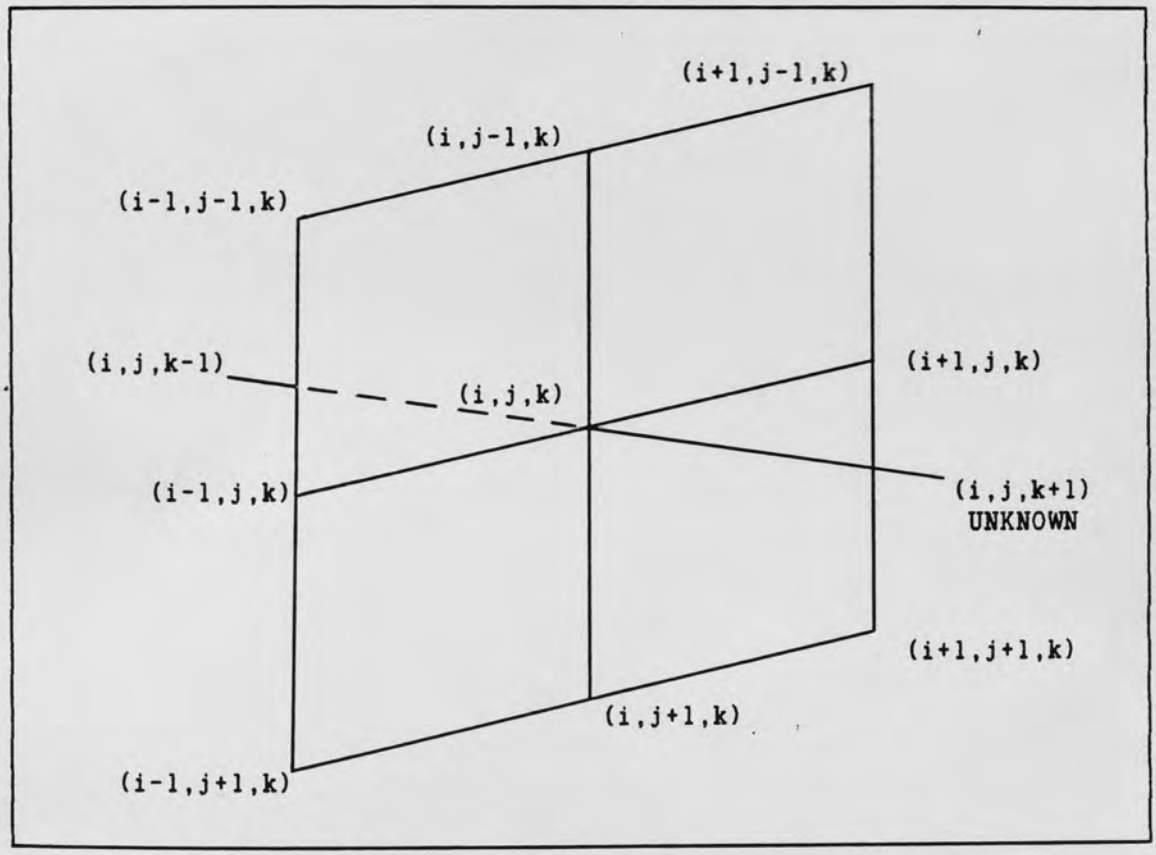

Figure 4. The Finite Difference Grid for the Wave Equations.

Boundary Conditions

While the wave equations are used to solve for displacements at interior mesh points, additional requirements must be met at the perimeter mesh points. Examples of such requirements are enforcing zero

shear and radial stress at the outer edge of the specimen. As a result, other relationships are used to establish equations which will allow for the solution of displacements at the perimeter mesh points.

Top and Bottom. Axial displacements at the top of the specimen are determined by the type of motion assumed for the upper pedestal. The most simple type of motion is that of constant velocity. In this case, the axial displacement at all points at the top is given by the product of the upper pedestal velocity and elapsed time. Or:

$$W(r,0,t) = Vt$$

where:

V = upper pedestal velocity

In finite difference form:

$$W(i,1,k) = V(k-1)dt$$

Another type of motion is that of a hyperbolically increasing function of velocity. Carroll [2] found that a two parameter hyperbola provides a good approximation of the upper pedestal motion produced in certain loading conditions in the laboratory. An appropriate function for this velocity is given by:

$$V(t) = V_o t/(t_o + t)$$

where:

V_o = limiting velocity (mils/msec)

A_o = initial acceleration (inches/second^2)

$t_o = V_o/A_o$ (25)

= characteristic time (seconds)

t = time (seconds)

Figure 5 shows this two parameter hyperbolic function.

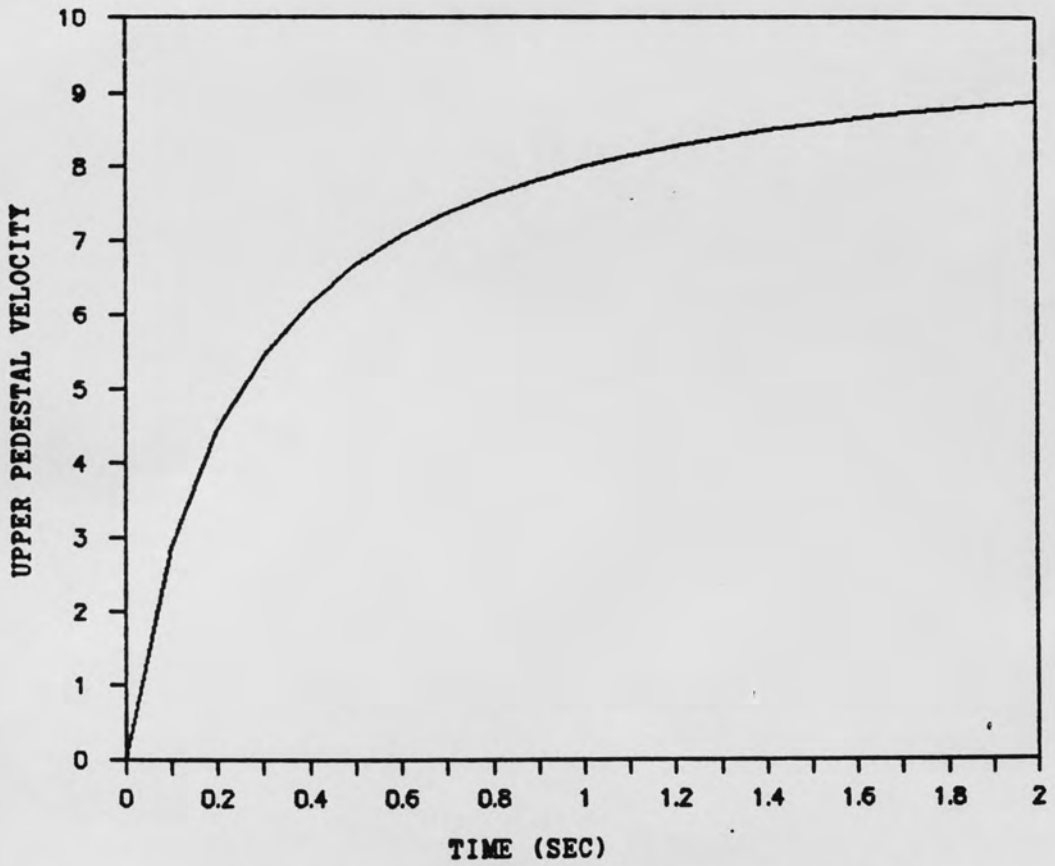

Figure 5. Two Parameter Hyperbolic Upper Pedestal Velocity.

The axial displacement of the upper pedestal is given by the integral of the hyperbolic velocity function:

$$W(r,0,t) = \int V(t)dt$$

$$= V_o t - V_o t_o \ln(1 + t/t_o)$$

Casting the equation in finite difference form:

$$W(i,1,k) = V_o(k-1)dt - V_o t_o \ln(1 + (k-1)dt/t_o)$$

A third type of motion, constant upper pedestal acceleration, can be assumed. This type of motion also closely approximates some of the loading conditions in the laboratory [2]. For this loading, the displacement of the upper pedestal is found by integrating the acceleration twice:

$$W(r,0,t) = \int\int A dt$$

$$= .5At^2$$

where:

A = acceleration of upper pedestal

Written in finite difference form:

$$W(i,1,k) = .5A((k-1)dt)^2$$

The axial displacements at the bottom of the specimen are forced to be zero in all cases since the pedestal on which the specimens rest does not move. Therefore:

$$W(i,jmax+1,k) = 0.0$$

The radial displacements at the specimen top and bottom are dependent on the type of lateral restraint assumed. The code allows for only two possibilities: full lateral restraint or no lateral restraint. With full restraint, radial displacements at the specimen top and bottom are set equal to zero. Or:

```
U(i,1,k) = 0.0
U(i,jmax+1,k) = 0.0
```

When assuming no lateral restraint, the code allows for the outward radial motion at the specimen top and bottom as the specimen is compressed. The radial displacements are found by noting that the shear stress must be zero at the specimen top and bottom. From equation 4d, zero shear stress requires that:

$$0 = U_z + W_r \tag{26}$$

Since W_r must be zero at the top and bottom, U_z must also be zero. By writing U_z with a forward difference approximation at the top, and a backward difference approximation at the bottom, the radial displacements at the top and bottom can be written as functions of displacements at nearby interior mesh points. From equations 13i and m,

```
U(i,1,k) = (1/3)(4U(i,2,k) - U(i,3,k))
U(i,jmax+1,k) = (1/3)(4U(i,jmax,k) - U(i,jmax-1,k))
```

Centerline and Outer Edge. The condition of zero shear stress must also be satisfied at the centerline and at the outer edge of the specimen. From this, the axial displacements at these points can be found. One

way to satisfy this condition at the outer edge is to write the equation for shear stress in finite difference form centered on a mesh point one radial increment in from the outer edge. That is, center the equations on point (imax,j,k) of Figure 6.

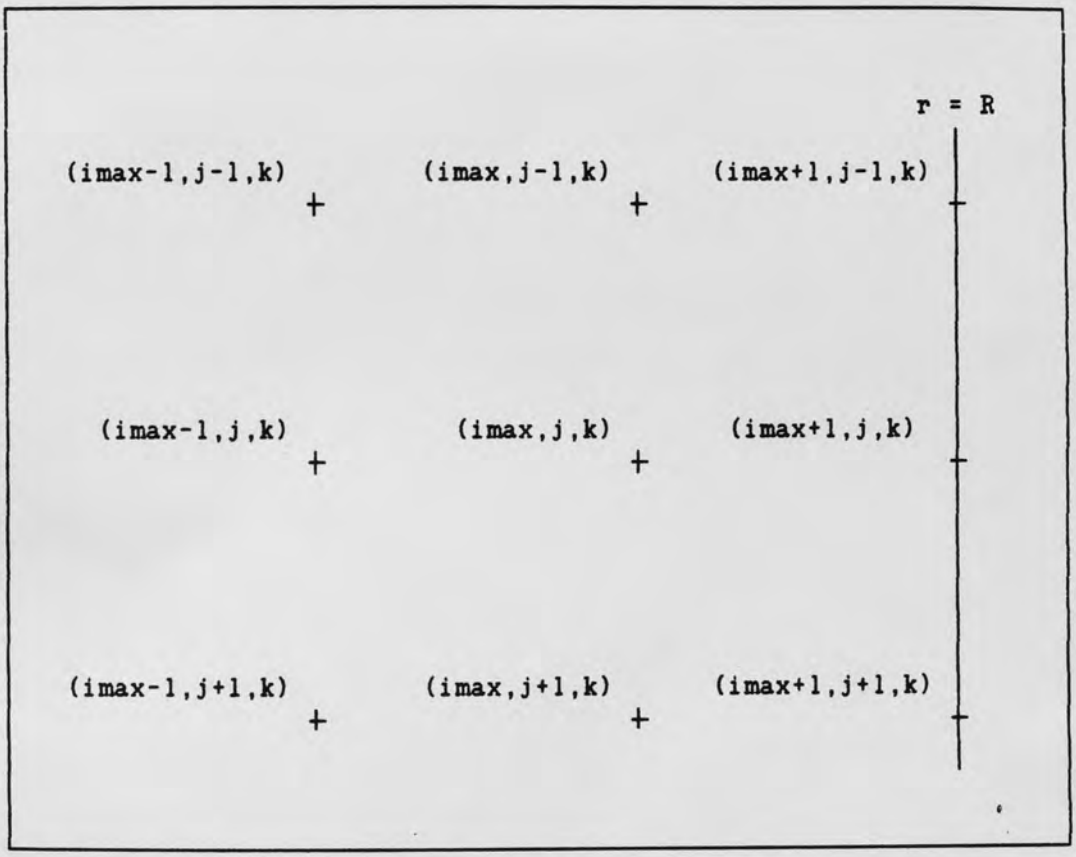

Figure 6. Finite Difference Mesh Near Outer Edge of Specimen.

Habberstad [7] showed that by using a forward difference approximation for W_r and a central difference approximation for U_z, the axial displacements at the outer edge can be written as a function of the displacements one increment in from the outer edge. These displacements at interior mesh points will already be known from the

solution of the wave equations. Applying Habberstad's method to Figure 6, and writing equation 26 in finite difference form:

$$0 = (U(imax,j+1,k) - U(imax,j-1,k))/(2dz) + (W(imax+1,j,k) - W(imax,j,k))/dr$$

Noting dr = dz, and solving for the unknown, W(imax+1,j,k):

$$W(imax+1,j,k) = W(imax,j,k) + .5(U(imax,j-1,k) - U(imax,j+1,k))$$

Although this actually satisfies the condition of zero shear stress at a surface somewhat inside the outer edge, as the mesh is made finer, the approximation becomes better.

The condition of zero shear stress can be enforced directly along the centerline. Since all radial displacements must be zero along the centerline for the axisymmetric case, U_z is zero, and therefore W_r must also be zero. By writing a forward difference approximation for W_r centered at the centerline, the axial displacement there is written as a function of displacements at nearby interior mesh points.

$$0.0 = -3W(1,j,k) + 4W(2,j,k) - W(3,j,k)$$

Solving for the unknown:

$$W(1,j,k) = (1/3)(4W(2,j,k) - W(3,j,k))$$

Finally, the radial displacements at the outer edge are found by enforcing zero radial stress there. Computationally, however, this once again is best achieved by centering the finite difference equation for radial stress at a point one increment in from the outer edge, as was

done with shear stress (see Figure 6). Recall equation 4a:

$$\sigma_1 = E'((1-nu)\varepsilon_1 + nu(\varepsilon_2 + \varepsilon_z))$$

This equation for radial stress, once set equal to zero, can be reduced to the form:

$$0.0 = U_r + (1 - 2\beta)(U/r + W_z)$$

Writing a forward difference approximation for U_r and a central difference approximation for W_z centered on point (imax,j,k) in Figure 6 yields:

$$\begin{aligned} 0.0 = {} & (U(imax+1,j,k) - U(imax,j,k))/dr \\ & + (1 - 2\beta)(U(imax,j,k)/(imax-1) \\ & + (W(imax,j+1,k) - W(imax,j-1,k))/(2dz)) \end{aligned}$$

Noting dr = dz and solving for the unknown:

$$\begin{aligned} U(imax+1,j,k) = {} & (1 - (1 - 2\beta)/(imax-1))U(imax,j,k) \\ & + .5(1 - 2\beta)(W(imax,j-1,k) - W(imax,j+1,k)) \end{aligned}$$

Thus, the radial displacement at the outer edge is written as a function of known displacements at interior mesh points.

The fact that zero shear and radial stress is enforced on a surface somewhat inside the outer edge is shown in Figure 7. Once again, as the number of radial increments is increased, the boundary conditions at the outer edge are better satisfied. Note that zero shear stress is satisfied exactly at the centerline of the specimen.

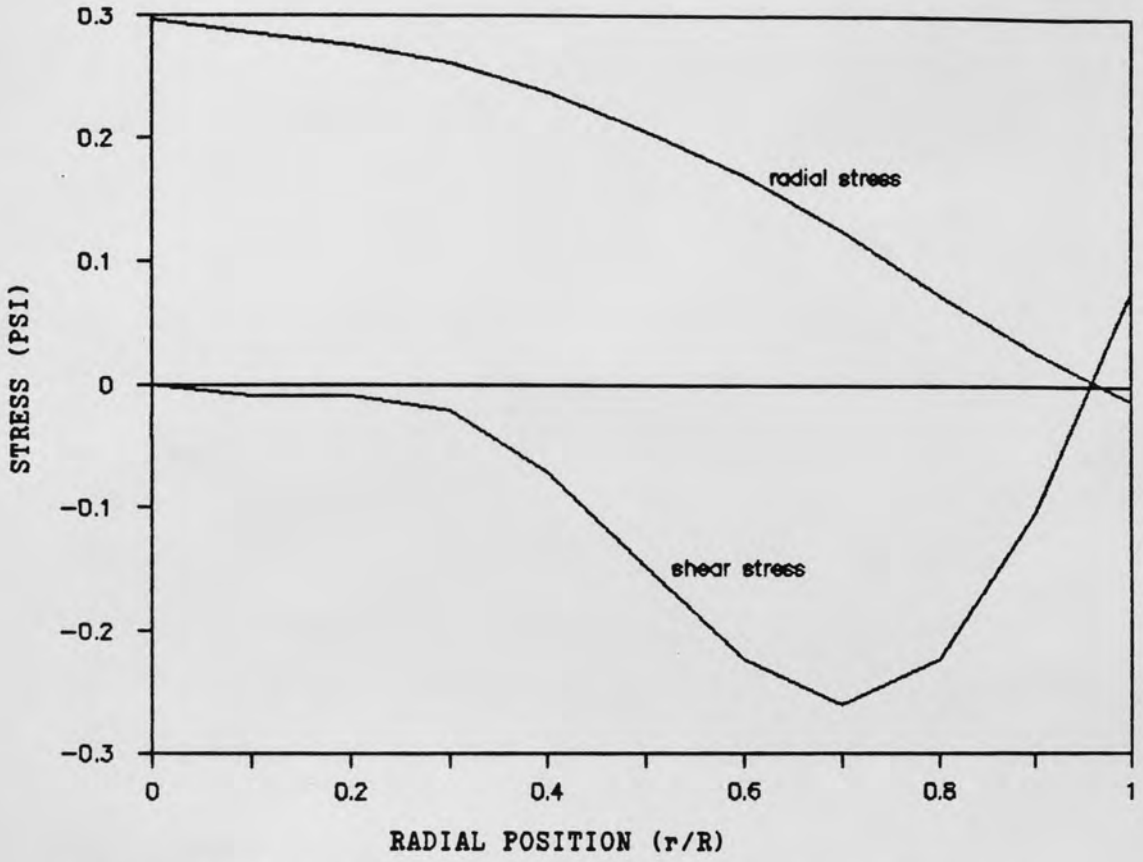

Figure 7. Radial Distribution of Shear and Radial Stresses.

Strains

Since stresses are to be calculated at points along the top, middle, and bottom of the specimen, the strains need only be found at these points as well. This is very different from the displacements which had to be calculated at every mesh point throughout the entire finite difference grid.

Once the displacements are known at a given time interval in the finite difference grid, strains are calculated using strain-displacement relationships. Recall equations 5:

$$\varepsilon_1 = U_r \qquad (5a)$$

$$\varepsilon_2 = U/r \tag{5b}$$

$$\varepsilon_3 = W_z \tag{5c}$$

Recall also that shear strain is given by $U_z + W_r$.

The type of finite difference approximation to use for a given derivative in the strain-displacement relationships is dependent on the position of the mesh point at which the derivative is to be approximated. Forward difference approximations must be used for U_r and W_r at the centerline and for U_z and W_z at the top of the specimen. Backward differences are used for U_r and W_r at the outer edge and for U_z and W_z at the bottom of the specimen. Central differences are used in all other cases.

Stresses

Once the strains are calculated at the points of interest, any stress can be found, using the stress-strain relationships of equations 4.

$$\begin{bmatrix} \sigma_1 \\ \sigma_2 \\ \sigma_3 \end{bmatrix} = E' \begin{bmatrix} 1\text{-nu} & nu & nu \\ nu & 1\text{-nu} & nu \\ nu & nu & 1\text{-nu} \end{bmatrix} \begin{bmatrix} \varepsilon_1 \\ \varepsilon_2 \\ \varepsilon_3 \end{bmatrix} \tag{4a, 4b, 4c}$$

$$\tau_{13} = (E/(2(1+nu)))(U_z + W_r) \tag{4d}$$

Recall also equations 7:

$$E'(1\text{-nu})/rho = C_d^2 \tag{7a}$$

$$E/(2(1+nu)rho) = C_t^2 \tag{7b}$$

$$E'/(2rho) = C_d^2 - C_t^2 \tag{7c}$$

Axial stresses are the only stresses of real interest for the triaxial test evaluation since they are the stresses that are measured in the triaxial tests. However, as a check on the accuracy of the code, shear and radial stresses were also calculated.

Multiplying equations 7 by rho, and inserting the results into equations 4a, 4c, and 4d, gives the stresses as a function of the known strains, rho, and the dilatational and shear wave velocities:

$$\begin{bmatrix} \sigma_1 \\ \sigma_3 \end{bmatrix} = \text{rho}(C_d^2) \begin{bmatrix} 1 & (1 - 2\beta) & (1 - 2\beta) \\ (1 - 2\beta) & (1 - 2\beta) & 1 \end{bmatrix} \begin{bmatrix} \varepsilon_1 \\ \varepsilon_2 \\ \varepsilon_2 \end{bmatrix}$$

$$\tau_{13} = \text{rho}(C_t^2)(U_z + W_r)$$

The discussion to this point has considered only the two-dimensional wave analysis. The general procedure of calculating displacements, strains, and then stresses also holds for the one-dimensional analysis. There are significant differences, however, between the two analyses, as noted below.

One-Dimensional Analysis

In the one-dimensional analysis, there are no radial increments or displacements to consider. As such, the only displacements to consider at a given time interval in the finite difference mesh are the axial displacements at each axial increment.

The displacement at the top of the specimen is once again a function of the upper pedestal motion, as discussed previously. The

displacement at the bottom of the specimen is zero. The displacements at all other mesh points are calculated with the wave equation. As in the two-dimensional analysis, the finite difference grid is applied at all interior mesh points at a given time interval, working from the top of the specimen toward the bottom. Once the calculations are completed at one time interval, they are repeated at subsequent time intervals throughout the remainder of the test.

Axial strain and stress are calculated at a given time interval in the same manner as in the two-dimensional analysis. With no centerline or outer edge boundary conditions to enforce, nor any radial increments to account for, however, the one-dimensional analysis is performed significantly faster than the two-dimensional analysis.

In either the one-dimensional or two-dimensional analysis, once the calculations of displacements, strains, and stresses are complete, the appropriate stresses are printed out as a function of dimensionless time.

CHAPTER 5

VALIDITY OF CODE

Pochhammer considered the problem of an infinite cylinder in which harmonic disturbances were propagated. He developed the wave equations, the solution of which would determine the radial and axial displacements in the cylinder as a function of time. The exact solution of these equations, however, was not obtained until many years later, and even then only at points far removed from the end of the cylinder [1].

In order to check the validity of the code used in this analysis, the portion of code which calculates displacements was used in a program which considered a semi-infinite cylinder and compared the displacements calculated to those of the exact solution to Pochhammer's equations. The end of a one inch diameter cylinder was displaced in the axial direction, according to a sine function, in order to generate a harmonic disturbance as in Pochhammer's problem. Let the input disturbance take the form:

$$W(r,0,t) = A\sin wt$$

Writing the circular frequency, w, as a function of the wavelength, L, and the dilatational wave velocity, C_d,

$$w = 2\pi f$$

$$f = C_d/L$$

$$w = 2\pi C_d/L$$

and substituting C_d = 1000 fps, L = 3.33 inches, and A = .05 inches gives:

$$W(r,0,t) = .05\sin(.04230246t)$$

Poisson's ratio was taken to be equal to 0.25, and the finite difference mesh was such that there were ten radial increments in the specimen.

Two different outputs were generated. The first checked displacements as a function of time, at points along a surface four inches from the end of the cylinder. This particular distance was chosen for several reasons. Bertholf [6] showed that a distance of at least four diameters from the end of the cylinder was required before a finite difference approximation agreed well with the Pochhammer solution. Also, four diameters is far enough from the end that an exact solution to Pochhammer's equations exists. If a further distance is chosen, however, many more time increments are required to elapse before the initial wavefront passes the point of interest and a good wave pattern is established. This requires an inordinate amount of computer time.

This first check was carried out twice: once assuming full lateral restraint at the end of the specimen, and once assuming no lateral restraint at the end. Each case gave essentially identical results for the displacments four diameters from the end of the semi-infinite rod. This is reasonable since the end conditions should

have little, if any, effect on the displacements at points far from the end.

The first type of output verified that indeed a harmonic disturbance was observed as a function of time, and that the proper radial distribution of displacements existed, as predicted by the solution to the Pochhammer equations. Table 2 shows the radial distribution of displacements according to the exact solution of Pochhammer's equations [6] and as given by the numerical results.

TABLE 2

RADIAL DISTRIBUTION OF DISPLACEMENTS IN A HARMONICALLY LOADED SEMI-INFINITE CYLINDER

	Pochhammer Solution (exact)		Numerical Solution (approximate)	
r/R	W/W_{max}	U/U_{max}	W/W_{max}	U/U_{max}
0.0	1.00000	0.00000	1.00000	0.00000
0.1	0.99854	0.11401	0.99862	0.11138
0.2	0.99419	0.22712	0.99446	0.22524
0.3	0.98699	0.33845	0.98762	0.34016
0.4	0.97702	0.44715	0.97723	0.44903
0.5	0.96439	0.55236	0.96295	0.55236
0.6	0.94924	0.65329	0.94599	0.65573
0.7	0.93173	0.74919	0.92733	0.75448
0.8	0.91206	0.83935	0.90730	0.84416
0.9	0.89044	0.92314	0.88595	0.92785
1.0	0.86711	1.00000	0.86390	1.00000
W_{max}/U_{max}	3.9112716		3.89599	

Note the excellent agreement between not only the radial distribution of displacements, but also between the exact and predicted ratios of maximum axial displacement to maximum radial displacements.

The second type of output found the displacements at mesh points along the first twenty inches of the semi-infinite cylinder. These displacements were calculated for only one instant in time. This output again showed the periodic nature of the disturbance as well as allowed for a direct measurement of the wavelength of the disturbance. Figure 8 shows the displacements as a function of axial position.

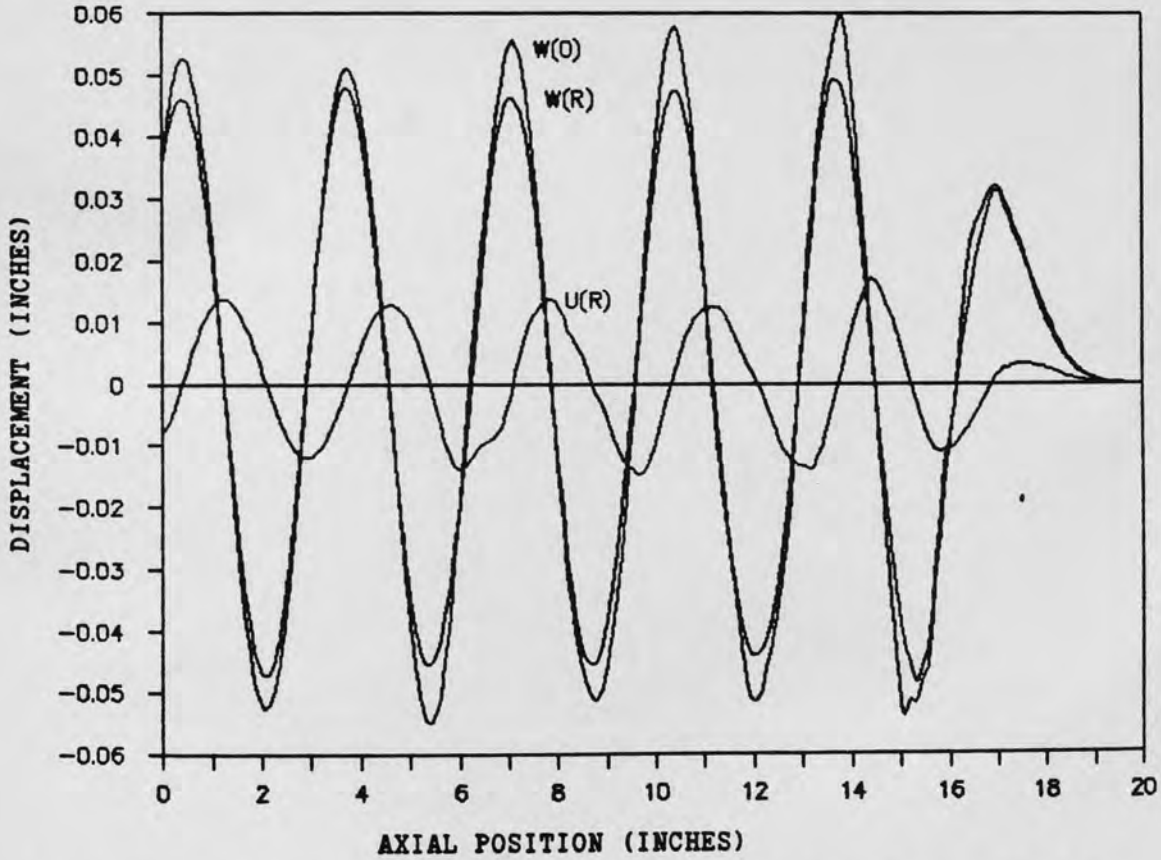

Figure 8. Axial Distribution of Radial and Axial Displacements in a Harmonically Loaded Semi-Infinite Elastic Cylinder.

From Figure 8, the wavelength is measured to be about 3.3 inches. This agrees well with the wavelength of 3.33 inches used to generate the code for the input disturbance.

As a result of these checks, it appears that the code that calculates displacements is being carried out properly. The fact that the code gives results for displacements which are so close to the exact solution lends credence to its accuracy.

Still other checks can be made. By entering an appropriate ratio of dilatational and shear wave velocities into the code, Poisson's ratio can be made equal to zero. In such cases, the specimen should behave as in the one-dimensional case. That is, the output should show zero radial or shear stresses, and no variation in axial stress with radial position. This indeed is what happens.

Figure 9 indicates that as Poisson's ratio approaches zero, the axial stresses predicted by the two-dimensional analysis approach those predicted by the one-dimensional analysis, with no radial variation in stress observed. The results of the one-dimensional and two-dimensional analyses are identical when Poisson's ratio is set equal to zero in the two-dimensional analysis.

Additionally, Figures 10 and 11 show that the radial and shear stresses approach zero as they should, indicating that the two-dimensional analysis approaches the one-dimensional analysis as Poisson's ratio goes to zero. Note also that the boundary conditions are being enforced with $\sigma_r = 0$ at the outer edge, and $\tau_{rz} = 0$ at the centerline and outer edge.

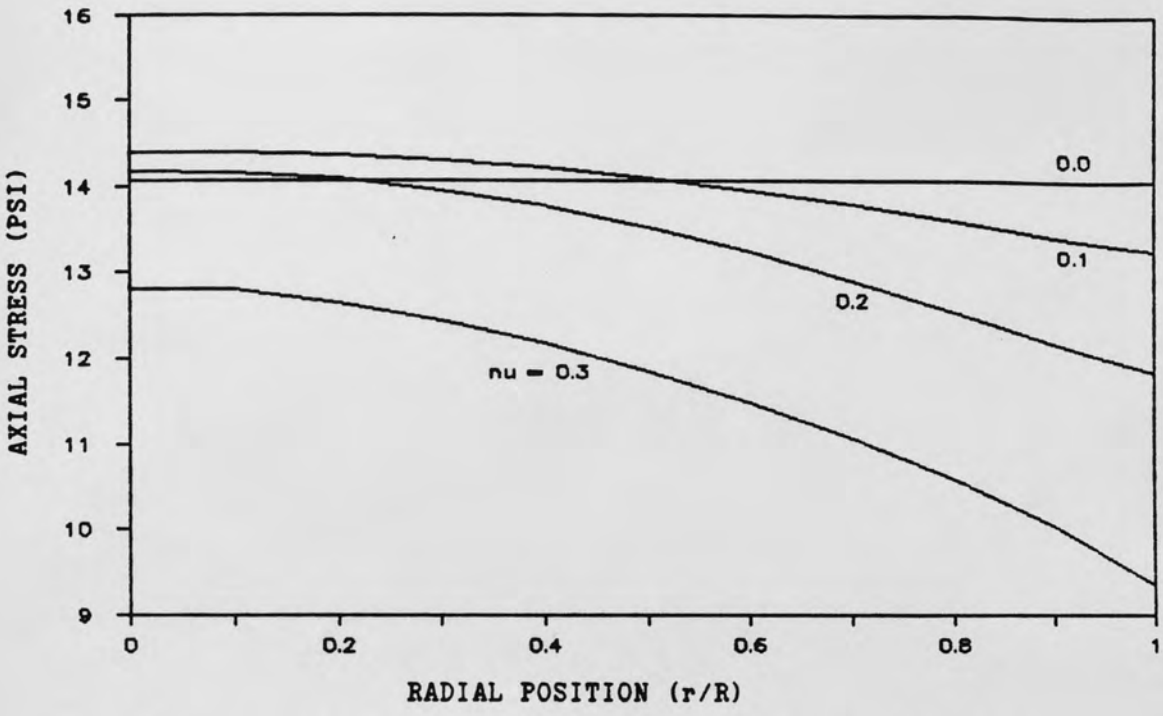

Figure 9. Axial Stress Variations with Poisson's Ratio.

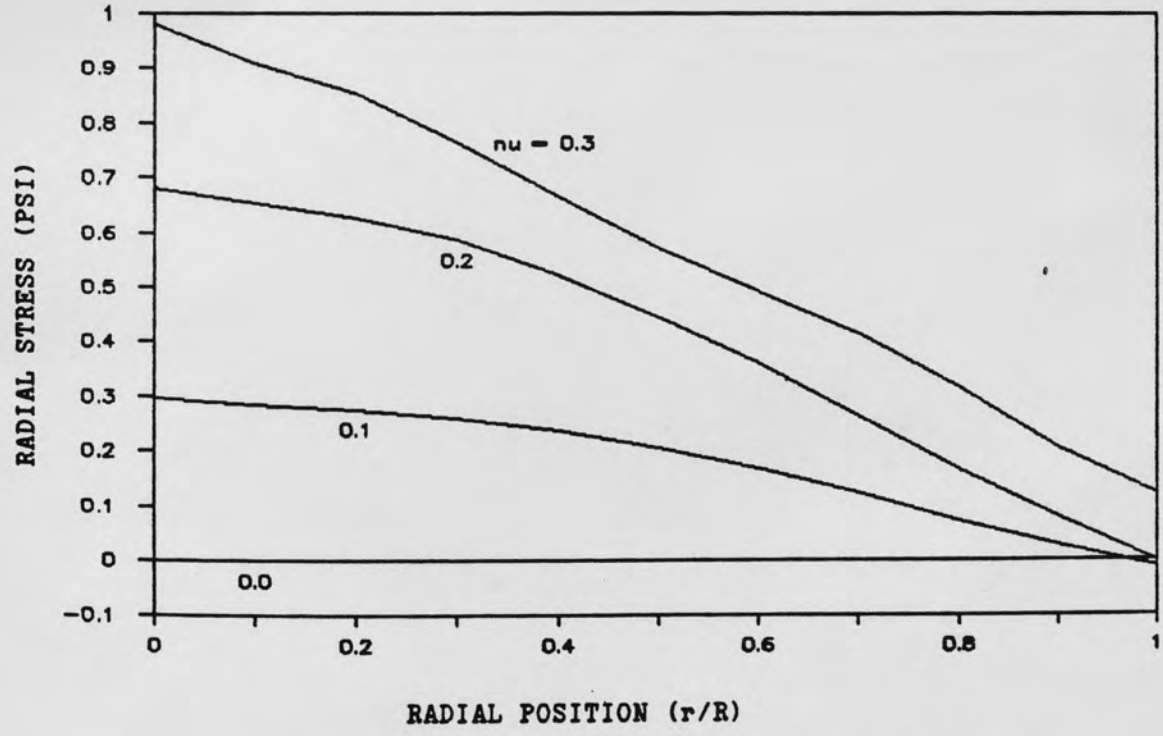

Figure 10. Radial Stress Variations with Poisson's Ratio.

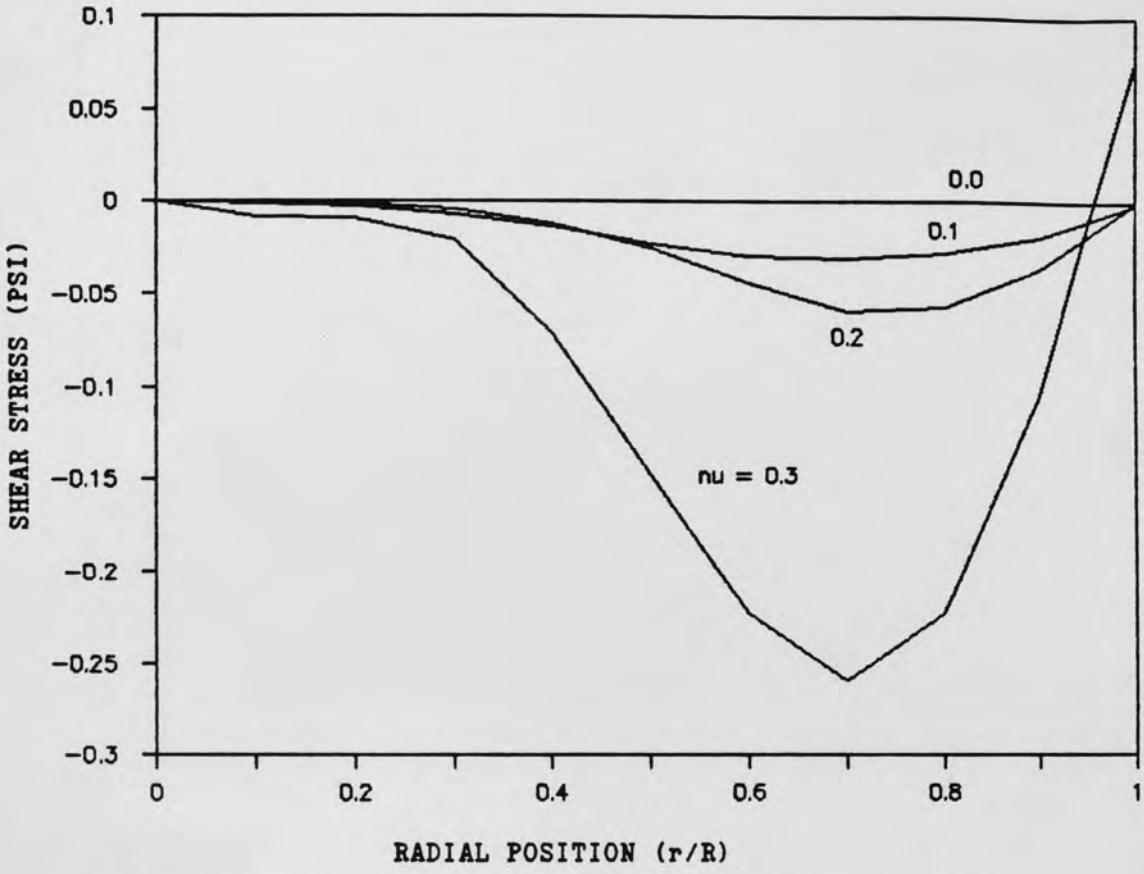

Figure 11. Shear Stress Variations with Poisson's Ratio.

Remember also that in the derivation of the wave equations, the two-dimensional wave equation reduced exactly to the one-dimensional wave equation when radial displacements and variations, as well as Poisson's ratio, were set equal to be zero. All these things taken together support the validity of the code. It appears that the basic equations used to calculate displacements, strains and stresses, and those used to enforce the boundary conditions are correct and are being carried out properly in the code.

CHAPTER 6

THE PROGRAMS

Two general programs have been devised in the problem considered. The first, called WAVES, allows the user to perform a one-dimensional or two-dimensional wave analysis for a variety of loading and boundary conditions. The output consists of a table of axial stresses versus dimensionless time and can include radial distributions of radial and shear stresses at selected time intervals in the case of a two-dimensional analysis.

The second program, titled COMPARE, performs three separate analyses for a given specimen under a given loading condition. Two of the analyses are two-dimensional, accounting for the two separate end constraint conditions, while the third analysis is one-dimensional. The output consists not only of axial stress as a function of dimensionless time for each analysis, but also includes the percent difference between the two-dimensional and one-dimensional analyses. Each program is discussed in greater detail below.

Program Waves

The program requires the input of several quantities which determine, among other things, the type of analysis to be performed, the specimen geometry and loading conditions, the wave velocities, the mesh size, and the format of the output.

The total time for the test is determined by the loading conditions chosen. Since the greatest effects of the wave phenomema are observed in the first few passes of the waves through the specimen, and since the governing equations are valid only for small strain theory, the test ends once the displacement at the top reaches fifteen percent of the specimen length, or once dimensionless time = 20, whichever occurs first. For a two-dimensional analysis, the output includes axial stresses versus dimensionless time at nine points in the specimen, as shown in Figure 12.

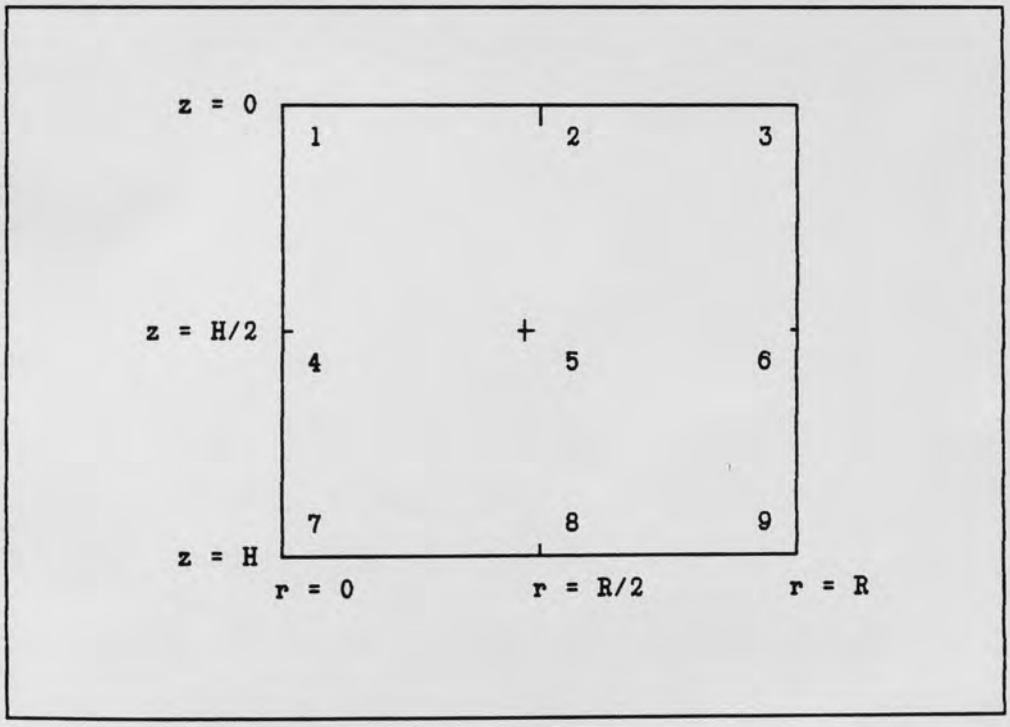

Figure 12. Points of Interest for Stresses in Elastic Cylinder.

For the stresses to be calculated at these points, each of the nine points must correspond to a mesh point in the finite difference

mesh. Thus, there must be an even number of axial and radial increments in the mesh. Hence, the choices for number of axial increments in the analysis is limited, and dependent on the height-to-diameter ratio of the specimen.

After initializing counters and calculating important constants, the program begins marching forward in time, calculating displacements at every mesh point at a given time interval, in the manner described earlier. At any time interval, however, the displacements are not a function of displacements from more than the two previous time intervals. Thus, in order to decrease the required computer storage space, only the displacements at the three latest time intervals are retained at any given time.

For example, displacements at points (i,j,3) are found to be functions of displacements at points (i,j,2) and (i,j,1). Once the calculations at the latest time interval, k=3, are completed, the displacements at points (i,j,1) will never be needed again. So, the displacements at points (i,j,2) and (i,j,3) can be renumbered as those of points (i,j,1) and (i,j,2), respectively, in preparation for the next cycle of displacement calculations. In this manner, the time interval at which the displacements are calculated always corresponds to k=3, and the storage requirements for the calculations are greatly reduced.

Before the renumbering process is carried out, however, strains and axial stresses are calculated at selected points in the specimen. If the user desires, radial and shear stresses at the top, middle, and bottom of the specimen are also calculated as a function of radial position at certain time intervals.

Axial stresses are also calculated at each radial mesh point at the top, middle, and bottom of the specimen at time increments selected by the user. In the actual triaxial testing, however, the radial distribution of the axial stresses is unknown. The load cell data allows only the calculation of an average axial stress at the top and bottom of the specimen. It is useful then, in the numerical analysis, to calculate an average axial stress at a given height in the specimen. This averaging technique is described below.

Finding Average Axial Stress

Consider the following distribution of axial stress versus radial position:

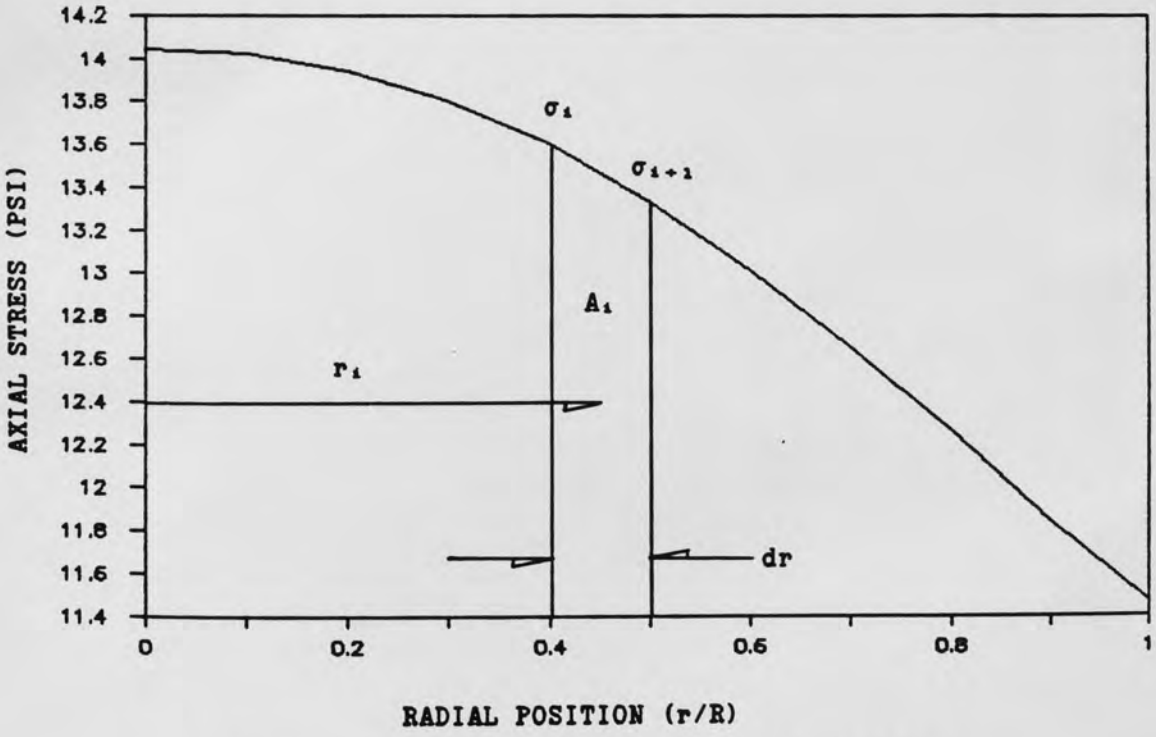

Figure 13. Radial Distribution of Axial Stress, Mid-Height of the Specimen.

Let:

σ_{ave} = average axial stress

A_i = incremental area, approximated by a trapezoid

$$= (\sigma_i + \sigma_{i+1})dr/2 \tag{27}$$

r_i = distance from centerline to centroid of A_i

$$= (i-1)dr + (\sigma_{i+1}/2 + (\sigma_i - \sigma_{i+1})/6)dr^2/A_i \tag{28}$$

The average stress for such a distribution is found by rotating this stress distribution about the centerline of the specimen and dividing the resulting volume by the cross-sectional area of the specimen. That is,

$$\sigma_{ave} = \text{Volume}/(\pi R)^2 \tag{29}$$

where:

$$\text{Volume} = \sum_{i=1}^{imax} (2\pi r_i A_i) \tag{30}$$

Substituting equations 27 and 28 into equation 30, and then equation 30 into equation 29, and simplifying:

$$\sigma_{ave} = (dr/R)^2 \sum_{i=1}^{imax} ((i-2/3)\sigma_i + (i-1/3)\sigma_{i+1})$$

Noting that $dr/R = 1/imax$:

$$\sigma_{ave} = (1/3imax^2) \sum_{i=1}^{imax} ((3i-2)\sigma_i + (3i-1)\sigma_{i+1}) \tag{31}$$

Once the axial stresses are known for each of the radial mesh points at a given height in the specimen, equation 31 is used to find the average axial stress at that height.

The need for such an averaging technique becomes most apparent when the specimen is assumed to be fully restrained in the lateral direction at the top and bottom of the specimen. In such cases, the two-dimensional analysis shows sharp increases in the axial stress at the top and bottom outer edge. Compare the axial stress distributions at the top of a specimen, assuming full and no lateral restraint, as shown in Figure 14.

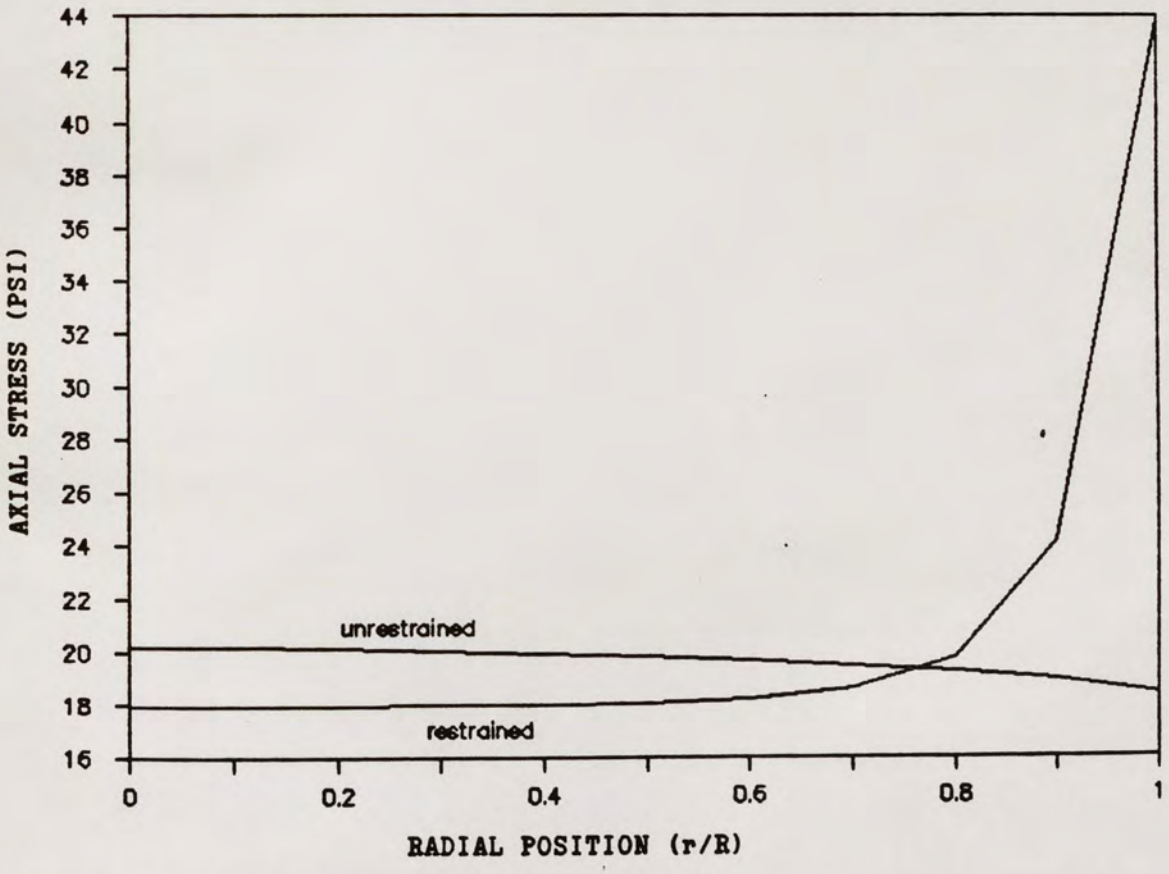

Figure 14. Radial Distribution of Axial Stress at the Top or Bottom of Laterally Restrained and Unrestrained Specimens.

A physical explanation for the high stress noted at the outer edge of the restrained specimen in Figure 14 is offered. In general, the closer a mesh point is to the centerline of the specimen, the smaller are the radial displacements that can be expected. When a radial displacement is observed, the mesh point is expected to undergo a smaller axial displacement. That is, the axial displacements are lessened when radial displacements occur simultaneously.

Therefore, near the centerline of the specimen, downward axial displacements cause similar downward displacements at mesh points below due to the small (if any) radial displacements there. Meanwhile, near the outer edge of the specimen, a given downward axial displacement results in smaller axial displacements at mesh points below due to the radial displacements that will simultaneously occur. Refer to Figure 15.

Thus, while no radial displacements are allowed at the very top or bottom of a fully restrained specimen, large radial displacements can exist near the outer edge only a few axial increments from the top or bottom. As a result of this, axial displacements also vary rapidly in the axial direction at the top and bottom outer edge of the specimen, giving rise to large W_z's. When σ_z is calculated there, the applicable equation is:

$$\sigma_z = E'(nu(U_r + U/r) + (1-nu)W_z)$$

Note that U_r and U/r are zero along the top and bottom of the specimen due to full lateral restraint. But, as noted above, large W_z's are observed at the top or bottom outer edge leading to large σ_z's there.

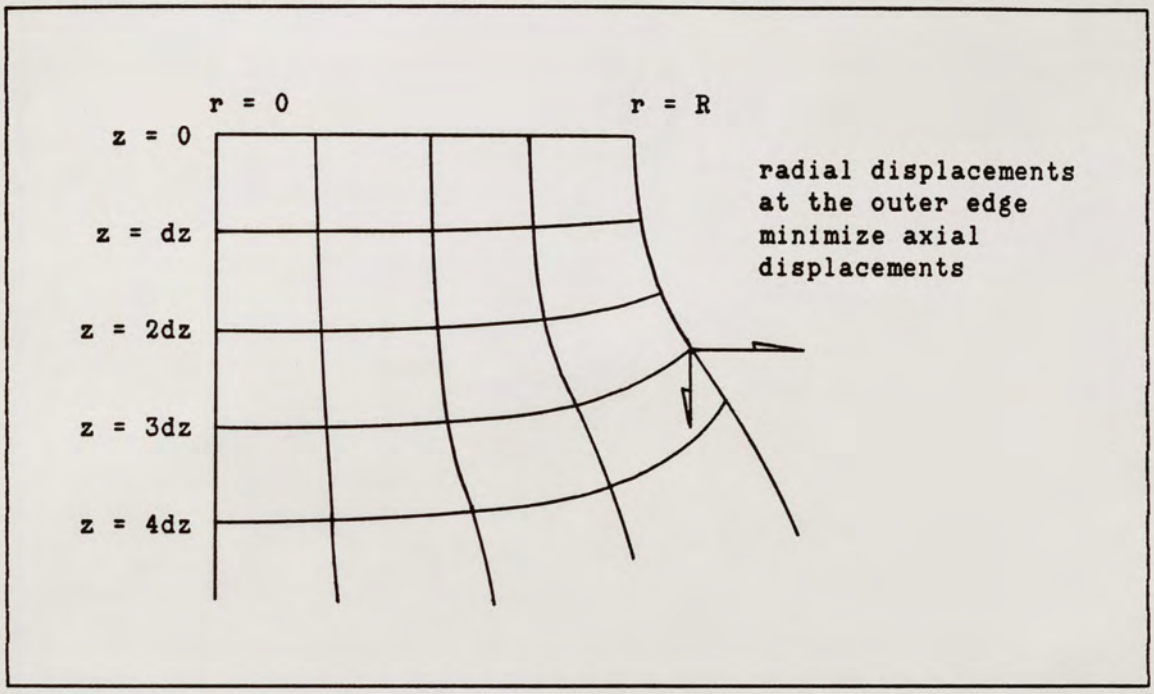

Figure 15. Distorted Finite Difference Mesh Near the Top of a Loaded Specimen.

In contrast, no unusual increases in axial stress are observed at the outer edge near the mid-height of the specimen, no matter the type of lateral restraint at the specimen top and bottom. Figure 16 shows the axial stress distribution at mid-height for the two possible boundary conditions.

The averaging technique discussed previously is used to find the average axial stresses in the two-dimensional analyses. There is no need to carry out this averaging technique in the one-dimensional analysis as there are no radial increments to consider. In all other respects, however, the steps taken in carrying out the one-dimensional and two-dimensional analyses are essentially the same. Once the calculations of displacements, strains, and stresses have been made at

all possible time intervals in the test, the stresses are output as a function of position and time.

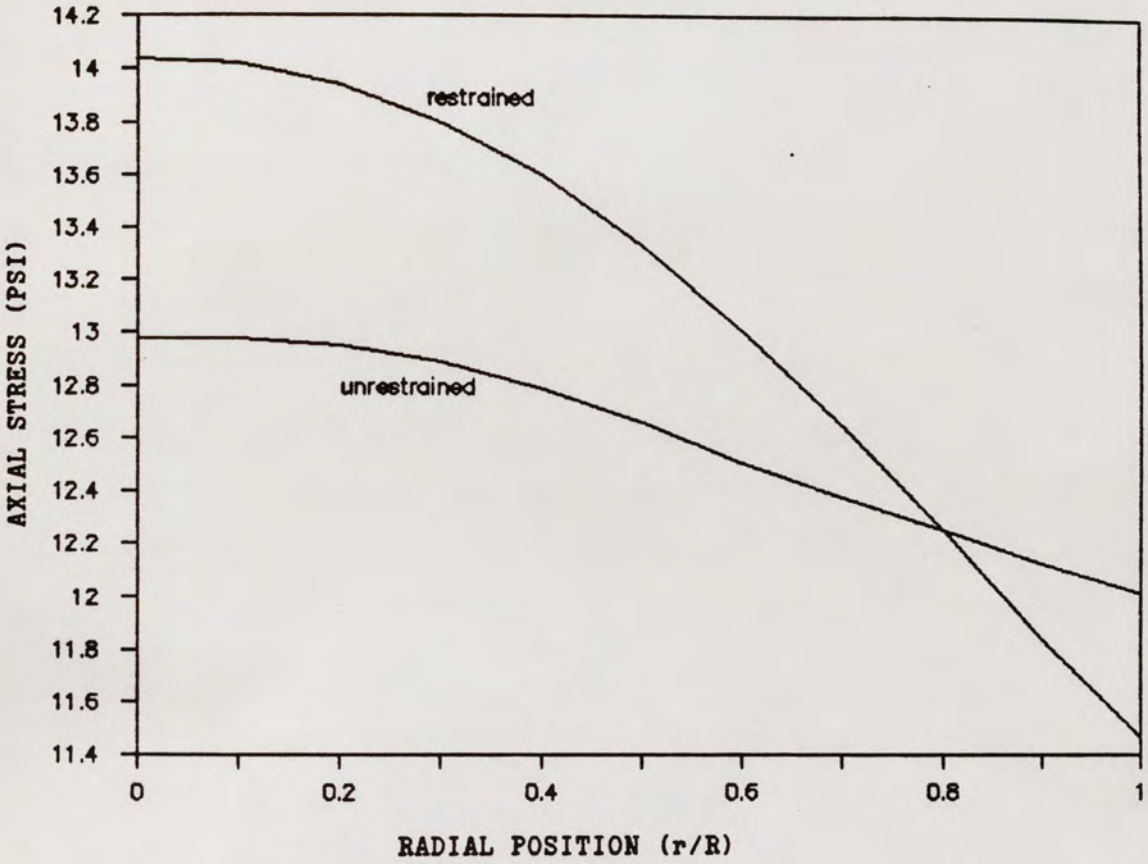

Figure 16. Radial Distribution of Axial Stress at Mid-Height of of Laterally Restrained and Unrestrained Specimens.

Program Compare

This program is very similar to WAVES in the methodology for finding displacements, strains, and stresses. COMPARE'S major purpose, however, is to compare the axial stresses calculated using a two-dimensional to those obtained from a one-dimensional analysis; as such, no radial or shear stresses are calculated as may be with WAVES. Three analyses are actually carried out: 1) a two-dimensional analysis,

assuming no lateral restraint at specimen top and bottom, 2) a two-dimensional analysis, assuming full lateral restraint at specimen top and bottom, and 3) a one-dimensional analysis.

In order to make useful comparisons between the one-dimensional and two-dimensional analyses, their finite difference meshes need to be compatible. That is, they need to have the same number of axial increments, and a comparable number of wave passes associated with each analysis. Due to the different time increments required for stability of each analysis, however, there are twice as many time increments in a two-dimensional analyis as in the one-dimensional analysis.

Another requirement for useful comparisons is that the proper rod wave velocity is used in the one-dimensional analysis based on the dilatational and shear wave velocities input for the two-dimensional analyses. Recall equations 10, 18, and 19:

$$(C_d/C_o)^2 = (1-nu)/((1-2nu)(1+nu)) \tag{10}$$

$$nu = (1-2\beta)/(2-2\beta) \tag{18}$$

$$\beta = (C_t/C_d)^2 \tag{19}$$

With a given set of shear and dilatational wave velocities, Poisson's ratio is calculated from equations 18 and 19, and a rod wave velocity is found from equation 10. Table 3 shows the ratio of C_d/C_o for various values of Poisson's ratio. Thus, with Poisson's ratio and C_d already input for a given specimen, C_o can be found.

Even with an appropriate rod wave velocity chosen, making a comparison between the stresses obtained from the one-dimensional and two-dimensional wave analyses can be somewhat misleading. Remember that

stresses are compared as a function of dimensionless time, which is just a measure of the number of times the wavefront has traversed the specimen. In the two-dimensional analysis, this wavefront is assumed to travel at the dilatational wave velocity. However, due to the interaction of the wave with the boundaries of the elastic cylinder, the energy of the wave is dispersed and much of it will actually travel at a slower velocity than the dilatational wave velocity. This slower velocity is referred to as the group velocity of the wave [1, 5, 10]. However, due to the mulitiple reflections and the complexity of the wave motion in the two-dimensional analysis, no attempt was made to determine or use the group velocity.

TABLE 3

DETERMINING THE PROPER C_o
FOR THE 1-D ANALYSIS

nu	C_d/C_o
0.0	1.0000
0.1	1.0113
0.2	1.0541
0.3	1.1602
0.4	1.4639
0.5	undefined

As a result, the actual number of times the energy of the wavefront traverses the specimen in the two-dimensional analysis is always somewhat less than the number of times the dilatational wavefront has traversed the specimen. Thus, the measure of dimensionless time in

the two-dimensional analysis is somewhat misleading, due to the dispersion of the wavefront that occurs. In the one-dimensional analysis, no dispersion of the wavefront occurs, and it always travels at the rod wave velocity. Although the comparisons made between the analyses as a function of dimensionless time may not be ideal, there does not appear to be a better basis on which to compare the stresses.

Once the data concerning specimen geometry and loading is input, COMPARE carries out the three analyses in succession, storing values of average axial stress versus dimensionless time for the top, middle, and bottom of the specimen for each analysis. The next step is to find the percent difference between the one-dimensional and two-dimensional analyses.

This percent difference is reported as a percentage of the two-dimensional analysis. That is,

percent difference = (1-D stress/2-D stress - 1)100%

Thus, when the 1-D stress is greater in magnitude than the 2-D stress, a positive percent difference is reported; a negative percent difference is reported whenever the 2-D stress is greater in magnitude than the 1-D stress.

The final step of the program is to output the axial stresses for each analysis and the percent differences versus dimensionless time. A block diagram for the WAVES and COMPARE programs appears in Appendix A. The actual codes for the programs appear in Appendix B, and Appendix C includes samples of the output generated from each program.

CHAPTER 7

RESULTS

In order to determine the conditions in which the one-dimensional and two-dimensional analyses give significantly different results for axial stress versus time, it is necessary to consider how the results of each analysis vary as a given parameter of the test is varied. The following parameters were considered as possibly influencing the differences noted between the one- and two-dimensional wave analyses:

1. Type of loading, as determined by the motion of the upper pedestal,
2. Rate of loading,
3. Type of lateral restraint at specimen top and bottom,
4. Position in specimen,
5. Mesh size of the finite difference scheme,
6. Height-to-diameter ratio of specimen, and
7. Poisson's ratio of the specimen.

Closer consideration of each of these parameters and their effects on the wave analyses follow. The discussions focus on the first few passes of the wave through the specimen, when the greatest variation in difference between the two analyses is observed. After the wave has travelled through the specimen many times, a constant difference between one- and two-dimensional analysis results is achieved. This appears to be due to the fact that after traversing the specimen several times,

the waves in the two-dimensional analysis are dispersed and appear to behave like a one-dimensional wave. Also, in each discussion below, the specimens are assumed to be fully laterally restrained at the top and bottom unless specifically stated otherwise.

Type of Loading

As noted earlier, three types of motion can be assumed for the upper pedestal: 1) constant velocity, 2) constant acceleration, and 3) hyperbolic velocity. The second type most closely approximates the actual loading conditions observed in the laboratory in the fastest triaxial tests. The other two types of motion are observed also, but only in slower tests [2]. The constant (step) velocity is also important due to its more easily visualized wave phenomena.

1-D, Step Velocity Input

Probably the most straightforward stress-time curve for a triaxial test is that for the one-dimensional analysis of a specimen loaded with a constant upper pedestal velocity. Figure 17 shows the stress at the top of the specimen as a function of dimensionless time.

Step-wise increases in stress should occur at even integers of dimensionless time, corresponding to the times when the stress wave arrives and is reflected at the top of the specimen. Rather than just a step-wise increasing function, however, Figure 17 shows sharp dips and peaks in the stress-time curve at the time increments just before and after the arrival of the wave at the top of the specimen.

These anomalies can be attributed to the way in which the strains are calculated at the top of the specimen. Using a three point backward

difference approximation for W_z causes the derivative to be approximated across the wavefront. That is, the displacements used to approximate W_z at the top of the specimen are at points on opposite sides of the wavefront. At the wavefront is a very large change in stress which is proportional to a change in strain and, in turn, to a change in particle velocity (acceleration). Note that the particle acceleration is directly related to the motion of the upper pedestal. For a step velocity input, this corresponds to an infinite acceleration at time, $t = 0$. Thus, the finite difference algorithm attempts to approximate infinite derivatives when the wavefront is one axial increment from the top, either approaching or departing.

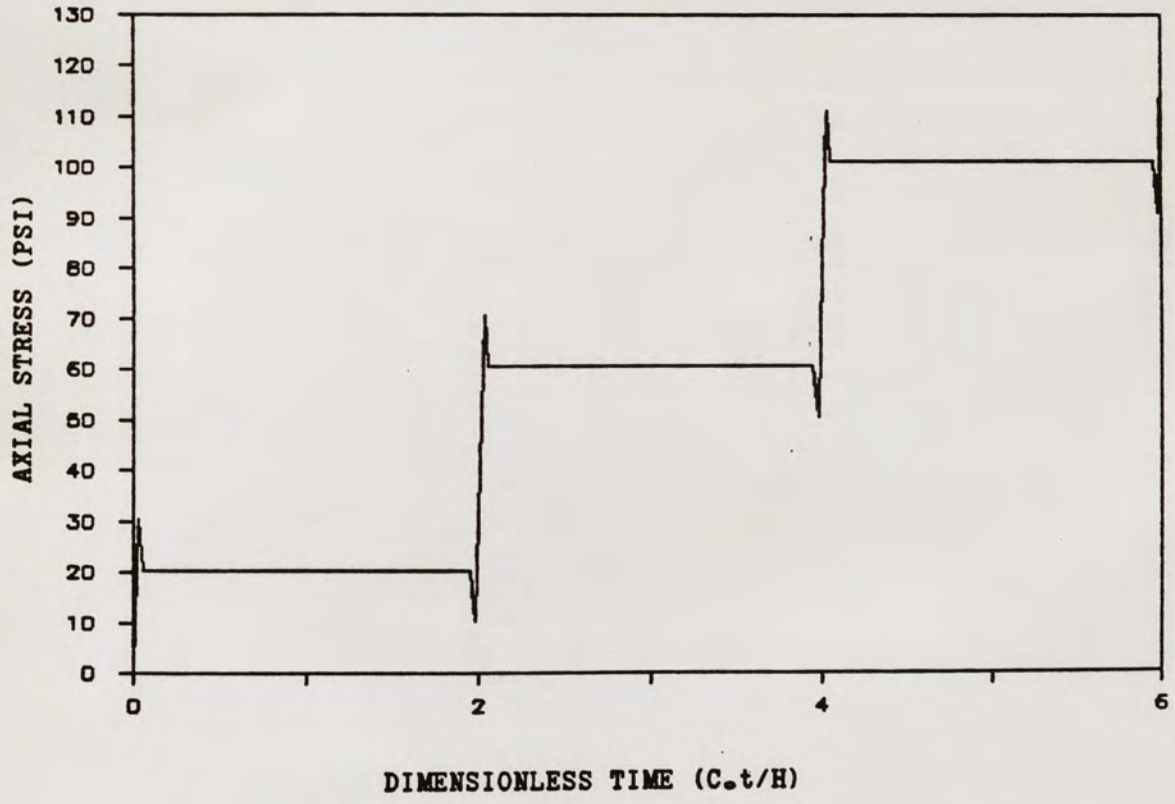

Figure 17. 1-D Axial Stress at Top of Specimen, Constant Upper Pedestal Velocity.

It appears then that the finite difference algorithm cannot accurately approximate derivatives when values vary sharply over only a few axial increments, as is the case with the step velocity loading. The sharp dips and peaks can be removed from Figure 17 by tracking the position of the wavefront with time. Whenever the wavefront is within one axial increment of the top, a two point backward difference approximation for W_z should be used, rather than the usual three point approximation. In this way, the finite difference algorithm used to calculate strain never crosses the wavefront.

Figure 18 shows the stress-time curve which results when such a 'peak suppressor' code is introduced into the one-dimensional analysis of the step velocity loading. Note that the plot more closely approximates the step increases in stress which are expected, without the sharp dips and peaks present in Figure 17.

More complicated is the stress-time curve resulting from a two-dimensional wave analysis of the same specimen under the same loading conditions. Figure 19 shows the oscillatory nature of the axial stress as computed with a two-dimensional analysis superimposed with the one-dimensional anyalysis results. Note that although the one-dimensional and two-dimensional analyses can predict very different axial stresses at any given time interval, the same general step-wise trend for axial stress is noted in each.

The oscillations noted in the two-dimensional analysis in Figure 19 appear to be due to two sources. In part, the oscillations are due to the presence of waves propagating and reflecting in the radial direction as well as the axial direction. This certainly would affect

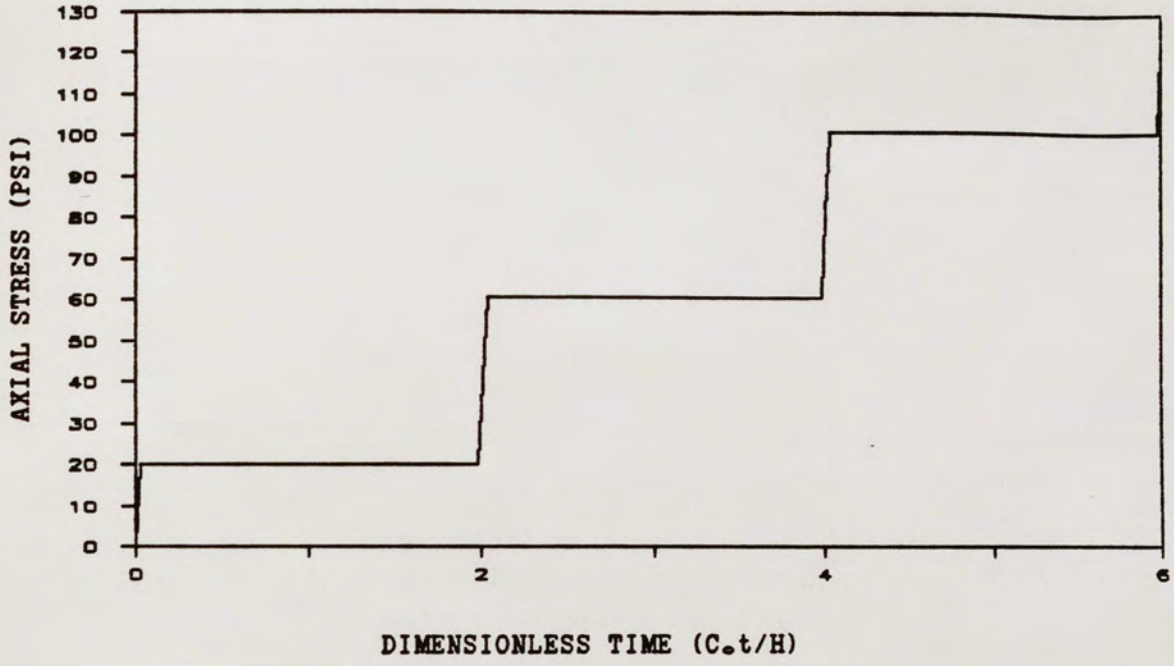

Figure 18. 1-D Axial Stress at Top of Specimen, Constant Upper Pedestal Velocity, with "Peak Suppressor Code."

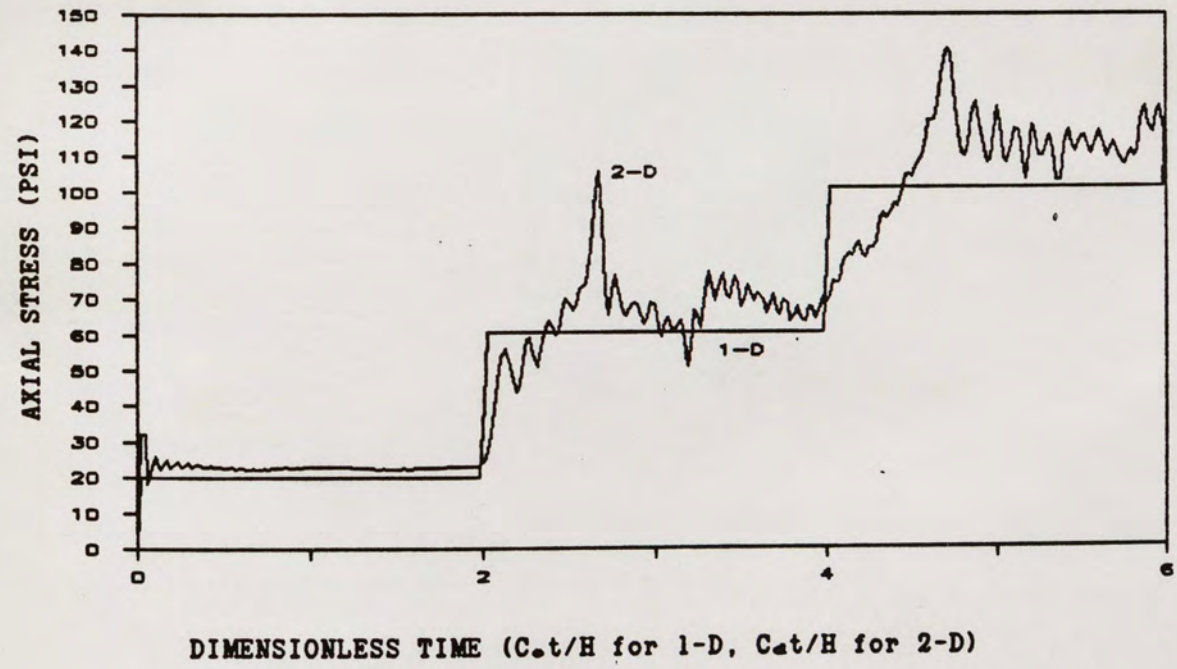

Figure 19. 1-D and 2-D Axial Stresses at Top of Specimen, Constant Upper Pedestal Velocity.

the axial stresses observed at the top of the specimen. However, the oscillations also, in part, appear to be due to the sharp wavefront associated with the step velocity input. To verify this, consider the other possible types of upper pedestal motion.

Other Types of Input

In order to determine to what degree the sharp wavefronts are the cause for the oscillations in the stress-time curves, consider the other types of loading conditions. The other types of upper pedestal motion are the constant acceleration and the hyperbolically increasing velocity, neither of which causes a sharp change in particle velocity and stress at the wavefront in normal laboratory loading conditions. Figure 20 shows that plots of axial stress at the top versus dimensionless time are essentially identical for both the one-dimensional and two-dimensional analyses for constant upper pedestal acceleration. The one- and two-dimensional plots are also essentially identical when considering the case of the hyperbolic velocity for the upper pedestal, under most conditions. See also Figure 21.

Notice that with these other types of upper pedestal motion, none of the oscillations of axial stress are observed in the two-dimensional analyses. Yet the radial waves thought to cause the oscillations in Figure 19 ought to be present with these other types of motion as well. This apparent conflict can be resolved by considering the hyperbolic velocity loading condition more closely.

Consider Figure 22, which shows axial stress at the top versus dimensionless time for varying initial accelerations associated with the

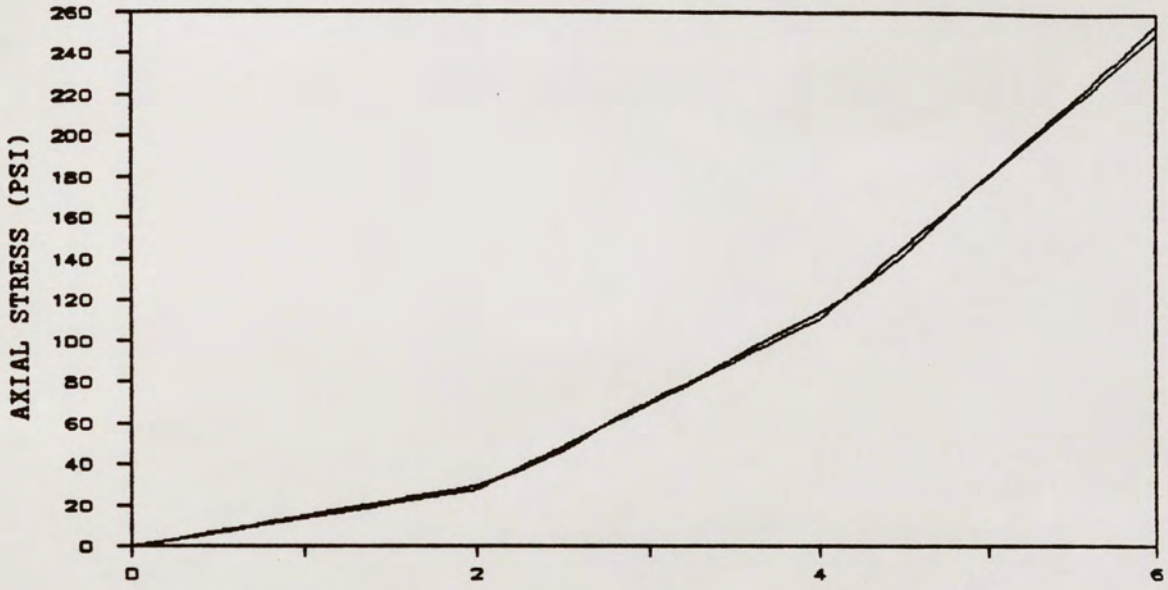

Figure 20. 1-D and 2-D Axial Stresses at Top of Specimen, Constant Upper Pedestal Acceleration.

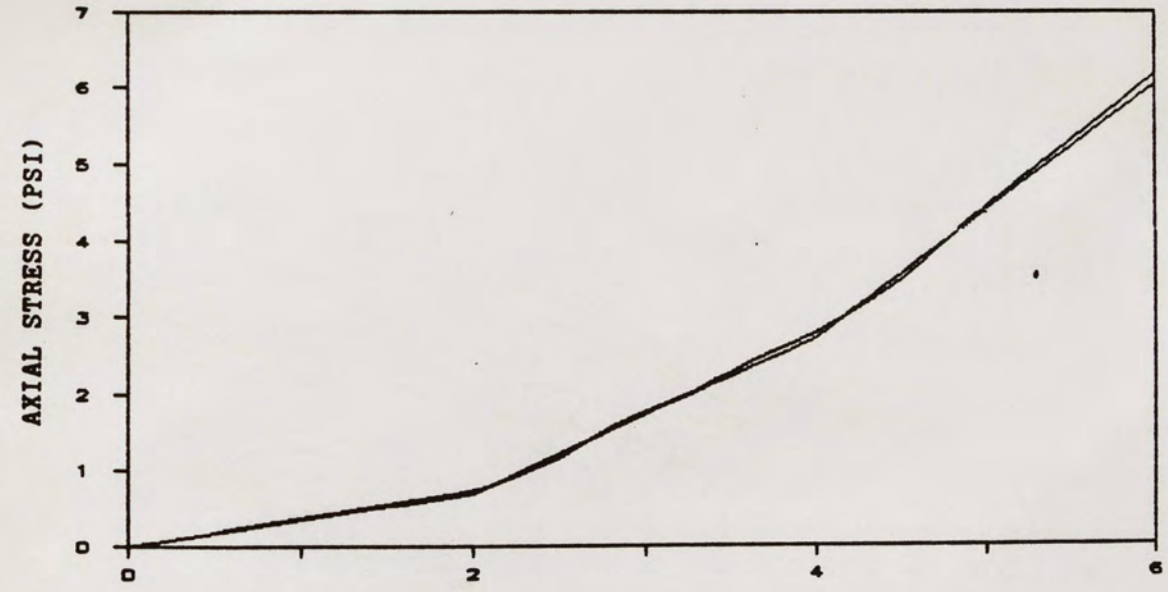

Figure 21. 1-D and 2-D Axial Stresses at Top of Specimen, Hyperbolic Upper Pedestal Velocity.

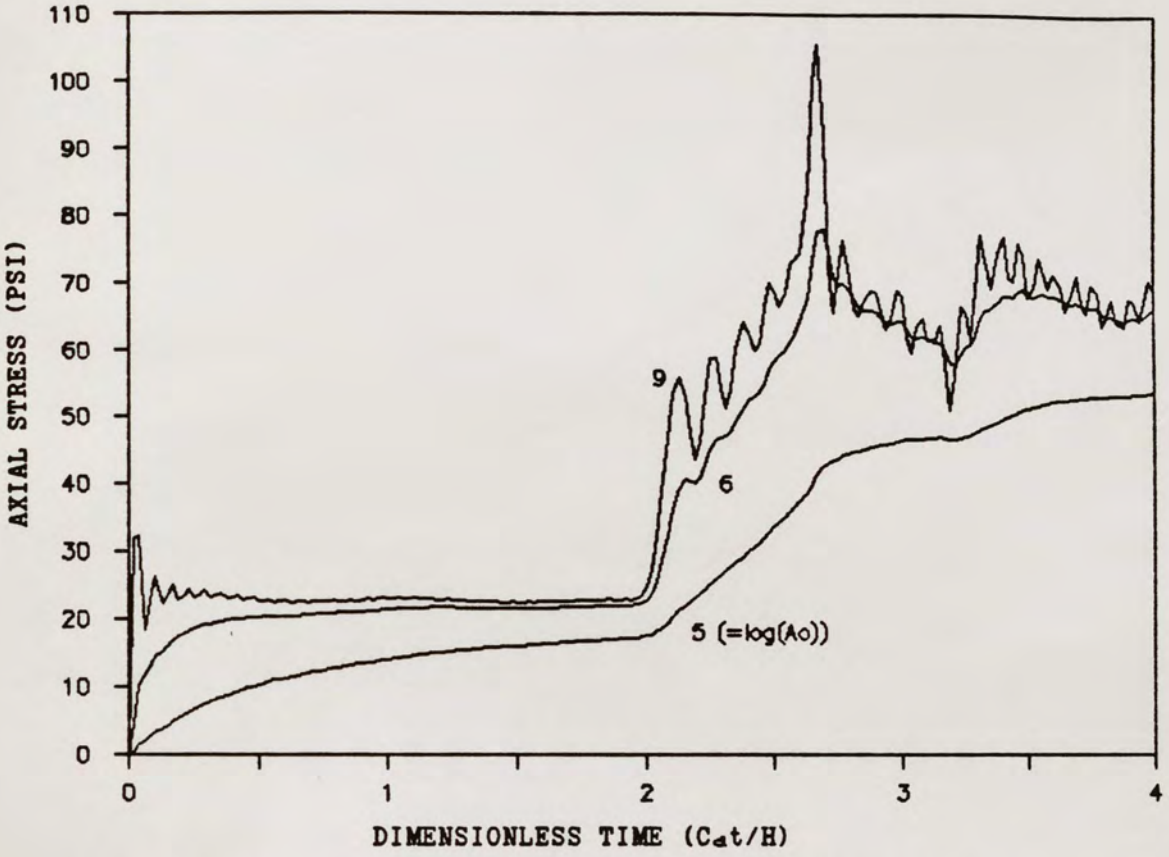

Figure 22. 2-D Axial Stresses at Top of Specimen, Varying Initial Acceleration of Hyperbolic Velocity.

hyperbolic upper pedestal velocity. The curves were generated using the two-dimensional analysis.

Recall equation 25:

$$t_o = V_o/A_o$$

For a given limiting upper pedestal velocity, V_o, the characteristic time, t_o, will decrease as the initial acceleration, A_o, increases. The curves in Figure 22 were generated assuming a constant V_o of ten inches per second. Thus, Figure 22 shows that the oscillations in the stress-time curves appear as t_o gets smaller. Note that as t_o

decreases, the motion of the upper pedestal approaches that of a step velocity. The top curve of Figure 22 is essentially identical to that of the two-dimensional analysis curve for the step velocity of Figure 19.

Consider how the nature of the oscillations of Figure 22 change as t_o decreases. The curve for $A_o = 10^5$ inches per second^2 shows rather broad oscillations in the axial stress occurring between dimensionless time equals two and four. The period of these oscillations remains about the same for $A_o = 10^6$ inches per second^2 although the amplitude of oscillations increases greatly. Note, however, the many rapid oscillations which occur when $A_o = 10^9$ inches per second^2. This curve has very much the same shape as that for $A_o = 10^6$ inches per second^2 but with many sharp oscillations superimposed.

It appears that the very broad oscillations in axial stress which occur after dimensionless time equals two can be attributed to the effects of radial wave phenomena. The amplitude of these oscillations increases as A_o increases and the hyperbolic velocity approaches the step velocity. There are limitations, however, to the loading rates which can presently be achieved in the laboratory. In the case of hyperbolic velocity, the maximum V_o is on the order of ten inches per second and maximum A_o on the order of 200 g's, or about 8×10^4 inches per second^2. Thus, for the present loading conditions in the laboratory, the oscillations due to radial wave phenomena would be minimal or non-existent. Note that such oscillations did not appear in the two-dimensional analysis of Figure 21, which had the identical loading conditions but with $A_o = 10^3$ inches per second^2.

The very sharp and rapid oscillations in the top curve of Figure 22 are due to the inability of the finite difference algorithm to accurately approximate the derivatives associated with a sharp wavefront. Unlike the one-dimensional analysis in which the effects of this limitation quickly dampen out, the oscillations in axial stress carry through the calculations for many time intervals in the two-dimensional analysis, masking the true behavior of the specimen.

There appears to be a relationship between the hyperbolic velocity loading rate and the appearance of the rapid oscillations in the stress-time curves. As noted earlier, as A_o increases for a given V_o, the characteristic time t_o decreases. The oscillations first appear when t_o has values on the same order magnitude of the time interval of the finite difference mesh. For the loading conditions of Figure 22, this corresponds to A_o between 10^6 and 10^7 inches per second^2. This is precisely when the oscillations begin to appear.

Further support for the idea of a sharp wavefront causing the sharp oscillations in stress is found by considering the stress-time variations as t_o is decreased in the one-dimensional analysis. Figure 23 shows these variations for the same loading conditions considered in Figure 22. Note that the oscillations in the one-dimensional analysis dampen out more quickly than in the two-dimensional analysis. The top curve of Figure 23 is identical to the step velocity of Figure 17. Again, the oscillations in Figure 23 only appear when t_o approaches the magnitude of the time increment of the finite difference algorithm.

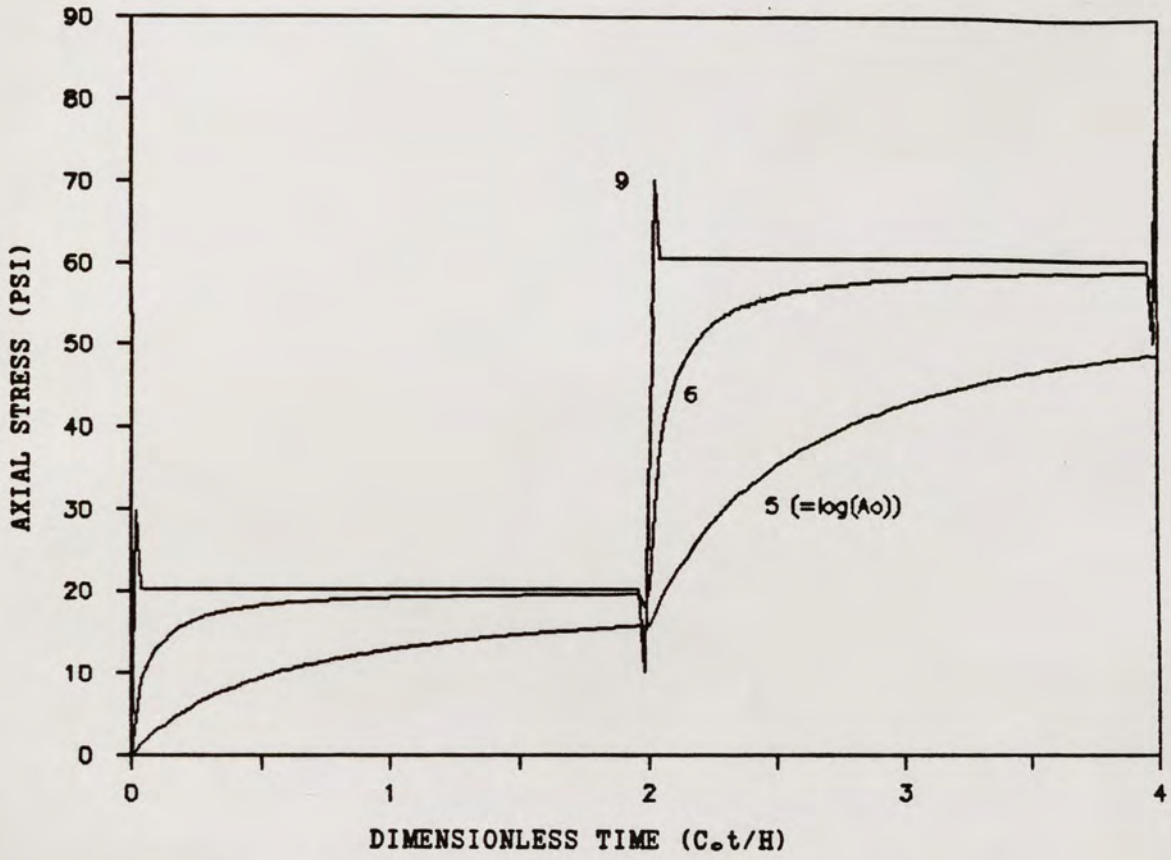

Figure 23. 1-D Axial Stresses at Top of Specimen, Varying Initial Acceleration of Hyperbolic Velocity.

It was shown earlier that the oscillations are easily removed from the stress-time curves in the one-dimensional analyses by incorporating a 'peak suppressor code.' Inserting such a 'peak suppressor' code into the two-dimensional analysis would be difficult. As noted previously, it is difficult to predict the shape or the position of the wavefront in the two-dimensional anlysis, and therefore difficult to know when to apply such a code. Furthermore, Figures 20 and 21 indicate that for many loading conditions, no oscillations in the two-dimensional stress-time curves are even observed. The oscillations do not appear with the constant acceleration input and are present with the hyperbolic

although it certainly will affect the actual stresses observed in either analysis. To see why no change in the percent differences occur, recall that the axial displacements at the top of the specimen are given by:

$$W(r,0,t) = .5At^2$$

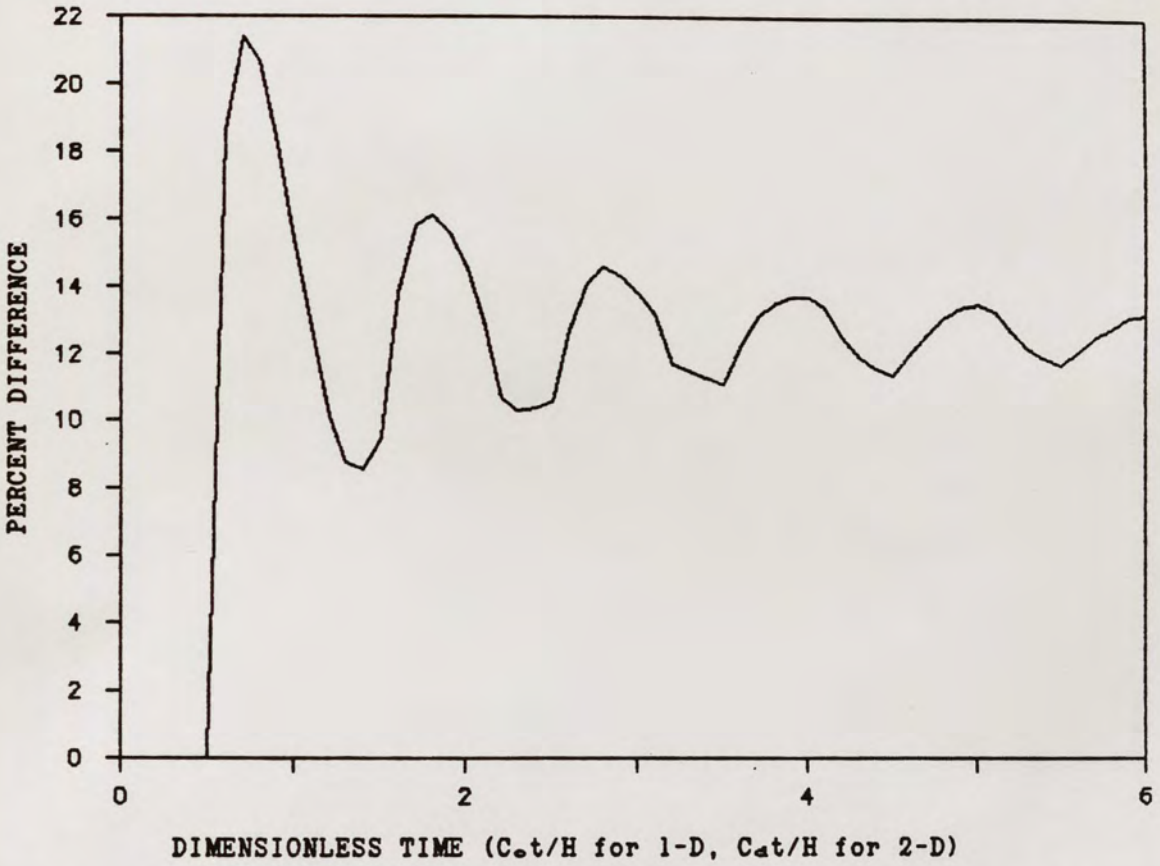

Figure 24. 1-D, 2-D Axial Stress Percent Difference at Middle of Specimen, Constant Upper Pedestal Acceleration.

By doubling the acceleration, for example, displacements at the top are exactly doubled at any given time interval. Displacements at any other point, as solved by the wave equations or various boundary conditions in finite difference form, are first order functions of previously solved

displacements. As such, displacements throughout the finite difference mesh will exactly double. Thus, the resulting strains and stresses also double due to the linear relationships that exist. This is the case in either the one-dimensional or two-dimensional analysis, and therefore the percent difference between the two is independent of the acceleration of the upper pedestal.

Hyperbolic Velocity

The percent difference between the one-dimensional and two-dimensional analyses is shown in Figure 25 for a specimen loaded by the hyperbolic velocity of the upper pedestal. Also shown are the variations in percent difference that occur as the limiting upper pedestal velocity, V_o, increases.

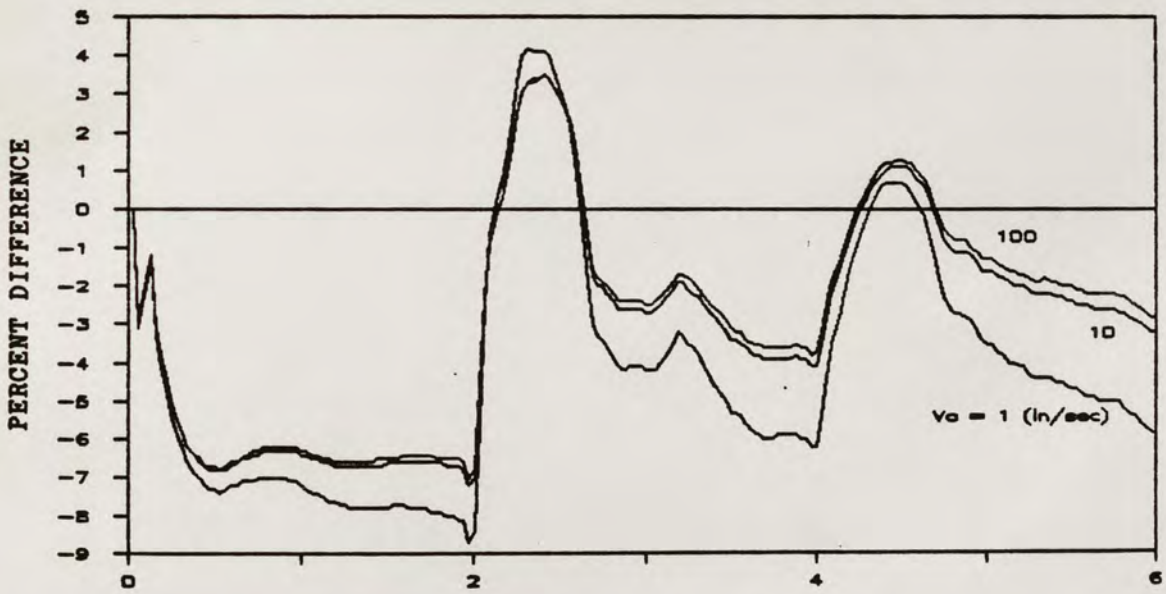

Figure 25. 1-D, 2-D Axial Stress Percent Difference at Top of Specimen, Hyperbolic Upper Pedestal Velocity, Varying Limiting Upper Pedestal Velocity.

Note that for any value of V_o, the maximum percent difference is achieved at dimensionless time equals two, corresponding to reflection of the wave at the top of the specimen. Between reflection times, the difference between the analyses is less. The percent difference between the two analyses decreases only slightly with increased values of V_o. In the laboratory, V_o = ten inches per second is a maximum presently attainable; V_o = 100 inches per second has been included in Figure 25 for comparison purposes only. For each curve in Figure 25, A_o = 1000 inches per second^2. Thus, in terms of t_o, Figure 25 shows that the maximum difference between the one-dimensional and two-dimensional analyses increases slightly as t_o decreases.

Another way to vary the loading rate is to increase the initial acceleration, A_o, rather than V_o. In Figure 26, V_o = ten inches per second for each curve while A_o is allowed to vary. Figure 26 shows that the maximum percent difference again increases slightly as t_o decreases. Figure 26 shows the percent differences for only the first two passes of the wave through the specimen. The curves look very similar to those of Figure 25 during equivalent time intervals.

So, as t_o decreases, either due to decreasing V_o or increasing A_o, the one-dimensional and two-dimensional solutions become more different. This change in the percent difference between the one-dimensional and two-dimensional analyses, however, appears to be minimal for present laboratory loading conditions, and of little consequence in determining when a two-dimensional analysis would be needed. It is apparent from Figures 22 and 23 that t_o should be maintained large enough (in comparison to the time interval of the finite difference algorithm) so

that unusual oscillations in the stress-time curves are avoided in either type of analysis.

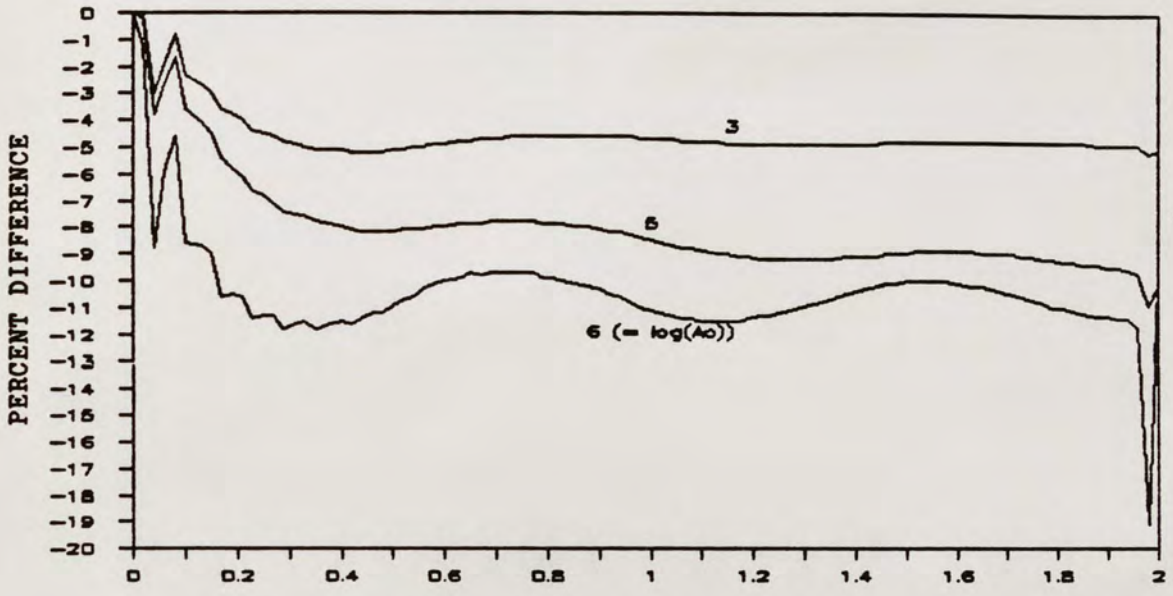

Figure 26. 1-D, 2-D Axial Stress Percent Difference at Top of Specimen, Hyperbolic Upper Pedestal Velocity, Varying Initial Acceleration of Upper Pedestal.

In summary, the variations noted with changing loading rates are non-existent for the case of constant upper pedestal acceleration, and small for the case of hyperbolic velocity, as long as t_o is maintained larger than the time increment of the finite difference mesh.

Type of Lateral Restraint

The top and bottom of the specimens can be assumed to have no lateral restraint, or full lateral restraint. These conditions represent limiting extremes of the actual constraints of the specimen.

In all practicality, however, the condition of full lateral restraint at the specimen top and bottom better approximates the actual constraints in the triaxial tests.

Since the one-dimensional analysis is equivalent to a two-dimensional analysis with zero lateral displacements, it is expected that the stresses the one-dimensional analysis predicts will be closer to those predicted by the two-dimensional analysis which allows no lateral deformation at the specimen top and bottom. Figures 27 and 28 show that this is the case.

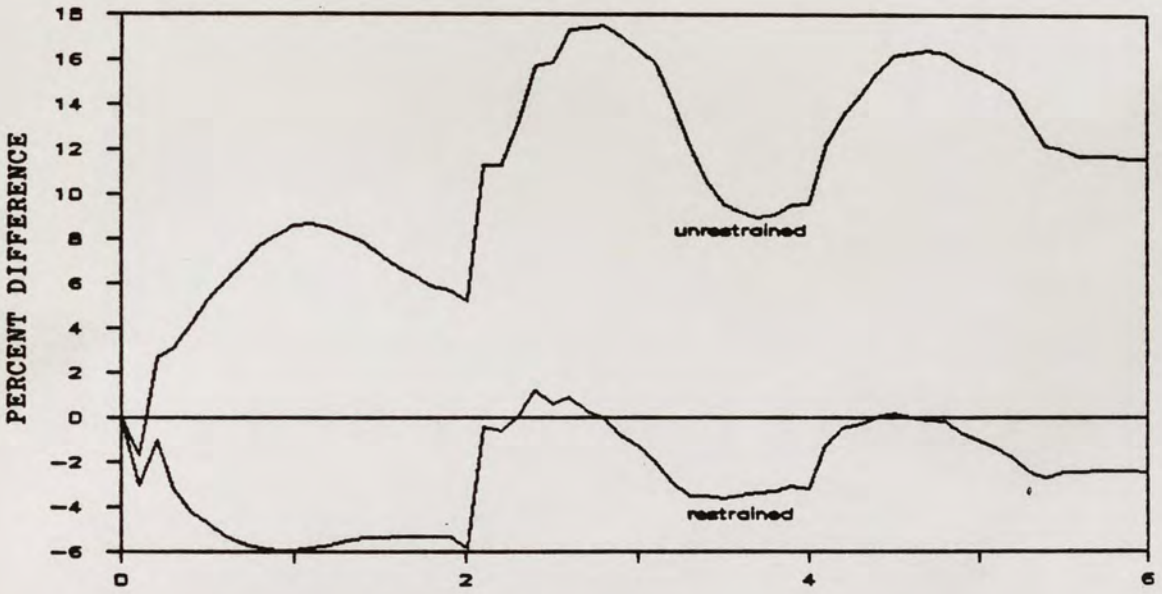

Figure 27. 1-D, 2-D Axial Stress Percent Difference at Top of Specimen, Constant Upper Pedestal Acceleration, Restrained Versus Unrestrained Specimens.

At the top of the specimen, as shown in Figure 27, the unrestrained two-dimensional analysis predicts stresses which differ

from the one-dimensional analysis by as much as 18%, while the restrained two-dimensional analysis remains within 6% of the one-dimensional analysis.

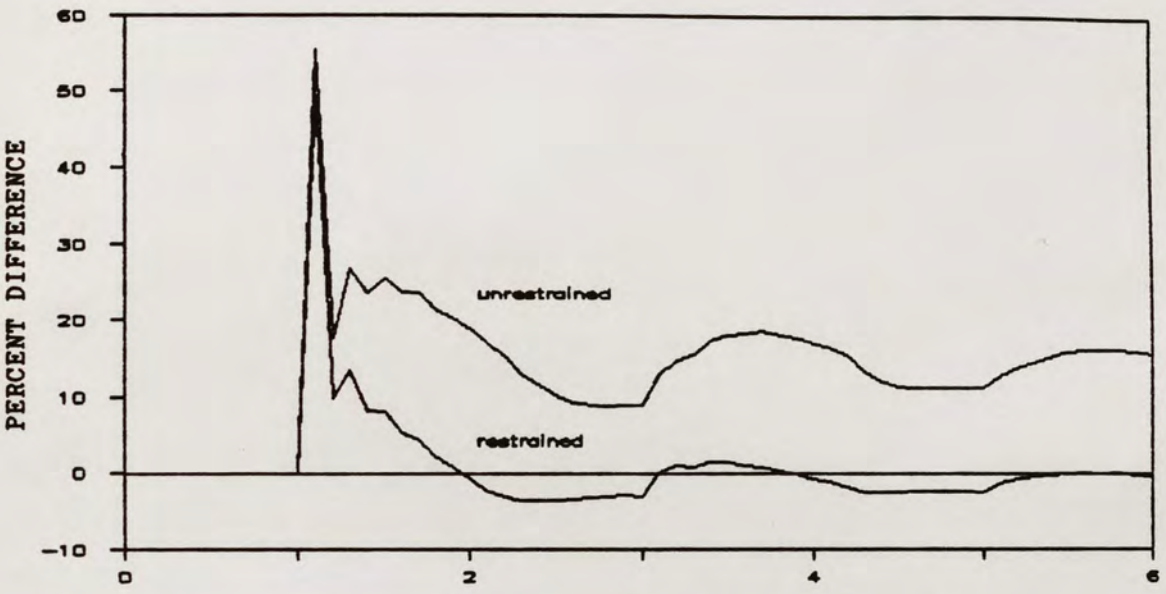

Figure 28. 1-D, 2-D Axial Stress Percent Difference at Bottom of Specimen, Constant Upper Pedestal Acceleration, Restrained Versus Unrestrained Specimens.

Figure 28 addresses the bottom of the specimen. Each of the two-dimensional analyses predicts large differences just after the arrival of the initial wavefront. Afterwards, though, the restrained two-dimensional analysis remains within 5% of the one-dimensional analysis while the unrestrained analysis differs by as much as 20% from the one-dimensional analysis.

At the middle of the specimen, it is expected that the end restraints should have little effect on the stress-time curves generated

in the two-dimensional analyses. This is due to the fact that end restraint effects should decrease with distance from the end of the specimen. As such, any end restraint effects observed at mid-height should be minimal, and should decrease as the length of the specimen increases.

Figure 29 shows the difference in axial stresses at mid-height as computed once by the restrained two-dimensional anlaysis and once by the unrestrained two-dimensional analysis. The percent difference for a given specimen height oscillates about an average percent difference. This difference represents the difference between the stresses at mid-height, as calculated from the restrained and unrestrained two-dimensional analyses, as opposed to the difference between the one-dimensional and two-dimensional analyses considered in earlier figures. Note that the average percent difference is small for any given height, and decreases as the height of the specimen increases.

These observations indicate that the code is generating the expected results, and that the end constraints have little effect on the stresses observed at the mid-height of the specimen. The end constraints have a larger effect on the stresses at the top and bottom of the specimen. At these points, the one-dimensional and restrained two-dimensional results approximate each other most closely, as discussed below.

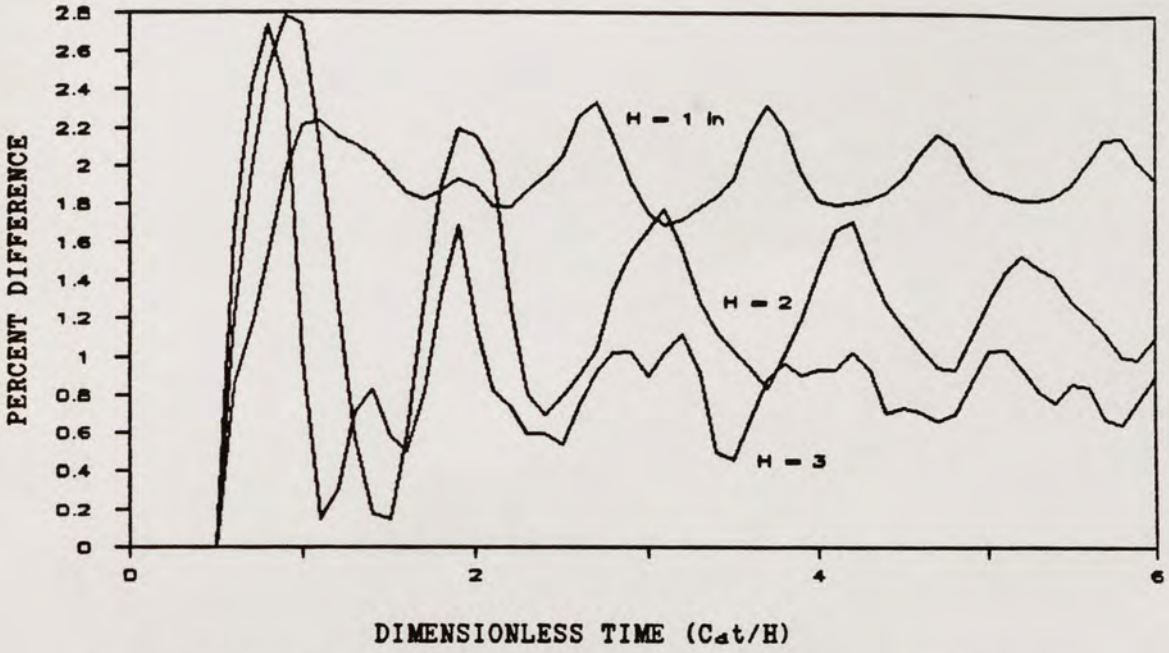

Figure 29. 2-D Axial Stress Percent Difference at Middle of Specimen, Constant Upper Pedestal Acceleration, Restrained Versus Unrestrained Specimens.

Position in Specimen

In general, larger differences between the one- and two-dimensional analyses exist at the middle of the specimen; the two analyses approximate each other more closely at the specimen top and bottom, especially when full lateral restraint is assumed, as expected. The largest radial displacements occur near the mid-height of the specimen in the two-dimensional analysis, thus axial stresses there are more different from those predicted with the one-dimensional analysis.

Figure 30 shows the percent difference between the two analyses observed at the top, middle, and bottom of the specimen as a function of dimensionless time. These curves are for the case of constant upper pedestal acceleration, with the full lateral restraint at the top and

bottom. Again, the percent difference is quoted as a percent of the two-dimensional values. Differences noted between the one-dimensional and two-dimensional analyses are very similar for the hyperbolic upper pedestal velocity and subsequent discussions in this section pertain to either loading condition.

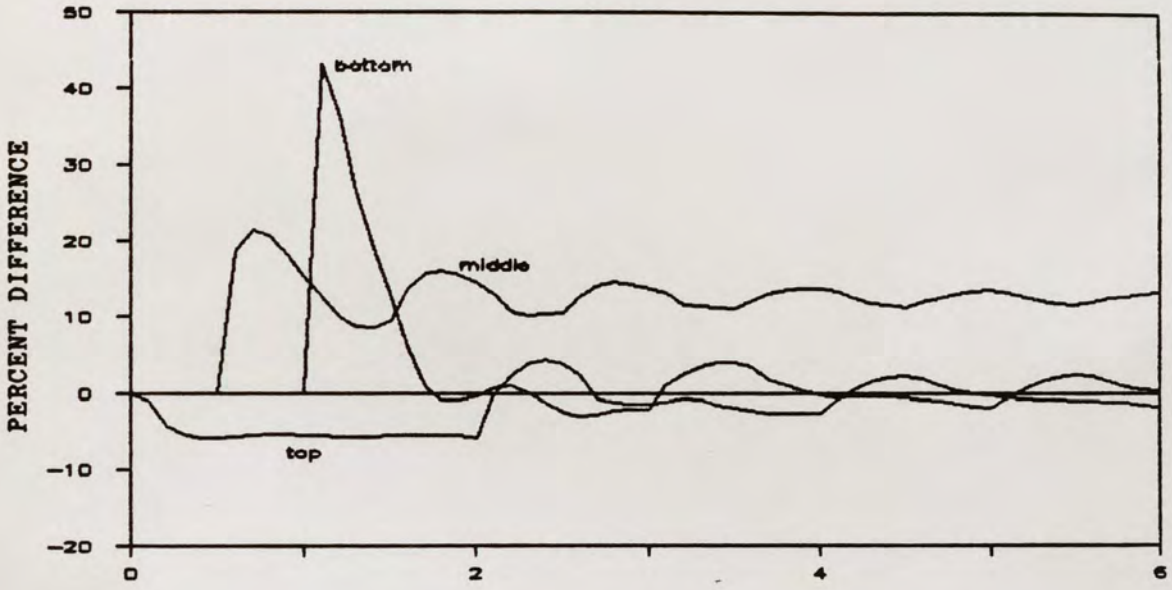

Figure 30. 1-D, 2-D Axial Stress Percent Difference as a Function of Axial Position, Constant Upper Pedestal Acceleration.

Note that after some large oscillations in the first wave pass, the differences at the top and bottom become rather small and essentially negligible. The difference at the middle is more significant; as noted earlier, this is expected. The very large differences between the two analyses, especially at the bottom of the specimen the instant after the initial wavefront is reflected (after

dimensionless time equals to one), can be explained by recalling how the stresses in the one- and two-dimensional are compared.

The comparisons are made in terms of dimensionless time where the wavefront is assumed to travel the length of the specimen during one unit of dimensionless time. However, due to the dispersive nature of the wave in the two-dimensional analysis, much of the energy associated with the wave lags behind the initial wavefront assumed to be travelling at the dilatational speed.

A seemingly better way to compare the different wave analyses would be to determine a group velocity for the wavefront which accounts for dispersion, and establish the time increments of the finite difference algorithm based on the group velocity, rather than the dilatational wave velocity. Actually carrying this out, however, would be difficult. With the multiple reflections occurring as the waves travel through the specimen, it is infeasible to define and track the position of a wavefront travelling at the group velocity.

The fact that some energy of the wave lags behind the dilatational wavefront is useful, however, in explaining some of the results observed in Figure 30. The large differences in the axial stresses noted at the bottom of the specimen indicate that the one-dimensional analysis is predicting much higher stresses at the bottom after the arrival of the initial wavefront than the two-dimensional analysis predicts. Note also that this difference decreases rapidly with time.

Since some energy lags behind the dilatational wavefront of the two-dimensional analysis, smaller stresses and strains will be predicted at the bottom, even though the dilatational wavefront may have already

arrived. On the other hand, in the one-dimensional analysis, no dispersion of the wave occurs, and all of the energy of the wave arrives at the bottom of the specimen when dimensionless time equals one. As such, larger strains and stresses are predicted, leading to the large differences noted. The differences decrease with time as more of the energy associated with the two-dimensional analysis reaches the bottom of the specimen, resulting in stresses closer to those observed in the one-dimensional analysis.

A similar argument can be used to explain the differences at the middle and top of the specimen. As shown in Figure 30, large differences also exist at the middle of the specimen just after the arrival of the initial wavefront. At the middle, however, the maximum difference is smaller than at the bottom of the specimen. Since the waves have not travelled as far through the specimen, there will be less dispersion of the wave in the two-dimensional analysis. As such, the energy does not lag as far behind the dilatational wavefront, thus yielding smaller maximum differences between the two analyses.

At the top of the specimen, negative differences are noted at early time intervals, indicating larger stresses predicted by the two-dimensional analysis. Once again, due to the ispersion of the wave in the two-dimensional analysis, the energy, on a dimensionless time basis, would not be carried away as fast as with the one-dimensional wave. Thus, higher stresses are initially predicted at the top with the two-dimensional analysis.

The explanation of Figure 30 to this point has dealt only with the times shortly after the initial wavefront passes a particular point.

Further explanation of the differences observed between the one-dimensional and two-dimensional analyses at later times would be difficult due to the complex nature of the waves and their various interactions in the two-dimensional analysis of the specimen. It is sufficient to say that the differences observed at the top and bottom of the specimen are only significant in the first few passes of the wave through the specimen. The large differences appear to be due to methodology of comparing the one-dimensional and two-dimensional analyses on the basis of dimensionless time and the inability to accurately predict the dispersion of the two-dimensional wave. At later times, the differences at the top and bottom of the specimen are small.

Although larger differences are observed at the middle, the actual fast triaxial tests only generate data for the top and bottom of the specimen. Since the one-dimensional and restrained two-dimensional analyses predict similar stresses at the top and bottom for most time intervals, either would appear to be adequate for approximating laboratory results. If it is thought, however, that data from the middle of the specimen better represent specimen behavior, then the differences between the two analyses become more significant.

The actual stress-strain behavior of a specimen should be more closely approximated by a two-dimensional analysis than a one-dimensional analysis. But the computer time and storage requirements to complete a two-dimensional analysis can become prohibitive. Therefore, it would be useful if a one-dimensional analysis could be performed, and its results converted, by use of some type of conversion factor, into the results that would be predicted by a two-dimensional analysis.

One such useful conversion factor is represented in Figure 31, which shows the ratio of the axial stress at the middle of a fully restrained specimen as predicted by a two-dimensional analysis, to the axial stress at the top of a specimen as predicted by a one-dimensional analysis. The curves are for height-to-diameter ratios of one, two, and three. Note that varying the height-to-diameter ratio has very little effect on the conversion factor.

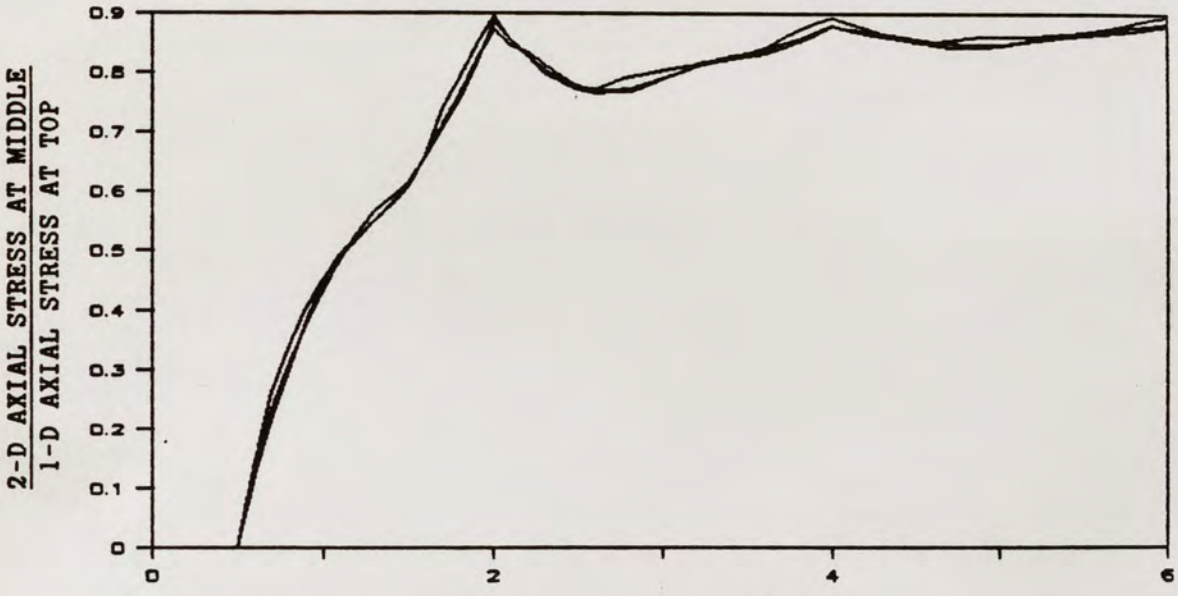

Figure 31. Ratio of Middle Axial Stress (2-D Analysis) to Top Axial Stress (1-D Analysis) for Constant Upper Pedestal Acceleration.

The conversion factor would be most useful since a two-dimensional analysis would never have to actually be carried out, other than to derive the conversion factor. Once obtained, one-dimensional analysis results from the top of the specimen can be multiplied by the conversion

factor to obtain the stresses that a restrained two-dimensional analysis would have predicted for the middle of the specimen.

Figure 32 shows a similar factor, but this time compares one-dimensional analysis stresses at the bottom of the specimen to the two-dimensional analysis stresses at the middle of the specimen. Again, the curves for height-to-diameter ratios of one, two, and three are shown, and appear to be almost identical. Note that a relatively constant ratio of 0.9 is achieved in both Figures 31 and 32 after dimensionless time equals two.

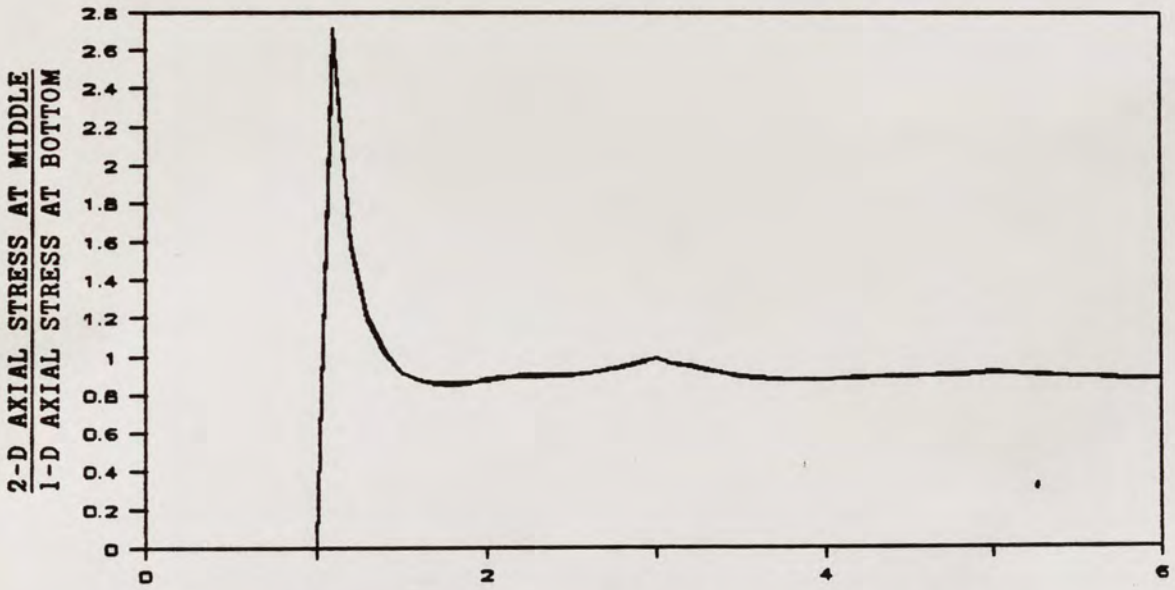

Figure 32. Ratio of Middle Axial Stress (2-D Analysis) to Bottom Axial Stress (1-D Analysis) for Constant Upper Pedestal Acceleration.

The very large conversion factor noted at dimensionless time equals one in Figure 32 occurs because the initial wavefront has already

passed the middle of the specimen, and large stresses exist there in comparison to those at the bottom. Note also that the conversion factor is undefined before dimensionless time equals one. Thus, stresses at the middle, although non-zero after dimensionless time is equal to 0.5, cannot be calculated until after dimensionless time equals one. For this reason, the conversion factor of Figure 31 appears to be the better of the two considered, since stress at the middle can be calculated at all time intervals.

Mesh Size

One important consideration in the two-dimensional analysis is the number of radial increments needed for reasonable output. The code is written for a mesh which has equal length increments in the axial and radial directions. Therefore, in a given specimen, increasing the number of radial increments will automatically increase the axial increments as well as time increments associated with the test. Thus, the computer time required for a solution increases rapidly as the mesh is made finer. It is desirable, therefore, to find the number of radial increments needed to obtain a good solution to the problem, yet not require an unreasonable amount of computer time.

It was found that the code gives very good results for average axial stress at the middle of the specimen versus time, even with as few as only six or eight radial increments in the specimen. However, when calculating radial or shear stresses versus radial position, reasonable results are not obtained with any fewer than about twelve radial increments. The minimum number of radial increments needed for

satisfactory results does not appear to be affected by the height-to-diameter ratio of the specimen.

Figures 33 and 34 show how a given distribution of radial or shear stress is approached as the number of radial increments is increased. The curves are for stresses computed using four, eight, twelve, and sixteen radial increments. Note that the curves generated using twelve and sixteen radial increments are almost identical. Also note also that the boundary conditions are also more closely approximated with more radial increments.

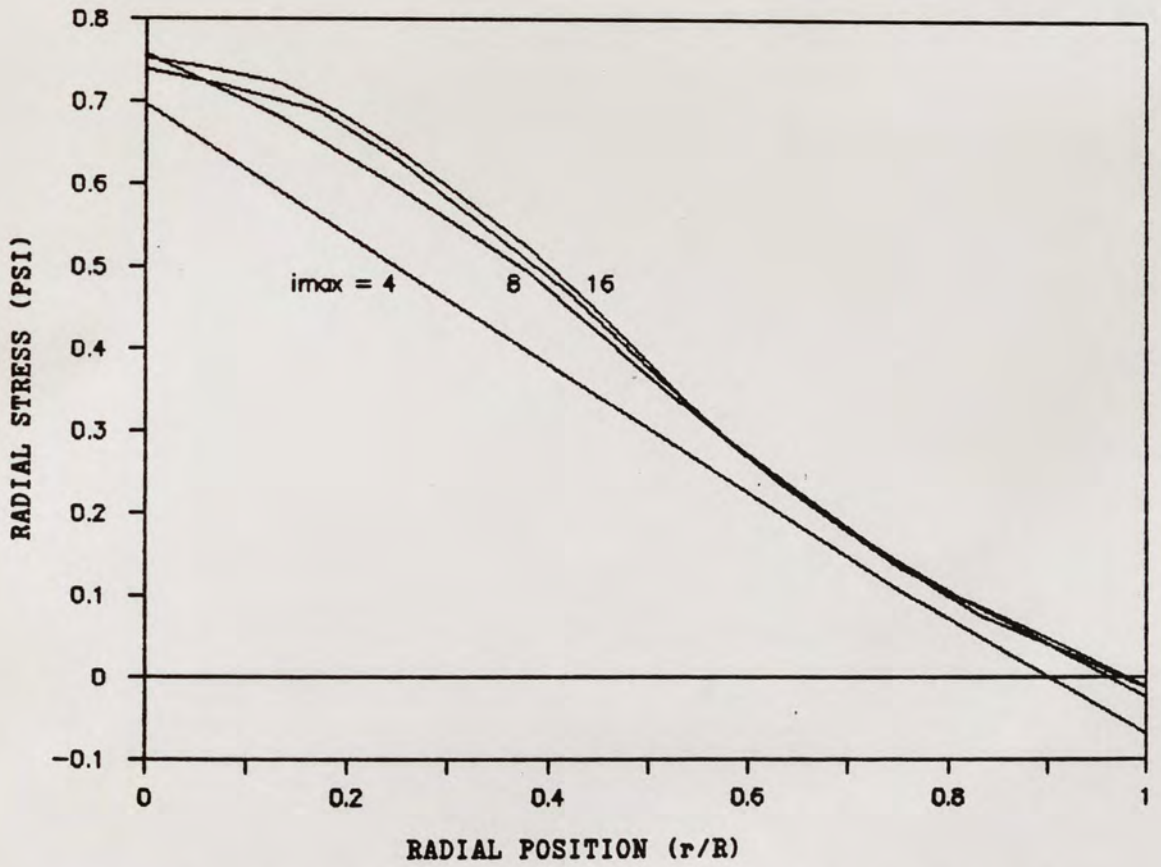

Figure 33. Radial Stress Distribution at Middle of Specimen, Constant Upper Pedestal Acceleration, Varying Mesh Size.

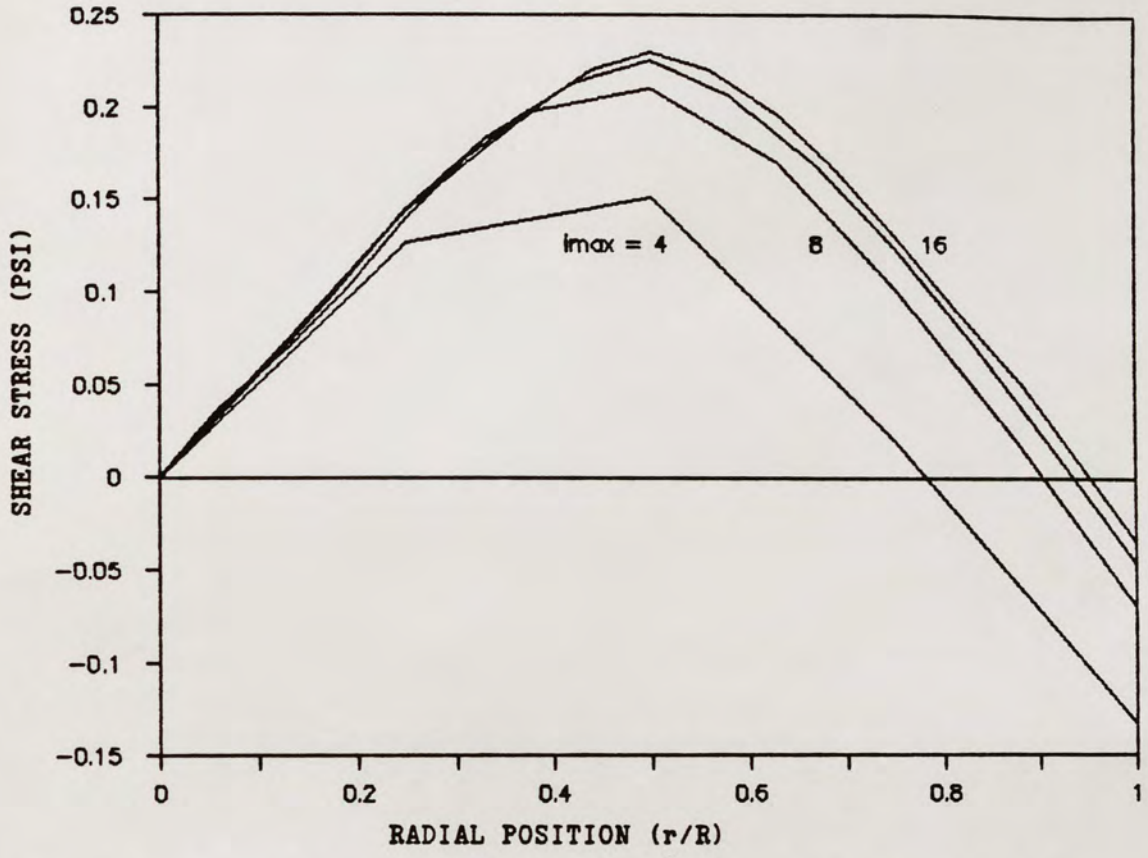

Figure 34. Shear Stress Distribution at Middle of Specimen, Constant Upper Pedestal Acceleration, Varying Mesh Size.

Although only six or eight radial increments are needed when finding axial stress versus time at the middle of the specimen, more are needed when calculating the average axial stress at the top or bottom in the specimens which are assumed to be fully laterally restrained. This is due to the fact that the stresses vary widely with radial position at these points, as discussed earlier (Figure 14), and a good approximation of the radial variation is not obtained without a sufficient number of radial increments. A good approximation of the average axial stress is obtained when, once again, at least twelve radial increments are used.

Another consideration is the variation in the differences observed between the one-dimensional and two-dimensional analyses as the mesh size is changed. Figures 35, 36, and 37 plot the percent difference between the two analyses at the top, middle, and bottom of a specimen as a function of dimensionless time. The curves are for specimens with a height-to-diameter ratio of two, and divided into twelve, twenty-four, and forty-eight axial increments. Thus, for the two-dimensional analysis, the curves correspond to specimens having six, twelve, and twenty-four radial increments, respectively.

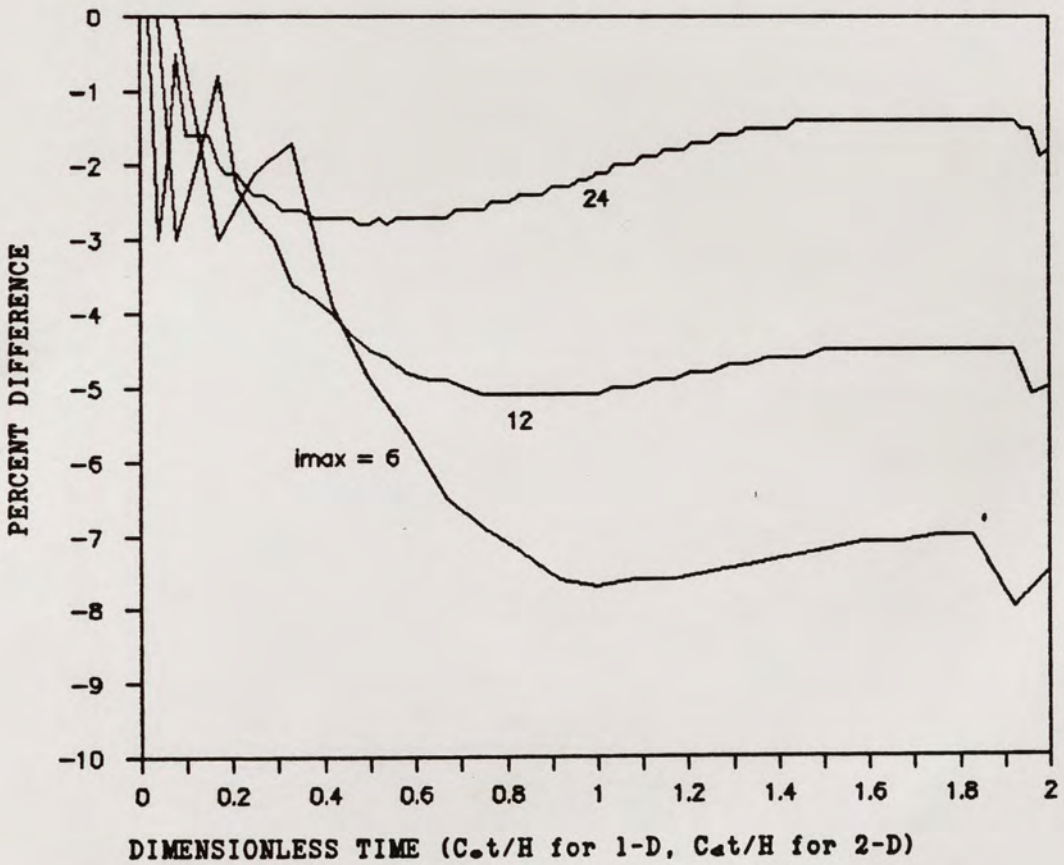

Figure 35. 1-D, 2-D Axial Stress Percent Difference at Top of Specimen, Constant Upper Pedestal Acceleration, Varying Mesh Size.

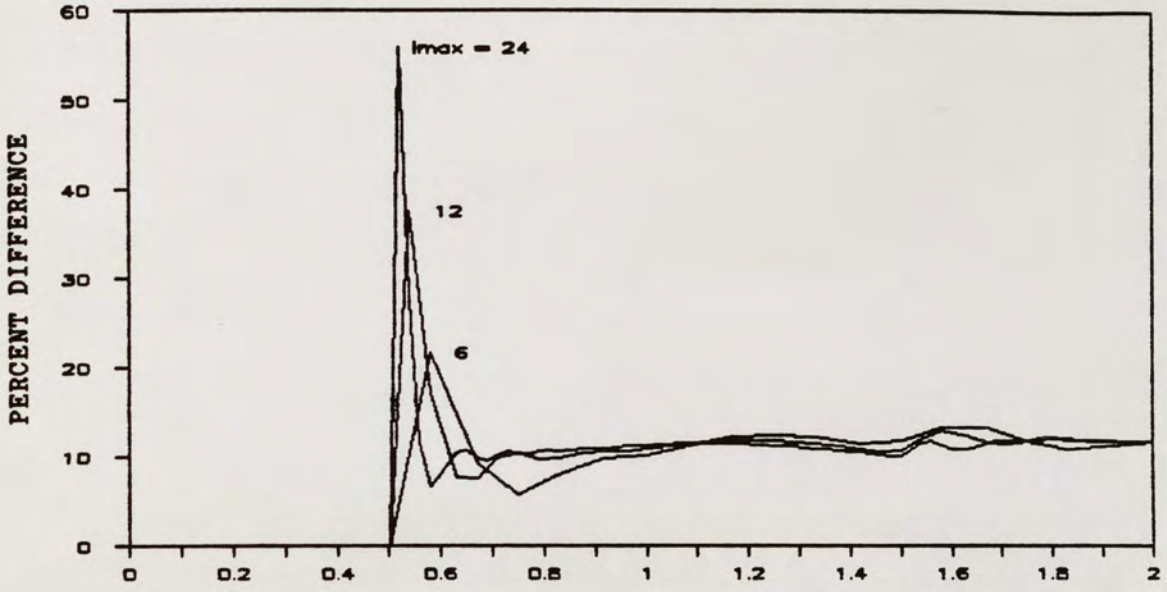

Figure 36. 1-D, 2-D Axial Stress Percent Difference at Middle of Specimen, Constant Upper Pedestal Acceleration, Varying Mesh Size.

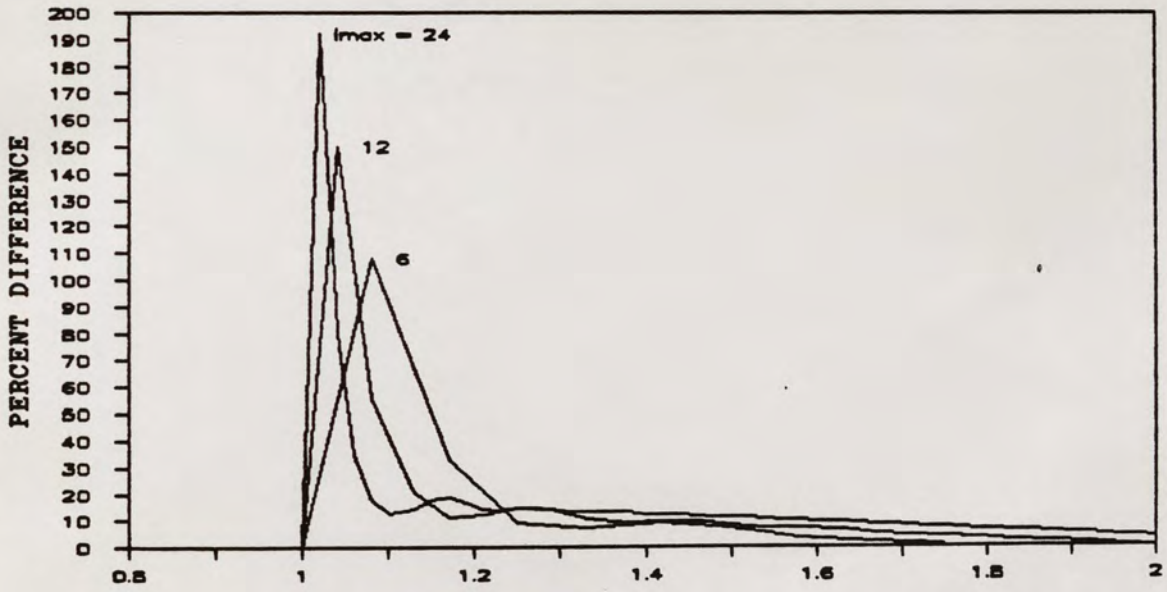

Figure 37. 1-D, 2-D Axial Stress Percent Difference at Bottom of Specimen, Constant Upper Pedestal Acceleration, Varying Mesh Size.

Note the similarities with Figure 30 in terms of the general shape of the curves at each point in the specimen. Figures 36 and 37 show that, at most time intervals, there is only a slight change in the differences between the one-dimensional and two-dimensional analyses as a result of changing the mesh size. The most notable change appears at times just after the initial wavefront arrives.

The finer mesh gives a larger difference immediately after the arrival of the first wavefront, but more quickly approaches a limiting difference than the coarser mesh. The higher peaks in the finer mesh curves occur because the difference between the two analyses is being calculated at an earlier value for dimensionless time than with the coarser mesh. As noted previously, the dispersion of the wave in the two-dimensional analysis can cause large differences between the one-dimensional and two-dimensional analysis results, especially just after the initial wavefront arrives.

Changing the mesh size appears to have a larger effect on the differences observed at the top of the specimen, as shown in Figure 35. For the most part, this is due to the scale of the vertical axis of Figure 35 in comparison to those of Figures 36 and 37. The changes that occur in Figure 35 as mesh size varies appear to be due to the averaging technique used to find the axial stress at the top. Recall Figure 14, which shows large axial stresses predicted at the top and bottom outer edge of the specimen. As the number of radial increments is increased, the radial distribution of axial stress becomes flatter, minimizing the effects of the peak at the outer edge. Hence, the average axial stress predicted at the top of the specimen gets smaller

as the number of radial increments increases, thereby reducing the differences between the one- and two-dimensional anlyses.

Thus, the mesh size appears not to have a large effect on the differences noted between the one-dimensional and two-dimensional analyses. Small variations with mesh size are observed at the top and bottom, but this appears to be due to the averaging technique used to calculate the axial stresses in the two-dimensional analysis. The mesh size is also important when determining the radial variation of a given quantity, and in accurately satisfying various boundary conditions.

Height-to-Diameter Ratio

Realistically, in testing the specimens, the height-to-diameter ratio could be increased in two different ways; the height can be kept constant while decreasing the diameter, or the diameter can be kept constant while increasing the height. Each case has been considered and was found to have the same effect on the differences between the one-dimensional and two-dimensional analyses.

The effects of increasing the height-to-diameter ratio were essentially the same for the case of constant upper pedestal acceleration and for hyperbolic upper pedestal velocity. Therefore, though the following discussion considers only constant upper pedestal acceleration, the results are applicable to both loading conditions.

Figures 38, 39, and 40 show the effects of changing the height-to-diameter ratio of the specimen. The differences between the one-dimensional and two-dimensional analyses are plotted as a function of dimensionless time at the top, middle, and bottom of the specimen.

Height-to-diameter ratios of one, two, and three have been considered. Longer specimens would be unreasonable for triaxial testing due to buckling considerations, while in shorter specimens, end condition effects would dominate throughout the specimen.

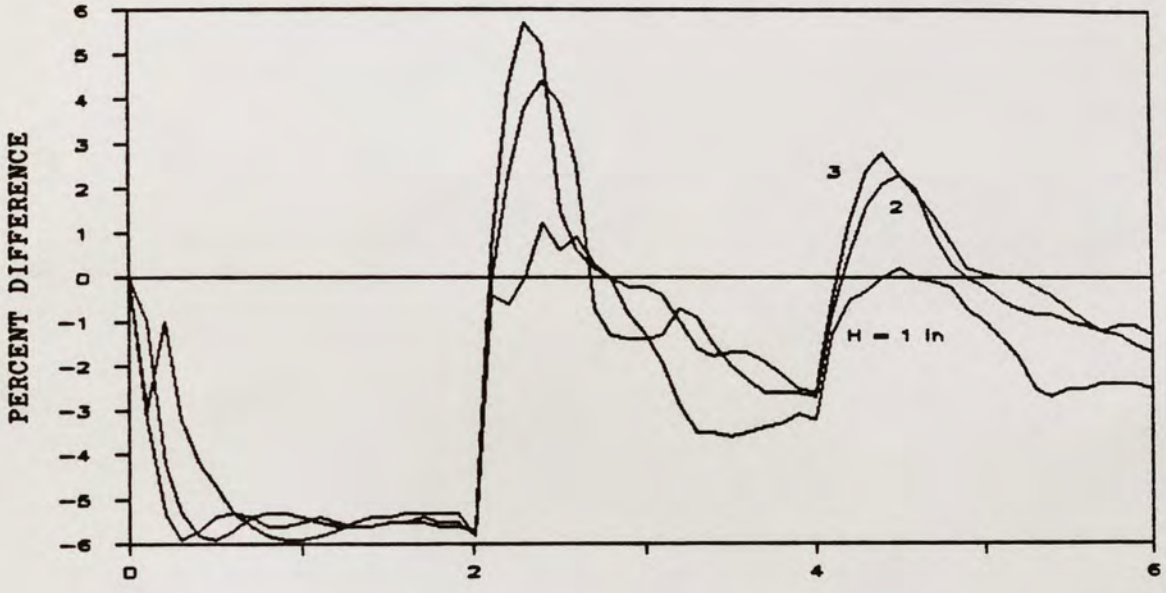

Figure 38. 1-D, 2-D Axial Stress Percent Difference at Top of Specimen, Constant Upper Pedestal Acceleration, Varying Height of Specimen.

Figures 38, 39, and 40 indicate that at all points in the specimen, increasing the height-to-diameter ratio causes an increase in the differences between the one-dimensional and two-dimensional wave analyses. This is due to the fact that as height-to-diameter ratio increases, more dispersion of the wave in the two-dimensional analysis will have occurred for a given value of dimensionless time.

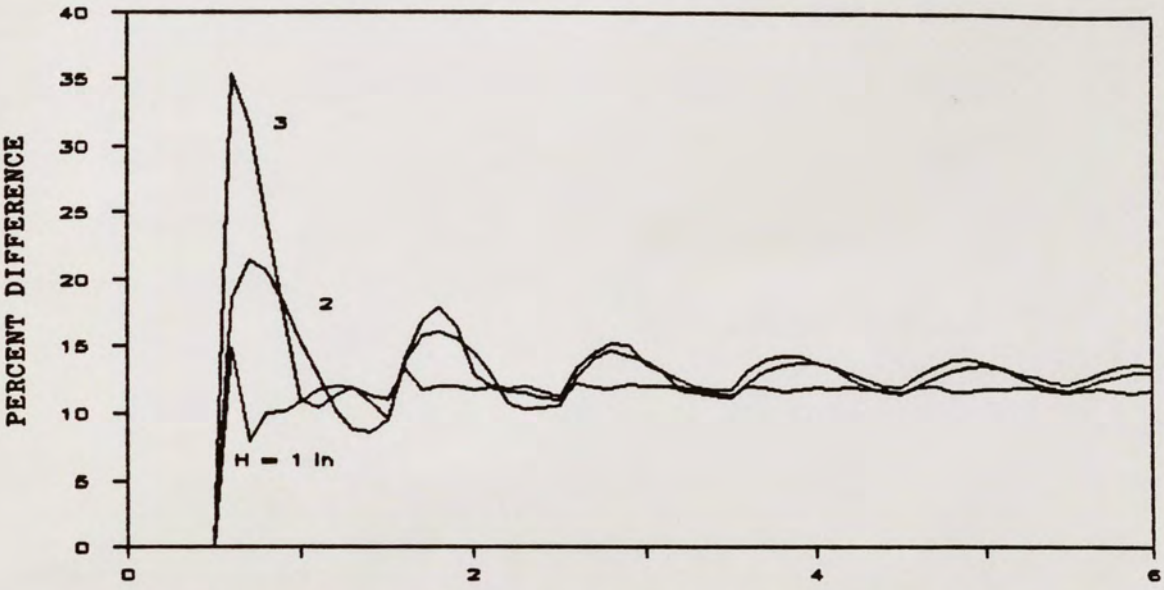

Figure 39. 1-D, 2-D Axial Stress Percent Difference at Middle of Specimen, Constant Upper Pedestal Acceleration, Varying Height of Specimen.

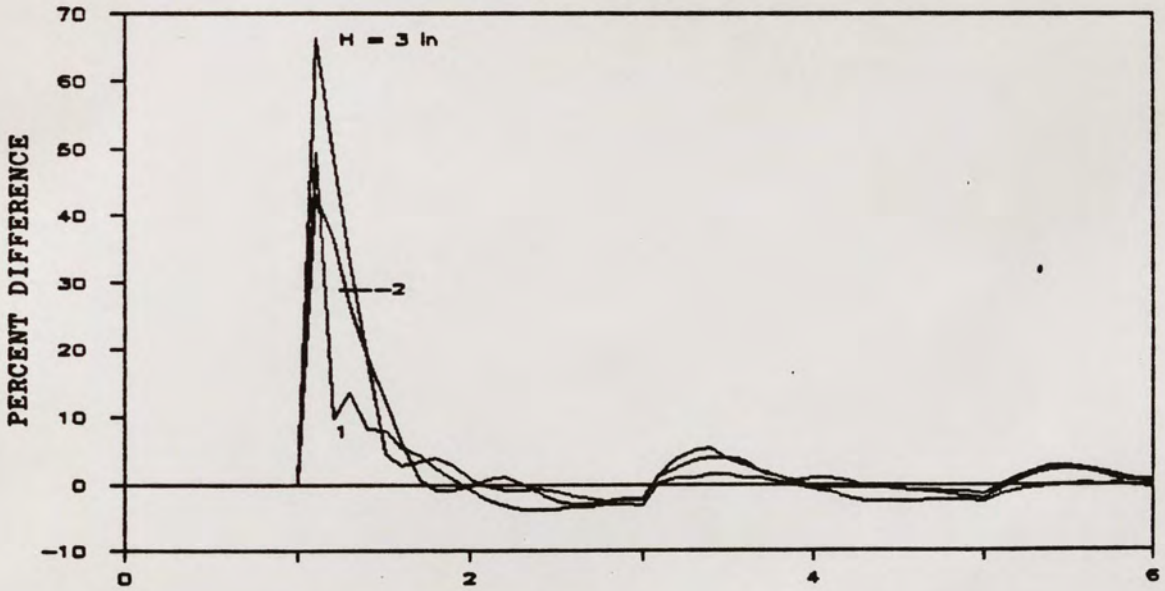

Figure 40. 1-D, 2-D Axial Stress Percent Difference at Bottom of Specimen, Constant Upper Pedestal Acceleration, Varying Height of Specimen.

Again, the only significant changes occur in the first few wave passes; as time goes on, each of the height-to-diameter ratios produces equivalent differences between the one- and two-dimensional analyses at a given point in the specimen. Even in the first few wave passes, the variations caused by changing the height-to-diameter ratio are not all that significant for the range of height-to-diameter ratios considered.

Poisson's Ratio

The only factor of any real consequence in affecting the differences noted between the one-dimensional and two-dimensional analyses appears to be Poisson's ratio. The one-dimensional analysis does not account for any radial variation of displacements or stresses; all radial displacements are assumed to be zero. This corresponds exactly to the two-dimensional case with Poisson's ratio equal to zero.

Thus, two-dimensional analysis results should approach those of the one-dimensional analysis as Poisson's ratio approaches zero. This was already shown to be the case for the radial distribution of axial, radial, and shear stresses. Refer to Figures 9, 10, and 11. Note also in Figure 41 how the plot of axial stress versus dimensionless time approaches the one-dimensional analysis as Poisson's ratio decreases.

As noted earlier, a relatively constant percent difference between the two-analyses is achieved at a given point in the specimen after several wave passes through the specimen. The only factor significantly affecting this difference over long time intervals is Poisson's ratio. Refer to Figure 42, which shows how the difference at a given point is affected by Poisson's ratio.

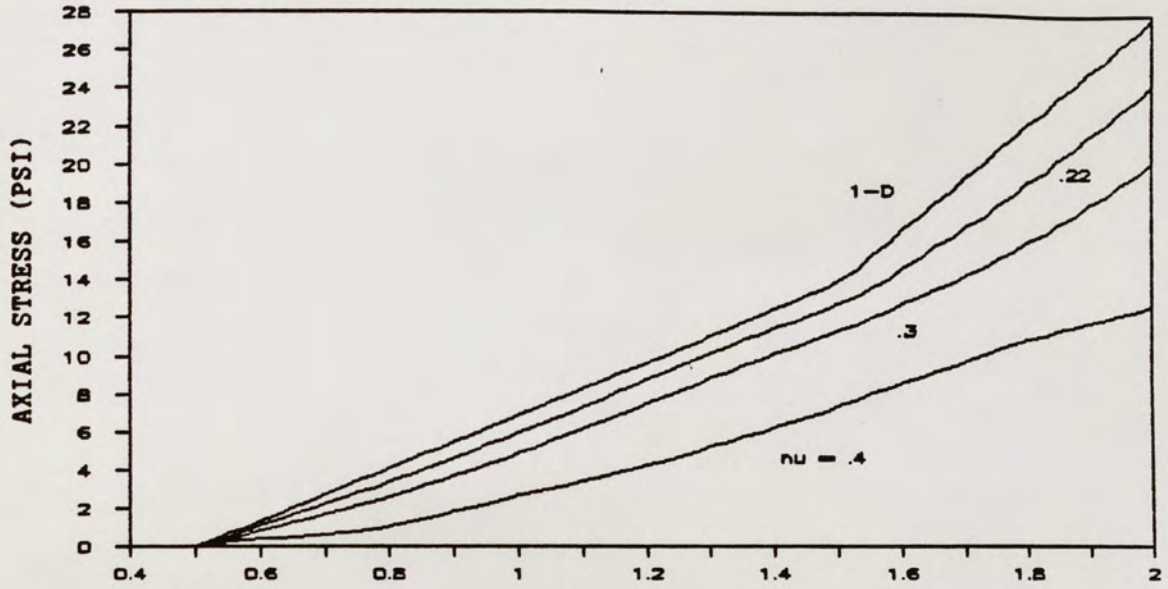

Figure 41. Axial Stress at Middle of Specimen, Constant Upper Pedestal Acceleration, Varying Poisson's Ratio.

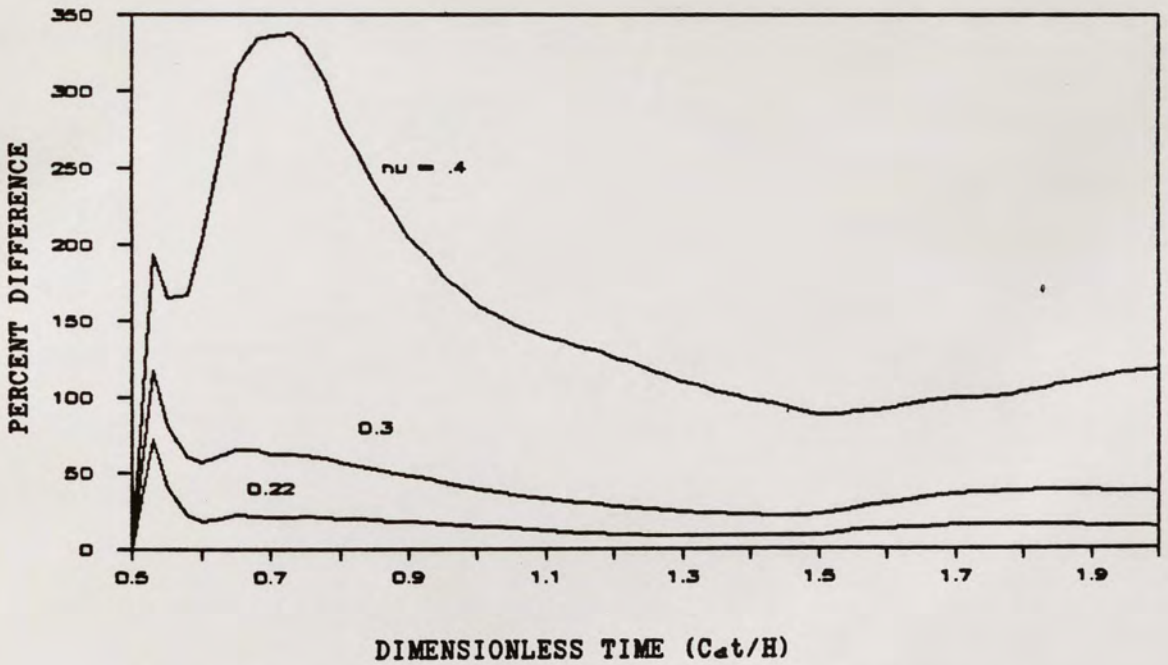

Figure 42. 1-D, 2-D Axial Stress Percent Difference at Middle of Specimen, Constant Upper Pedestal Acceleration, Varying Poisson's Ratio.

As Poisson's ratio increases, a significant contributor to the large differences between the two analyses is the differences in the time scales for the one-dimensional and two-dimensional analyses. Recall that the comparisons are made based on dimensionless time, TD, and that in the one-dimensional analysis,

$$TD = C_o t/H$$

while in the two-dimensional analysis,

$$TD = C_d t/H$$

As Poisson's ratio varies, C_d can become very different from C_o (refer to Table 3). Thus, although the comparisons are made at the same value of dimensionless time, they are made at potentially very different values of real time.

One way of accounting for this would be to divide the dimensionless times of the two-dimensional analyses by the ratio C_d/C_o, thus converting their time scales into dimensionless time based on C_o rather than C_d. Dividing the time scales directly, however, leads to the unreasonable result of non-zero stresses at the middle of the specimen before dimensionless time = 0.5. Therefore, there must a translation of the time scales before the conversion factor is applied. By making time = 0 when the initial wavefront arrives at the middle of the specimen, reasonable results are achieved. Hence, a revised dimensionless time TD' for the two-dimensional analyses is obtained from the equation,

$$TD' = (TD - .5)/(C_d/C_o)$$

By applying this change in time scales to the curves of Figure 41, Figure 43 is generated.

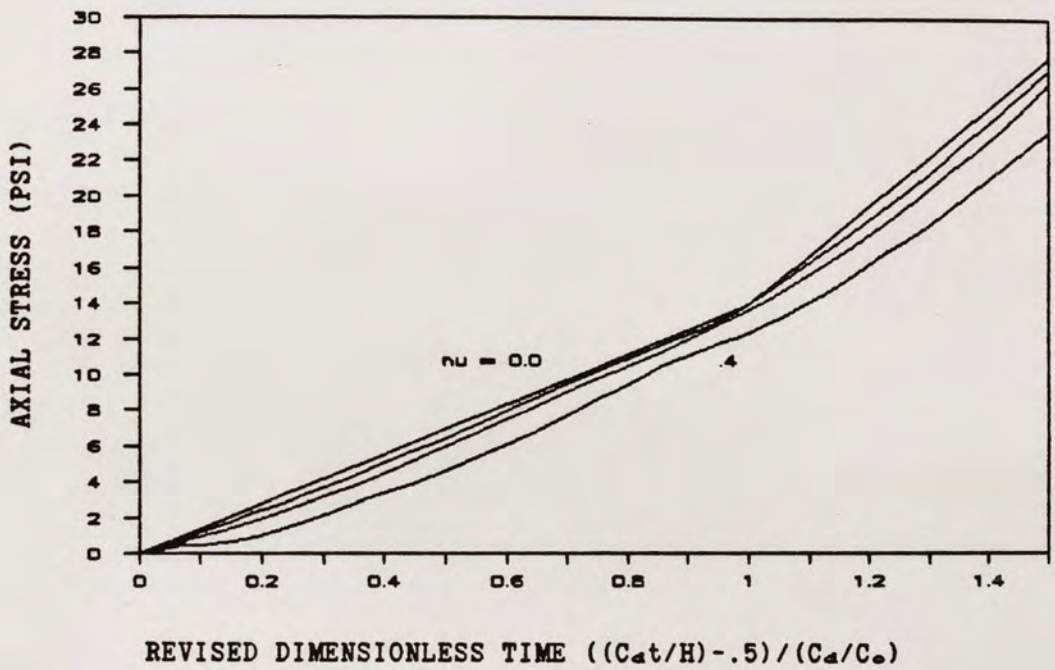

Figure 43. Axial Stress at Middle of Specimen, Constant Upper Pedestal Acceleration, Varying Poisson's Ratio, with Revised Time Scale.

Note that curves of Figure 43 with the revised time scale approximate each other much more closely than those of Figure 41 with the original dimensionless time scale. Thus, applying the correction factor to the time scale serves to minimize the differences between the one-dimensional and two-dimensional analyses, but does not completely erradicate them.

In summary, Poisson's ratio appears to be the one factor of those considered which has a significant effect on the differences noted

between the one-dimensional and two-dimensional wave analyses. Poisson's ratio should have the greatest effect since it determines the amount of lateral deformation the specimen will undergo during the test. As the lateral deformations increase, the two analyses' predictions become more different. The differences can be made smaller by comparing the stresses of the two analyses on a revised dimensionless time scale in which the differences between C_d and C_o are minimized.

CHAPTER 8

CONCLUSIONS AND RECOMMENDATIONS

For the most part, the factors considered as possibly influencing differences between the one-dimensional and two-dimensional wave analyses of the FTRXD have only small bearing on the outcomes. Both analyses predict very similar axial stresses, no matter the type of loading assumed, the mesh size for the finite difference algorithm, or the height-to- diameter ratio of the specimen. Minor differences between the analyses are observed, but often each analysis yields stress-time curves of similar shape that are only five to ten percent different in magnitude at the top and bottom of the specimen, and often ten to fifteen percent different in magnitude at the middle of the specimen.

In all cases, the most significant differences appear in the first few passes of the wave through the specimen, especially at points immediately after the arrival of the initial wavefront. These differences can be attributed to the dimensionless time scale on which the stresses are compared. These differences would be significant only if the specimens could be brought to failure in the time required for five to ten passes of the wave through the specimen. Assuming constant upper pedestal acceleration in a 1.5 inch specimen, with failure occurring at fifteen percent gross strain after six wave passes through the specimen, requires an acceleration of approximately 1200 g's for the

upper pedestal. Such loading rates have not been achieved in the FTRXD, but may be possible with modifications to the device.

Concerning the type of loading, significant differences between the analyses were observed only with the step velocity of the upper pedestal or the hyperbolic velocity with very short t_c, such that it approaches the step velocity. In such cases, the differences are, in part, due to radial wave effects and, in part, due to the inability of the two-dimensional finite difference algorithm to accurately account for the presence of a sharply defined wavefront. In reality, this type of loading cannot presently be achieved in the very fast tests, and thus these differences between the two analyses are of little concern.

When assuming the hyperbolic upper pedestal velocity, it is important to ensure that the time interval of the finite difference mesh, dt, is smaller than the characteristic time, t_c, of the upper pedestal. If not, either the one-dimensional or two-dimensional wave analysis yields inaccurate stress-time data, with unusual oscillations.

The mesh size used in the two-dimensional analysis is of little concern in calculating axial stresses at the middle of the specimen. As few as six or eight radial increments yield accurate average axial stresses at the middle. However, at least twelve radial increments should be used in order to obtain accurate radial distributions of stresses and to accurately satisfy radial boundary conditions.

The height-to-diameter ratio appears to have only a small effect on the differences observed between the wave analyses. Increasing the height-to-diameter ratio amplifies the differences in the analyses, but not significantly. Significant differences might appear in specimens

with height-to-diameter ratios larger than three, but as noted earlier, these specimens would present buckling problems in the triaxial testing.

One factor that strongly affects the outcome of the comparison between the one-dimensional and two-dimensional wave analyses is Poisson's ratio. In fact, it appears to be the one factor which determines the differences between the two wave analyses at a given point after several passes of the wave through the specimen. However, much of the differences noted between the two analyses can be attributed to the time scales on which the stresses are compared. Although dimensionless time is a convenient factor on which to base the comparisons, it can be somewhat misleading since it does not directly account for the difference between the governing wave velocities, namely, C_d and C_o. One method of comparison which minimizes the differences observed with changing Poisson's ratio is to use a revised dimensionless time scale instead of a strict dimensionless time scale. The merits of the revised time scale are not fully apparent at this time and may warrant further investigation.

A final, but very important, factor to consider is the computer time necessary for each analysis. A one-dimensional analysis usually requires only seconds to complete, whereas a two-dimensional anlysis can take several minutes. The storage requirements for the two-dimensional analysis are also significantly greater than for the one-dimensional analysis.

Thus, the two-dimensional analysis presented gives insights into the range of validity for the one-dimensional analysis, at least for the linear elastic behavior considered. It appears that the one-dimensional

analysis gives very good results, for the most part, for the present specimen geometry and loading conditions in the laboratory. Future modifications of the FTRXD may allow for faster loading rates or the use of larger specimens and different height-to-diameter ratios. With such modifications, significant variations may be noted between the one-dimensional and two-dimensional analyses.

Furthermore, the present insights into the two-dimensional wave analysis concern only the linear elastic behavior of the specimen. Since the FTRXD deals with shear strength, the entire stress-strain curve incorporating linear and non-linear behavior needs to be considered. Thus, an understanding of the non-linear behavior associated with a two-dimensional wave analysis is needed before definitive statements can be made regarding the validity of the one-dimensional versus the two-dimensional analysis.

APPENDIX A

BLOCK DIAGRAMS FOR PROGRAMS 'WAVES' AND 'COMPARE'

PROGRAM 'WAVES'

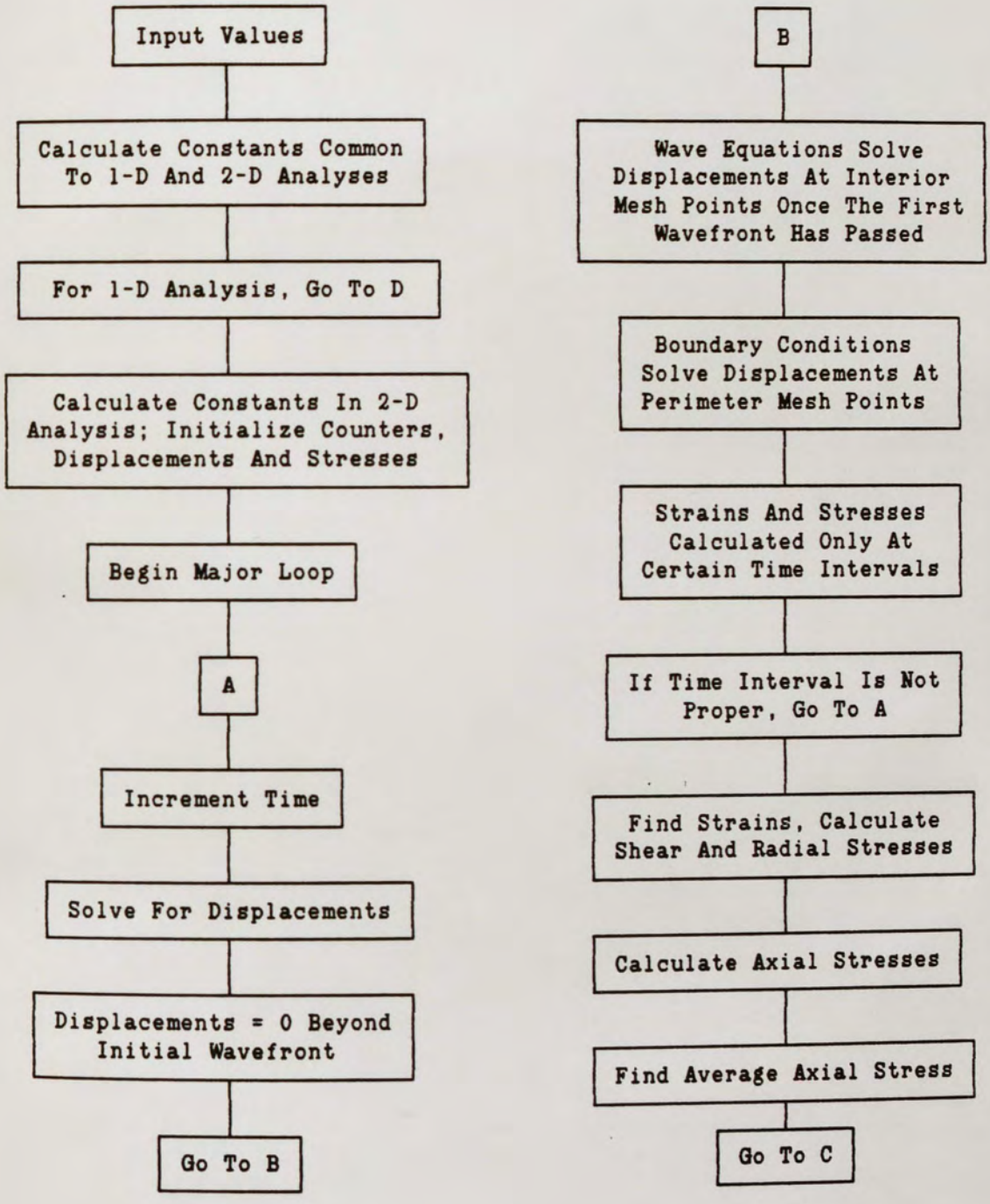

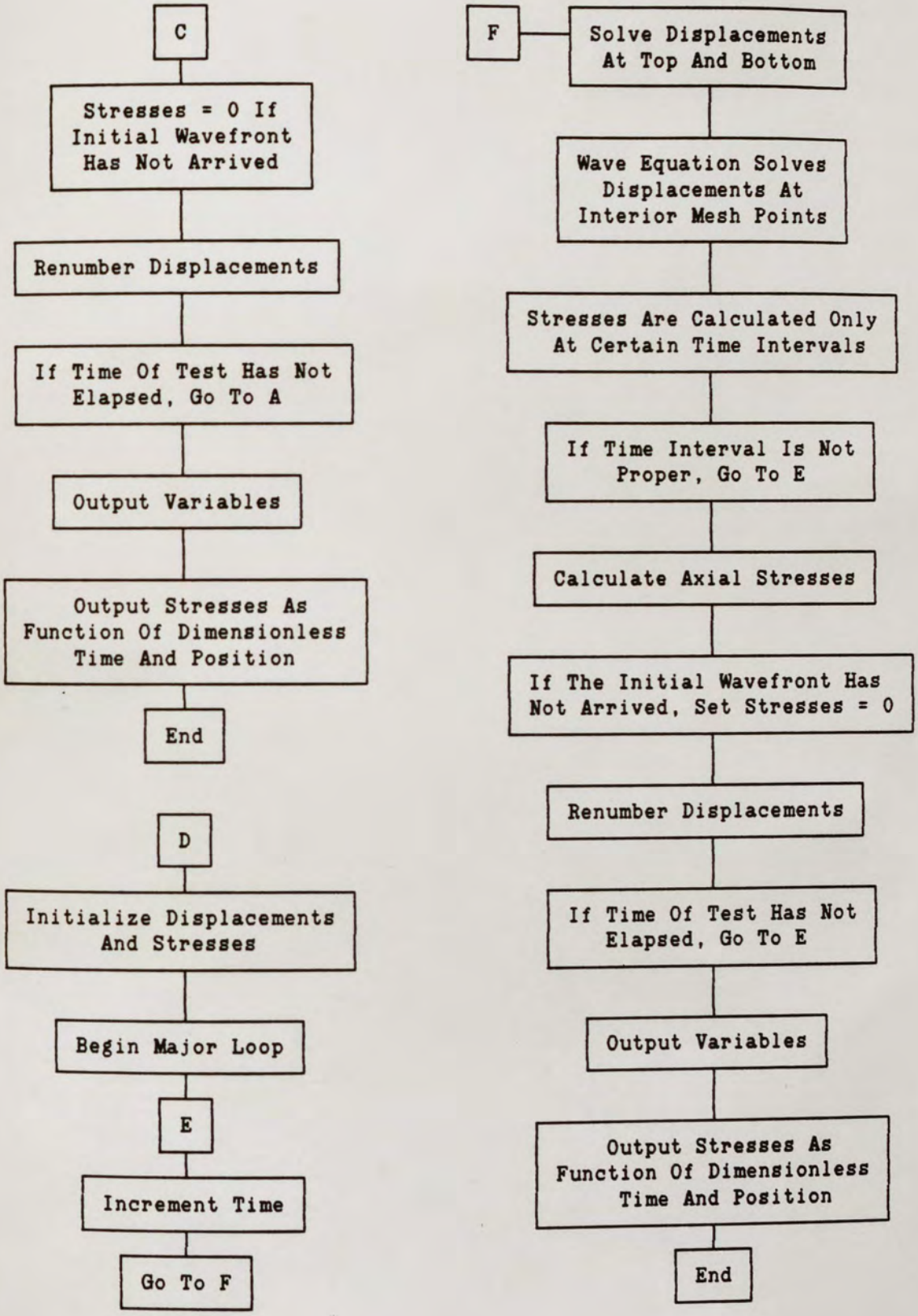
C
Stresses = 0 If Initial Wavefront Has Not Arrived
Renumber Displacements
If Time Of Test Has Not Elapsed, Go To A
Output Variables
Output Stresses As Function Of Dimensionless Time And Position
End
D
Initialize Displacements And Stresses
Begin Major Loop
E
Increment Time
Go To F
F
Solve Displacements At Top And Bottom
Wave Equation Solves Displacements At Interior Mesh Points
Stresses Are Calculated Only At Certain Time Intervals
If Time Interval Is Not Proper, Go To E
Calculate Axial Stresses
If The Initial Wavefront Has Not Arrived, Set Stresses = 0
Renumber Displacements
If Time Of Test Has Not Elapsed, Go To E
Output Variables
Output Stresses As Function Of Dimensionless Time And Position
End

PROGRAM 'COMPARE'

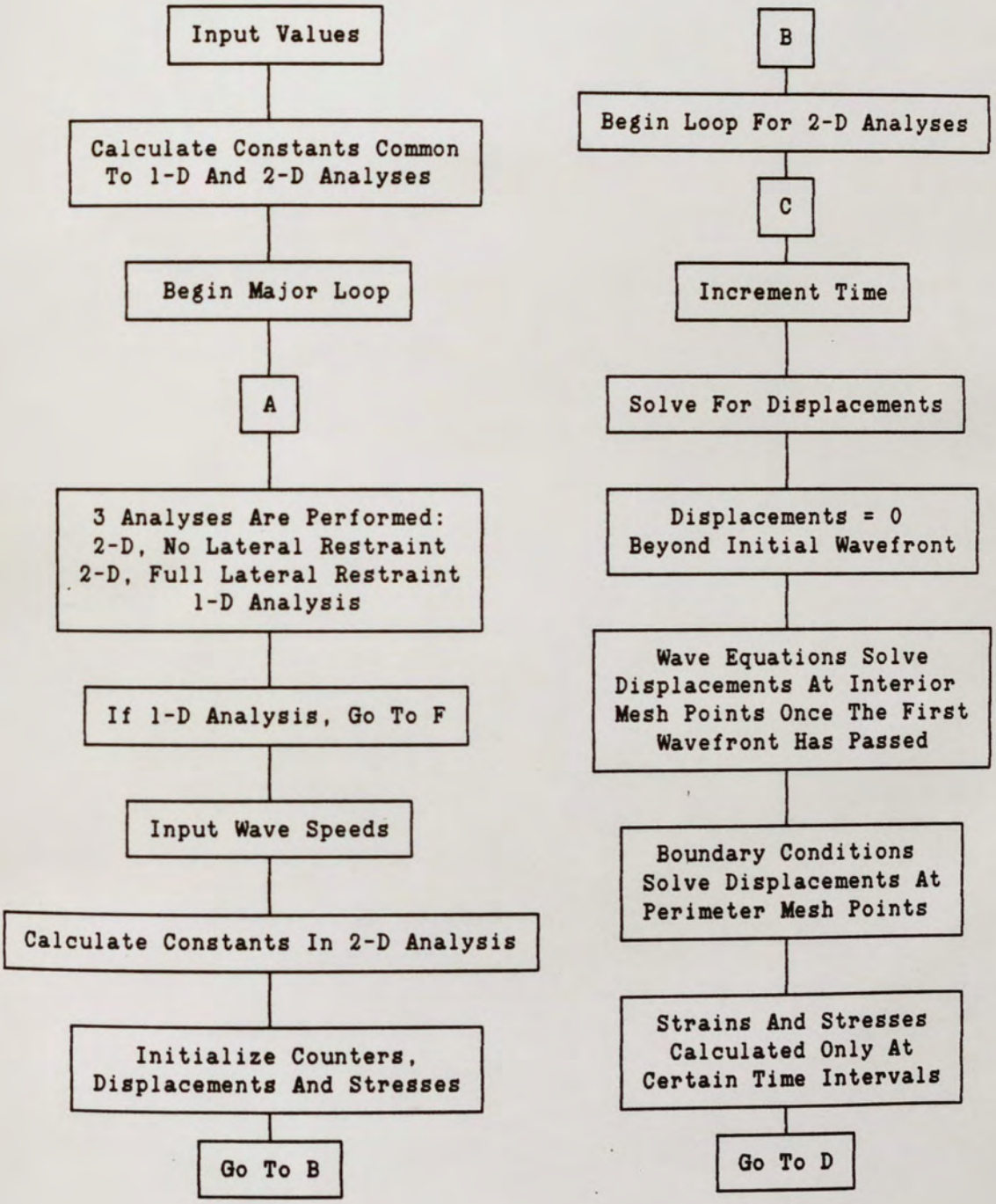

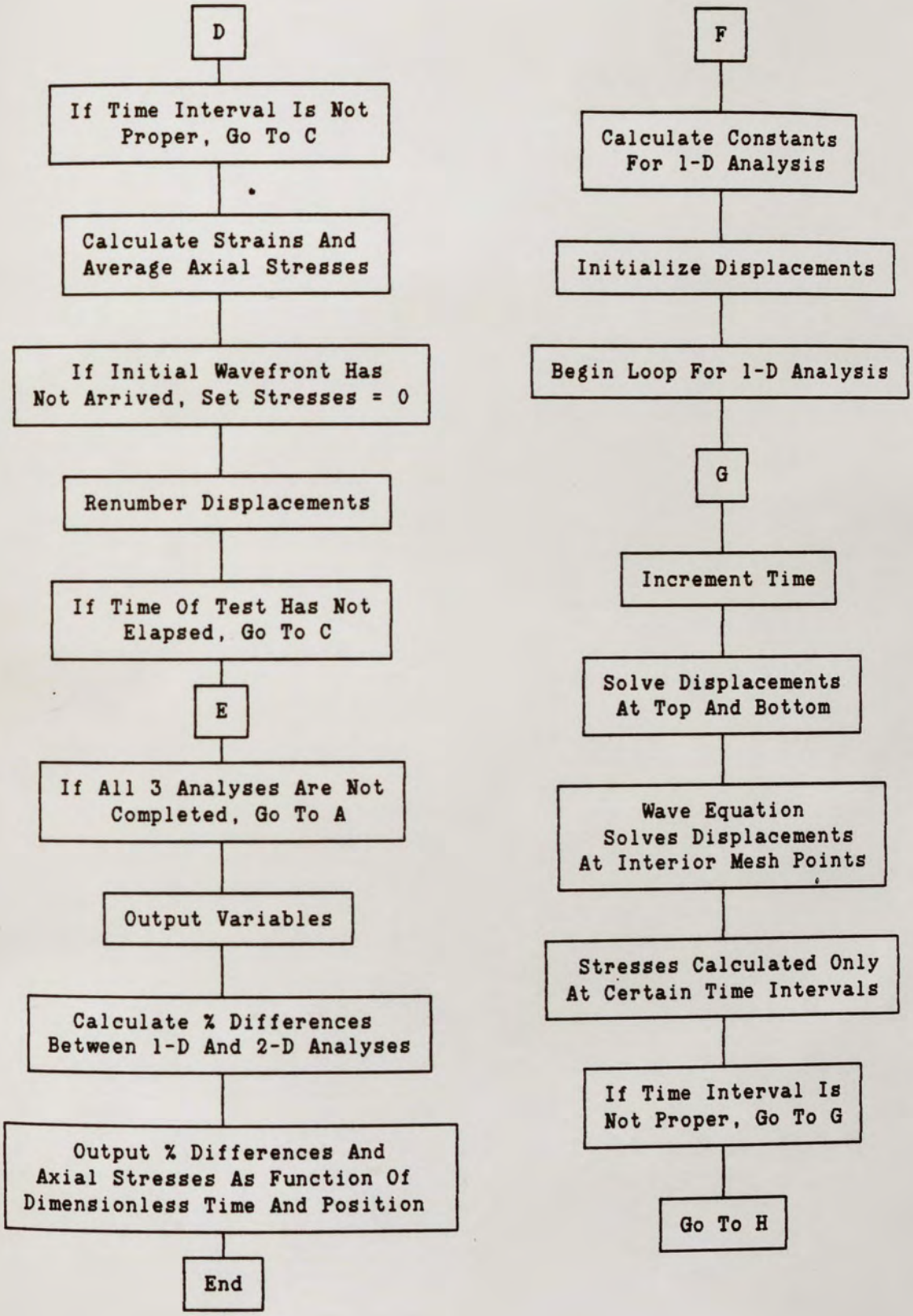
D
If Time Interval Is Not Proper, Go To C
Calculate Strains And Average Axial Stresses
If Initial Wavefront Has Not Arrived, Set Stresses = 0
Renumber Displacements
If Time Of Test Has Not Elapsed, Go To C
E
If All 3 Analyses Are Not Completed, Go To A
Output Variables
Calculate % Differences Between 1-D And 2-D Analyses
Output % Differences And Axial Stresses As Function Of Dimensionless Time And Position
End
F
Calculate Constants For 1-D Analysis
Initialize Displacements
Begin Loop For 1-D Analysis
G
Increment Time
Solve Displacements At Top And Bottom
Wave Equation Solves Displacements At Interior Mesh Points
Stresses Calculated Only At Certain Time Intervals
If Time Interval Is Not Proper, Go To G
Go To H

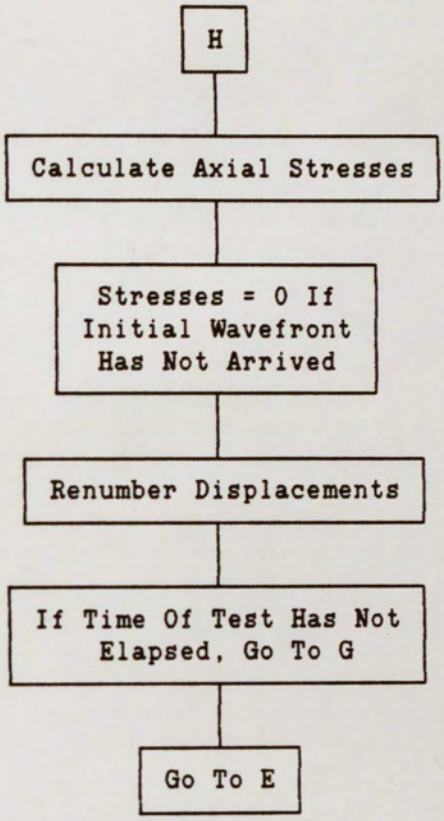
H
Calculate Axial Stresses
Stresses = 0 If Initial Wavefront Has Not Arrived
Renumber Displacements
If Time Of Test Has Not Elapsed, Go To G
Go To E

APPENDIX B

CODE FOR PROGRAMS 'WAVES' AND 'COMPARE'

PROGRAM 'WAVES'

```
$LARGE
      PROGRAM WAVES
c
c This program solves for stresses resulting from axisymmetric wave
c propagation in an elastic cylinder.  Constant or hyperbolic velocity
c or constant acceleration can be assumed for the upper pedestal.  The
c solution uses finite difference approximations, and allows a one or
c two dimensional analysis to be performed.  In the one dimensional
c case, the finite difference mesh is such that it takes one time
c increment for a wave to travel the length of one axial increment. In
c the two dimensional case, the mesh is such that radial and axial
c increments are of equal length and time increments are equal to an
c axial increment divided by twice the dilatational wave velocity.
c
c The variables used include:
c
c    H - specimen height
c  HDR - height to diameter ratio
c    G - wet unit weight of specimen
c  MUP - specifies motion of upper pedestal
c  NRS - specifies restraint of specimen
c  NDW - specifies 1-D or 2-D wave analysis
c  NST - specifies stresses to be calculated
c  NWP - maximum number of passes of wavefront through specimen
c IMAX - number of radial increments in specimen
c JMAX - number of axial increments in specimen
c KMAX - number of time increments in test
c TMAX - maximum dimensionless time in test
c   TD - dimensionless time
c    T - time
c   TO - characteristic time for hyperbolic upper pedestal velocity
c    V - constant velocity of upper pedestal
c   VO - limiting hyperbolic upper pedestal velocity
c    A - constant acceleration of upper pedestal
c   AO - initial acceleration of upper pedestal
c   C1 - dilatational wave velocity for 2-D analysis
c      - rod wave velocity for 1-D analyis
c   C2 - shear wave velocity
c  C1S - dilatational (or rod) wave velocity squared
c  C2S - shear wave velocity squared
c    B - C2S/C1S
c   NT - number of time increments between data output
c   DZ - length of one axial increment
```

```
c   DT - length of one time increment
c   DI - dimensionless radius
c    U - radial displacement
c    W - axial displacement
c   E1 - radial strain
c   E2 - tangential strain
c   E3 - axial strain
c   E4 - component of shear strain
c   E5 - component of shear strain
c   S1 - radial stress
c   S2 - axial stress
c  S2T - axial stress as a function of time
c   S3 - shear stress
c
      IMPLICIT DOUBLE PRECISION (A-H,O-Z)
      REAL*8 U(31,61,3), W(31,61,3), E1(31,3), E2(31,3), E3(31,3),
     :   E4(31,3), E5(31,3), S1(31,3,4), S2(31,3), S2T(4,3,1201),
     :   S3(31,3,4)
      OPEN(9,FILE='WV4.OUT',STATUS='NEW')
      WRITE(*,25)
25    FORMAT(/1X,'ENTER:  type of wave analysis to be performed:'/
     :9X,'1 for 1-D wave analysis'/9X,'2 for 2-D wave analysis'/)
      READ(*,*) NDW
      WRITE(*,50)
50    FORMAT(/1X,'ENTER:  wet unit weight of specimen (pcf)'/)
      READ(*,*) G
      WRITE(*,75)
75    FORMAT(/1X,'ENTER:  specimen height (inches)'/)
      READ(*,*) H
      IF (NDW .EQ. 1) THEN
        WRITE(*,100)
100     FORMAT(/1X,'ENTER:  rod wave velocity (ft/sec)'/)
        READ(*,*) C1
        WRITE(*,105)
105     FORMAT(/1X,'ENTER:  the number of axial increments'/
     :9X,'choose a multiple of 2 up to a maximum of 60'/)
        READ(*,*) JMAX
      ELSE
        WRITE(*,110)
110     FORMAT(/1X,'ENTER:  specimen height to diameter ratio'/
     :9X,'(choose from 1.0, 1.5, 2.0, 2.5, or 3.0)'/)
        READ(*,*) HDR
120     WRITE(*,125)
125     FORMAT(//1X,'ENTER:  dilatational wave velocity (ft/sec)'/
     :9X,'shear wave velocity (ft/sec)'//
     :9X,'(be sure the shear wave velocity is less than'/
     :9X,' .707 times the dilatational wave velocity)'/)
        READ(*,*) C1, C2
        IF (C2 .GT. .7071*C1) THEN
          WRITE(*,140)
140       FORMAT(/1X,'SHEAR WAVE VELOCITY TOO HIGH; TRY AGAIN'/)
```

```
          GOTO 120
        ENDIF
        WRITE(*,145)
145     FORMAT(/1X,'ENTER:  type of restraint of specimen:'/
     :9X,'1 for NO lateral restraint of specimen at top and bottom'/
     :9X,'2 for FULL lateral restraint of specimen at top and bottom'/)
        READ(*,*) NRS
        WRITE(*,150)
150     FORMAT(/1X,'ENTER:  types of stresses to be calculated:'/
     :9X,'1 for axial stresses only'/
     :9X,'2 for radial, axial, and shear stresses'//)
        READ(*,*) NST
c
c Ensure JMAX is consistent with HDR and desired output
c
        JM=IDINT(4*HDR)
        WRITE(*,175) JM
175     FORMAT(/1X,'ENTER:  number of axial increments'/
     :9X,'choose a multiple of', I3,' up to a maximum of 60'/)
        READ(*,*) JMAX
       ENDIF
       WRITE(*,200)
200    FORMAT(/1X,'ENTER:  type of upper pedestal motion:'/
     :9X,'1 for constant acceleration'/
     :9X,'2 for constant velocity'/
     :9X,'3 for hyperbolic velocity'/)
       READ(*,*) MUP
       IF (MUP .EQ. 1) THEN
         WRITE(*,225)
225      FORMAT(/1X,'ENTER:  acceleration of upper pedestal (in g''s)'/)
         READ(*,*) A
       ELSEIF (MUP .EQ. 2) THEN
         WRITE(*,250)
250      FORMAT(/1X,'ENTER:  velocity of upper pedestal (mils/msec)'/)
         READ(*,*) V
       ELSE
         WRITE(*,275)
275      FORMAT(/1X,'ENTER:  limiting velocity of upper pedestal (mils/ms
     :ec)'/9X,'and initial acceleration of upper pedestal (inches per se
     :cond squared)'/)
         READ(*,*) V0, A0
         T0= V0/A0
       ENDIF
       WRITE(*,300)
300    FORMAT(//1X,'ENTER:  maximum number of passes of wavefront '
     :'through specimen'/9X,'choose a multiple of 2 up to a maximum '
     :'of 20'/)
       READ(*,*) NWP
c
c Find max time increments for test.  KMAX1 is based on stopping test
c when 15% nominal strain is reached; KMAX2 is based on stopping test
```

```
c when the wavefront has travelled through the specimen a specified
c number of times.
c
      IF (MUP .EQ. 1) THEN
        KMAX1=IDINT(DSQRT(.1119/(A*H))*NDW*JMAX*C1)
      ELSEIF (MUP .EQ. 2) THEN
        KMAX1=IDINT(1.8*NDW*JMAX*C1/V)
      ELSE
        KMAX1=IDINT(1.8*NDW*JMAX*C1/V0)
      ENDIF
      KMAX2=NDW*NWP*JMAX
      KMAX=MIN(KMAX1,KMAX2)
      WRITE(*,325) KMAX
325   FORMAT(/1X,'ENTER:  number of time increments between data output'
     :/9X,'(1,2,3, etc.) up to a maximum of ', I4/)
      READ(*,*) NT
c
c Find axial (= radial, for 2-D analysis) and time increments lengths
c
      DZ=H/JMAX
      DT=DZ/(C1*NDW*12)
c
c Important constants for both 1-D and 2-D analyses
c
      C1S=C1**2
      L=0
      J1= JMAX/2
      J2= J1 + 1
      J3= J2 + 1
      J4= JMAX - 1
      J5= JMAX
      J6= JMAX + 1
c
c For one dimensional analysis, go to another portion of the code
c
      IF (NDW .EQ. 1) GOTO 2000
c
c
c  *** TWO DIMENSIONAL CODE ***
c
c
c Find number of radial increments and max dimensionless time
c
      IMAX=JMAX/(2*HDR)
      TMAX=.5*KMAX/JMAX
c
c Initializing variables and calculating constants
c
      DI1= 0.0
      DI2= 0.5
      DI3= 1.0
```

```
      C2S= C2**2
      B= C2S/C1S
      A1= (1-B)/16
      A2= 1.5 - B/2
      A3= B/4
      A4= 2*B - 1
      A5= 2*A1
      A6= 1./(3*IMAX**2)
      I1= 1
      I2= IMAX/2 + 1
      I3= IMAX + 1
      J7= 2*JMAX + 1
      KN= NWP/2*JMAX + 1
      K2= 0
c
c Set displacements = 0 along ficticious first two passes of finite
c difference algorithm
c
      DO 350 K=1,2
      DO 350 J=1,JMAX+1
      DO 350 I=1,IMAX+1
         U(I,J,K)=0.0
         W(I,J,K)=0.0
350   CONTINUE
c
c Set axial stresses = 0 at time t = 0
c
      DO 375 J=1,3
      DO 375 I=1,4
         S2T(I,J,1)=0.0
375   CONTINUE
c
c Begin major loop:  calculate displacements first, and then strains
c and stresses.  Finally, displacements are renumbered in preparation
c for the next calculation of displacements.
c
      DO 825 K=2,KMAX+1
      L=L+1
      M=0
      IF (K .LE. 2*JMAX) THEN
        KM=NINT((K+1.01)/2)
      ELSE
        KM=JMAX+1
      ENDIF
      DO 450 J=2,JMAX
c
c Displacements equal zero before initial wavefront arrives
c
        IF (J .GE. KM) THEN
          DO 400 I=1,IMAX+1
             U(I,J,3)=0.0
```

```
            W(I,J,3)=0.0
400         CONTINUE
c
c Wave equations solve displacements at interior mesh points
c
          ELSE
            DO 425 I=2,IMAX
               U(I,J,3)= -U(I,J,1) +.25*((1+1./(2*(I-1)))
     :           *U(I+1,J,2) + (1-1./(2*(I-1)))*U(I-1,J,2)) +
     :           A3*(U(I,J+1,2) + U(I,J-1,2)) + A1*(W(I+1,J+1,2)
     :           - W(I+1,J-1,2) - W(I-1,J+1,2) + W(I-1,J-1,2))
     :           + (1.5 - .25*(2*B + 1./(I-1)**2))*U(I,J,2)
               W(I,J,3)= -W(I,J,1) + .25*(W(I,J+1,2) + W(I,J-1,2)) +
     :           A2*W(I,J,2) + A3*(1+1./(2*(I-1)))*W(I+1,J,2) +
     :           A3*(1-1./(2*(I-1)))*W(I-1,J,2) + A5/(I-1)*
     :           (U(I,J+1,2) - U(I,J-1,2)) + A1*(U(I+1,J+1,2)
     :           - U(I+1,J-1,2) - U(I-1,J+1,2) + U(I-1,J-1,2))
425         CONTINUE
c
c Satisfy centerline boundary conditions
c
            U(1,J,3)= 0.0
            W(1,J,3)= (4*W(2,J,3) - W(3,J,3))/3
          ENDIF
450     CONTINUE
        T= DT*(K-1)
c
c Solve axial displacements at specimen top and bottom
c
        IF (MUP .EQ. 1) THEN
          DO 475 I=1,IMAX+1
             W(I,1,3)= 193.032*A*T**2
             W(I,J6,3)= 0.0
475       CONTINUE
        ELSEIF (MUP .EQ. 2) THEN
          DO 500 I=1,IMAX+1
             W(I,1,3)= V*T
             W(I,J6,3)= 0.0
500       CONTINUE
        ELSE
          DO 525 I=1,IMAX+1
             W(I,1,3)= VO*(T-TO*DLOG(1+T/TO))
             W(I,J6,3)= 0.0
525       CONTINUE
        ENDIF
c
c Solve radial displacements at specimen top and bottom
c
        IF (NRS .EQ. 1) THEN
          DO 550 I=1,IMAX
             U(I,1,3)= (4*U(I,2,3) - U(I,3,3))/3
```

```
            U(I,J6,3)= (4*U(I,J5,3) - U(I,J4,3))/3
550       CONTINUE
        ELSE
          DO 575 I=1,IMAX+1
             U(I,1,3)= 0.0
             U(I,J6,3)= 0.0
575       CONTINUE
        ENDIF
c
c Satisfy boundary conditions at outer edge of specimen
c
        DO 600 J=2,KM-1
           U(IMAX+1,J,3)= U(IMAX,J,3) + A4*(U(IMAX,J,3)/(IMAX-1)
     :        + .5*(W(IMAX,J+1,3) - W(IMAX,J-1,3)))
           W(IMAX+1,J,3)= W(IMAX,J,3) + .5*(U(IMAX,J-1,3) - U(IMAX,J+1,3))
600     CONTINUE
        IF (NRS .EQ. 2) GOTO 625
        U(IMAX+1,1,3)= (4*U(IMAX+1,2,3) - U(IMAX+1,3,3))/3
        IF (K .LE. J7) THEN
          U(IMAX+1,J6,3)= 0.0
        ELSE
          U(IMAX+1,J6,3)= (4*U(IMAX+1,J5,3) - U(IMAX+1,J4,3))/3
        ENDIF
c
c Calculation of strains and stresses performed at certain time
c intervals
c
625     IF (NST .EQ. 2 .AND. K .EQ. KN) THEN
          K2=K2+1
          KN=KN+NWP/2*JMAX
          DO 650 J=1,3
          DO 650 I=1,IMAX+1
             IF (J .EQ. 1) THEN
               JC= 1
               E4(I,J)= (-3*U(I,1,3) + 4*U(I,2,3) - U(I,3,3))/(2*DZ)
               E3(I,J)= (-3*W(I,1,3) + 4*W(I,2,3) - W(I,3,3))/(2*DZ)
             ELSEIF (J .EQ. 2) THEN
               JC= J2
               E3(I,J)= (W(I,J3,3) - W(I,J1,3))/(2*DZ)
               E4(I,J)= (U(I,J3,3) - U(I,J1,3))/(2*DZ)
             ELSE
               JC= J6
               E4(I,J)= (3*U(I,J6,3) - 4*U(I,J5,3) + U(I,J4,3))/(2*DZ)
               E3(I,J)= (3*W(I,J6,3) - 4*W(I,J5,3) + W(I,J4,3))/(2*DZ)
             ENDIF
             IF (I .EQ. 1) THEN
               E1(I,J)= (-3*U(I,JC,3) + 4*U(I+1,JC,3) -
     :           U(I+2,JC,3))/(2*DZ)
               E2(I,J)= E1(I,J)
               E5(I,J)= (-3*W(I,JC,3) + 4*W(I+1,JC,3) -
     :           W(I+2,JC,3))/(2*DZ)
```

```
            ELSE
              E2(I,J)= U(I,JC,3)/((I-1)*DZ)
              IF (I .EQ. IMAX+1) THEN
                E1(I,J)= (U(I-2,JC,3) - 4*U(I-1,JC,3) +
     :            3*U(I,JC,3))/(2*DZ)
                E5(I,J)= (W(I-2,JC,3) - 4*W(I-1,JC,3) +
     :            3*W(I,JC,3))/(2*DZ)
              ELSE
                E1(I,J)= (U(I+1,JC,3) - U(I-1,JC,3))/(2*DZ)
                E5(I,J)= (W(I+1,JC,3) - W(I-1,JC,3))/(2*DZ)
              ENDIF
            ENDIF
c
c Radial and shear stress calculation
c
            S1(I,J,K2)= G/4632.768*(C1S*E1(I,J) + (C1S-2*C2S)*
     :        (E2(I,J) + E3(I,J)))
            S3(I,J,K2)= G/4632.768*C2S*(E4(I,J) + E5(I,J))
650       CONTINUE
          M=1
        ENDIF
        IF (L .EQ. NT) THEN
          IF (M .EQ. 0) THEN
            DO 675 J=1,3
            DO 675 I=1,IMAX+1
              IF (J .EQ. 1) THEN
                JC= 1
                E3(I,J)= (-3*W(I,1,3) + 4*W(I,2,3) - W(I,3,3))/(2*DZ)
              ELSEIF (J .EQ. 2) THEN
                JC= J2
                E3(I,J)= (W(I,J3,3) - W(I,J1,3))/(2*DZ)
              ELSE
                JC= J6
                E3(I,J)= (3*W(I,J6,3) - 4*W(I,J5,3) + W(I,J4,3))/(2*DZ)
              ENDIF
              IF (I .EQ. 1) THEN
                E1(I,J)= (-3*U(I,JC,3) + 4*U(I+1,JC,3) -
     :            U(I+2,JC,3))/(2*DZ)
                E2(I,J)= E1(I,J)
              ELSE
                E2(I,J)= U(I,JC,3)/((I-1)*DZ)
                IF (I .EQ. IMAX+1) THEN
                  E1(I,J)= (U(I-2,JC,3) - 4*U(I-1,JC,3) +
     :              3*U(I,JC,3))/(2*DZ)
                ELSE
                  E1(I,J)= (U(I+1,JC,3) - U(I-1,JC,3))/(2*DZ)
                ENDIF
              ENDIF
675         CONTINUE
          ENDIF
c
```

```
c Axial stress calculation
c
        DO 750 J=1,3
           S2T(4,J,K)= 0.0
           DO 700 I=1,IMAX+1
             S2(I,J)= G/4632.768*((C1S-2*C2S)*(E1(I,J) + E2(I,J))
     :       + C1S*E3(I,J))
700        CONTINUE
           S2T(1,J,K)= S2(I1,J)
           S2T(2,J,K)= S2(I2,J)
           S2T(3,J,K)= S2(I3,J)
           DO 725 I=1,IMAX
              S2T(4,J,K)= S2T(4,J,K) + A6*((3*I-2)*S2(I,J) +
     :          (3*I-1)*S2(I+1,J))
725        CONTINUE
750     CONTINUE
        L=0
      ENDIF
c
c If the initial wavefront hasn't arrived yet, set stresses equal to
c zero
c
      IF (K .LE. J6) THEN
        DO 780 J=2,3
           DO 775 I=1,4
              S2T(I,J,K)= 0.0
775        CONTINUE
           DO 780 I=1,IMAX+1
              S1(I,J,K2)=0.0
              S3(I,J,K2)=0.0
780     CONTINUE
      ELSEIF (K .LE. J7) THEN
        DO 790 I=1,4
           S2T(I,3,K)= 0.0
790     CONTINUE
        DO 800 I=1,IMAX+1
           S1(I,3,K2)=0.0
           S3(I,3,K2)=0.0
800     CONTINUE
      ENDIF
      IF (K .EQ. KMAX+1) GOTO 850
c
c Renumber the second and third passes of displacements as the first
c and second passes.
c
      DO 825 K1=1,2
      DO 825 J=1,JMAX+1
      DO 825 I=1,IMAX+1
         U(I,J,K1)= U(I,J,K1+1)
         W(I,J,K1)= W(I,J,K1+1)
825   CONTINUE
```

```
c
c End of major loop.  Upon completing the displacement, strain, and
c stress calculations, output many of the input variables.
c
850   WRITE(9,900)
900   FORMAT(/5X,'TWO DIMENSIONAL WAVE ANALYSIS'//)
      WRITE(9,925) H, HDR, C1, C2, G, IMAX, JMAX, KMAX, NT
925   FORMAT(/6X,'H = ',F4.2,6X,'HDR = ',F4.2,6X,'C1 = ',F5.0,
     :6X,'C2 = ',F5.0/6X,'G = ',F4.0,6X,'IMAX = ',I3,5X,'JMAX = ',
     :I3,6X,'KMAX = ',I4,6X,'NT = ',I4)
      IF (MUP .EQ. 1) THEN
        WRITE(9,950) A
      ELSEIF (MUP .EQ. 2) THEN
        WRITE(9,975) V
      ELSE
        WRITE(9,1000) V0, A0
      ENDIF
950   FORMAT(6X,'A = ',F4.0)
975   FORMAT(6X,'V = ',F4.0)
1000  FORMAT(5X,'V0 = ',F4.0,6X,'A0 = ',F9.0)
      IF (NRS .EQ. 1) THEN
        WRITE(9,1025)
      ELSE
        WRITE(9,1050)
      ENDIF
1025  FORMAT(/5X,'NO LATERAL RESTRAINT AT SPECIMEN TOP AND BOTTOM')
1050  FORMAT(/5X,'FULL LATERAL RESTRAINT AT SPECEIMEN TOP AND BOTTOM')
      IF (NST .EQ. 2) THEN
c
c Output radial and shear stresses as a function of dimensionless
c radius for certain values of dimensionless time
c
        IF (TMAX .LT. NWP/4.) GOTO 1200
        WRITE(9,1075)
1075    FORMAT(//35X,'STRESSES'//16X,'TOP',17X,'MIDDLE',16X,'BOTTOM'/
     :1X,'DIM'/1X,'TIME',4X,3('RADIAL',5X,'SHEAR',6X),'r/R')
        DO 1175 K2=1,4
           T= NWP/4.*K2
           IF (T .GT. TMAX) GOTO 1200
           WRITE(9,1100) T
1100       FORMAT(//1X,F4.1)
           DO 1150 I=1,IMAX+1
              DI= (I-1.)/IMAX
              WRITE(9,1125) S1(I,1,K2),S3(I,1,K2),S1(I,2,K2),S3(I,2,K2),
     :          S1(I,3,K2),S3(I,3,K2),DI
1125          FORMAT(7X,6(E10.4,1X),1X,F4.2)
1150       CONTINUE
1175    CONTINUE
      ENDIF
c
c Output axial stress as a function of dimensionless time for nine
```

```
c dimensionless positions.  Also output average axial stress for three
c dimensionless heights.
c
1200  WRITE(9,1225) DI1,DI2,DI3
1225  FORMAT(/////34X,'AXIAL STRESS'/34X,'DISTRIBUTION'///
     :3X,'AXIAL',16X,'RADIAL POSITION',19X,'AVERAVE',7X,'DIM'/
     :2X,'POSITION',19X,'(r/R)',25X,'AXIAL',7X,'TIME'/
     :3X,'(z/H)',50X,'STRESS',6X,'(C1T/H)'/14X,F3.1,12X,F3.1,13X,F3.1)
      DO 1300 J=1,3
         IF (J .EQ. 1) THEN
           DJ=DI1
         ELSEIF (J .EQ. 2) THEN
           DJ=DI2
         ELSE
           DJ=DI3
         ENDIF
         WRITE(9,1250) DJ
1250     FORMAT(//4X,F3.1)
      DO 1300 K=1,KMAX+1,NT
         TD= .5*(K-1)/JMAX
         WRITE(9,1275) S2T(1,J,K), S2T(2,J,K), S2T(3,J,K),
     :     S2T(4,J,K), TD
1275     FORMAT(7X,4(3X,E12.5),4X,F5.2)
1300  CONTINUE
      GOTO 3000
c
c
c   **** END OF TWO DIMENSIONAL ANALYSIS ****
c
c      **** ONE DIMENSIONAL ANALYSIS ****
c
c
c Set displacements equal to zero on ficticious first two passes of
c finite difference algorithm
c
2000  DO 2025 K=1,2
      DO 2025 J=1,JMAX+1
         W(1,J,K)= 0.0
2025  CONTINUE
c
c Set axial stresses equal to zero at time equal zero
c
      DO 2050 J=1,3
         S2T(1,J,1)= 0.0
2050  CONTINUE
c
c Begin major loop; calculate displacements first, and then stresses.
c Finally, displacements are renumbered in preparation for the next
c calculation of displacements.
c
      DO 2600 K=2,KMAX+1
```

```
        L= L+1
        IF (K .LE. JMAX) THEN
          KM= K
        ELSE
          KM= JMAX+1
        ENDIF
        T= DT*(K-1)
c
c Solve displacements at top and bottom of specimen
c
        IF (MUP .EQ. 1) THEN
          W(1,1,3)= 193.032*A*T**2
        ELSEIF (MUP .EQ. 2) THEN
          W(1,1,3)= V*T
        ELSE
          W(1,1,3)= VO*(T-TO*DLOG(1+T/TO))
        ENDIF
        W(1,JMAX+1,3)= 0.0
c
c Solve for displacements at other points in the specimen.
c Displacements equal zero before the initial wavefront arrives, and the
c wave equation solves for displacements after the initial wavefront
c arrives.
c
        DO 2500 J=2,JMAX
           IF (J .GE. KM) THEN
             W(1,J,3)= 0.0
           ELSE
             W(1,J,3)= -W(1,J,1) + W(1,J-1,2) + W(1,J+1,2)
           ENDIF
2500    CONTINUE
c
c Stresses are calculated at the top, middle, and bottom of the specimen
c only at certain time increments.
c
        IF (L .EQ. NT) THEN
          S2T(1,1,K)= G/4632.768*C1S*(-3*W(1,1,3) + 4*W(1,2,3) -
     :      W(1,3,3))/(2*DZ)
          S2T(1,2,K)= G/4632.768*C1S*(W(1,J3,3) - W(1,J1,3))/(2*DZ)
          S2T(1,3,K)= G/4632.768*C1S*(3*W(1,J6,3) - 4*W(1,J5,3) +
     :      W(1,J4,3))/(2*DZ)
          L= 0
        ENDIF
c
c If the initial wavefront hasn't arrived, set stress equal to zero
c
        IF (K .LE. J2) THEN
          S2T(1,2,K)= 0.0
          S2T(1,3,K)= 0.0
        ELSEIF (K .LE. J6) THEN
          S2T(1,3,K)= 0.0
```

```
        ENDIF
        IF (K .EQ. KMAX+1) GOTO 2650
c
c Renumber the first and second passes of displacements at the
c first and second passes
c
      DO 2600 K1=1,2
      DO 2600 J=1,JMAX+1
         W(1,J,K1)= W(1,J,K1+1)
2600  CONTINUE
c
c End of major loop.  Upon completion of displacement and stress
c calculations, output many of the input variables.
c
2650  WRITE(9,2675)
2675  FORMAT(/5X,'ONE DIMENSIONAL WAVE ANALYSIS'//)
      WRITE(9,2700) H, C1, G, JMAX, KMAX, NT
2700  FORMAT(/10X,'H = ',F4.2,10X,'C1 = ',F5.0,10X,'G = ',F4.0/10X,
     :'JMAX = ',I3,8X,'KMAX = ',I3,9X,'NT = ',I4)
      IF (MUP .EQ. 1) THEN
        WRITE(9,2725) A
      ELSEIF (MUP .EQ. 2) THEN
        WRITE(9,2750) V
      ELSE
        WRITE(9,2775) V0, A0
      ENDIF
2725  FORMAT(10X,'A = ',F4.0)
2750  FORMAT(10X,'V = ',F4.0)
2775  FORMAT(10X,'V0 = ',F4.0,9X,'A0 = ',F9.0)
c
c Output axial stress as a function of dimensionless time at the top,
c middle, and bottom of the specimen
c
      WRITE(9,2800)
2800  FORMAT(///33X,'AXIAL STRESSES'///14X,'TOP',14X,'MIDDLE',12X,
     :'BOTTOM',10X,'DIM'/65X,'TIME'/)
      DO 2900 K=1,KMAX+1,NT
         TD= 1.*(K-1)/JMAX
         WRITE(9,2850) S2T(1,1,K), S2T(1,2,K), S2T(1,3,K), TD
2850     FORMAT(10X,3(E12.5,6X),F5.2)
2900  CONTINUE
3000  CLOSE(9,STATUS='KEEP')
      STOP
      END
```

PROGRAM 'COMPARE'

```
$LARGE
      PROGRAM COMPARE
c
c This program solves for axial stresses resulting from axisymmetric
c wave propagation in an elastic cylinder.  Constant or hyperbolic
c velocity or constant acceleration can be assumed for the upper
c pedestal.  One and two dimensional wave analyses are performed, and
c the resulting axial stresses are compared.  For the one dimensional
c analysis, the wave travels the distance of one axial increment in the
c time of one time increment.  In the two dimensional case, it takes the
c dilatational wave two time increments to traverse one axial increment.
c
c The variables used include:
c
c    H - specimen height
c  HDR - height to diameter ratio
c    G - wet unit weight of specimen
c  MUP - specifies motion of upper pedestal
c  NRS - specifies restraint of specimen
c  NDW - specifies 1-D or 2-D wave analysis
c  NWP - maximum number of passes of wavefront through specimen
c IMAX - number of radial increments in specimen
c JMAX - number of axial increments in specimen
c KMAX - number of time increments in test
c   TD - dimensionless time
c    T - time
c   TO - characteristic time for hyperbolic upper pedestal velocity
c    V - constant velocity of upper pedestal
c   VO - limiting hyperbolic upper pedestal velocity
c    A - constant acceleration of upper pedestal
c   AO - initial acceleration of upper pedestal
c   C1 - dilatational wave velocity
c   C2 - shear wave velocity
c   C3 - rod wave velocity
c  C1S - dilatational wave velocity squared
c  C2S - shear wave velocity squared
c   PR - Poisson's ratio
c   NT - number of time increments between data output
c   DZ - length of one axial increment
c   DT - length of one time increment
c   DI - dimensionless radius
c    U - radial displacement
c    W - axial displacement
```

```
c   E1 - radial strain
c   E2 - tangential strain
c   E3 - axial strain
c   S2 - axial stress
c  S2T - average axial stress as a function of time, and percent
c        difference between 1-D and 2-D average axial stresses
c
      IMPLICIT DOUBLE PRECISION (A-H,O-Z)
      REAL*8 U(31,61,3), W(31,61,3), E1(31,3), E2(31,3), E3(31,3),
     :   S2(31,3), S2T(5,3,1201)
      OPEN(9,FILE='CP4.OUT',STATUS='NEW')
      WRITE(*,75)
75    FORMAT(//1X,'ENTER:  specimen height (inches)'/
     :9X,'height to diameter ratio (1.0, 1.5, 2.0, 2.5, or 3.0)'/
     :9X,'wet unit weight (pcf)'//)
      READ(*,*) H, HDR, G
      WRITE(*,150)
150   FORMAT(//1X,'ENTER:  maximum number of passes of wavefront '
     :'through specimen'/9X,'choose a multiple of 2 up to a maximum '
     :'of 20'/)
      READ(*,*) NWP
c
c Ensure JMAX is consistent with HDR and desired 2-D output
c
      JM=IDINT(4*HDR)
      WRITE(*,175) JM
175   FORMAT(/1X,'ENTER:  number of axial increments'/
     :9X,'choose a multiple of', I3,' up to a maximum of 60'/)
      READ(*,*) JMAX
      WRITE(*,200)
200   FORMAT(/1X,'ENTER:  type of upper pedestal motion:'/
     :9X,'1 for constant acceleration'/
     :9X,'2 for constant velocity'/
     :9X,'3 for hyperbolic velocity'/)
      READ(*,*) MUP
      IF (MUP .EQ. 1) THEN
        WRITE(*,225)
225     FORMAT(/1X,'ENTER:  acceleration of upper pedestal (in g''s)'/)
        READ(*,*) A
      ELSEIF (MUP .EQ. 2) THEN
        WRITE(*,250)
250     FORMAT(/1X,'ENTER:  velocity of upper pedestal (mils/msec)'/)
        READ(*,*) V
      ELSE
        WRITE(*,275)
275     FORMAT(/1X,'ENTER:  limiting velocity of upper pedestal (mils/ms
     :ec)'/9X,'and initial acceleration of upper pedestal (inches per se
     :cond squared)'/)
        READ(*,*) V0, A0
        T0= V0/A0
      ENDIF
```

```
            ELSE
              KMAX1= IDINT(3.6*JMAX*C1/V0)
            ENDIF
            KMAX2= 2*NWP*JMAX
            KMAX= MIN(KMAX1,KMAX2)
c
c Ensure KMAX is a multiple of two
c
            KMAX= KMAX/2*2
            WRITE(*,335) KMAX
335         FORMAT(/1X,'ENTER:  number of time increments between data ou
     :tput'/9X,'choose a multiple of 2 up to a maximum of ',I4/)
            READ(*,*) NT
          ELSEIF (NDW .EQ. 1) THEN
            KMAX3= KMAX/2
            GOTO 900
          ENDIF
          IF (NRS .EQ. 2) GOTO 345
c
c
c     **** TWO DIMENSIONAL ANALYSIS ****
c
c
      WRITE(*,340)
340   FORMAT(/1X,'TWO DIMENSIONAL ANALYSIS IN PROGRESS')
c
c Find time increment and other constants
c
      DT=DZ/(C1*24)
      C1S= C1**2
      C2S= C2**2
      B= C2S/C1S
      PR= (1-2*B)/(2-2*B)
      C3= C1*DSQRT((1-PR-2*PR**2)/(1-PR))
      A1= (1-B)/16
      A2= 1.5 - B/2
      A3= B/4
      A4= 2*B - 1
      A5= 2*A1
      A6= 1./(3*IMAX**2)
      J7= 2*JMAX + 1
c
c Set displacements = 0 along ficticious first two passes of finite
c difference algorithm
c
345   DO 350 K=1,2
      DO 350 J=1,JMAX+1
      DO 350 I=1,IMAX+1
         U(I,J,K)=0.0
         W(I,J,K)=0.0
350   CONTINUE
```

```
c
c Set axial stresses = 0 at time t = 0
c
      DO 375 J=1,3
      DO 375 I=1,3
         S2T(I,J,1)=0.0
375   CONTINUE
c
c Begin stepping through time increments; find displacements, then
c strains and stresses.  Finally, displacements are renumbered in
c preparation for the next calculation of displacements.
c
      DO 825 K=2,KMAX+1
      L=L+1
      IF (K .LE. 2*JMAX) THEN
        KM=NINT((K+1.01)/2)
      ELSE
        KM=JMAX+1
      ENDIF
      DO 450 J=2,JMAX
c
c Displacements equal zero before initial wavefront arrives
c
        IF (J .GE. KM) THEN
          DO 400 I=1,IMAX+1
             U(I,J,3)=0.0
             W(I,J,3)=0.0
400       CONTINUE
c
c Wave equations solve displacements at interior mesh points
c
        ELSE
          DO 425 I=2,IMAX
             U(I,J,3)= -U(I,J,1) +.25*((1+1./(2*(I-1)))
     :          *U(I+1,J,2) + (1-1./(2*(I-1)))*U(I-1,J,2)) +
     :          A3*(U(I,J+1,2) + U(I,J-1,2)) + A1*(W(I+1,J+1,2)
     :          - W(I+1,J-1,2) - W(I-1,J+1,2) + W(I-1,J-1,2))
     :          + (1.5 - .25*(2*B + 1./(I-1)**2))*U(I,J,2)
            W(I,J,3)= -W(I,J,1) + .25*(W(I,J+1,2) + W(I,J-1,2)) +
     :          A2*W(I,J,2) + A3*(1+1./(2*(I-1)))*W(I+1,J,2) +
     :          A3*(1-1./(2*(I-1)))*W(I-1,J,2) + A5/(I-1)*
     :          (U(I,J+1,2) - U(I,J-1,2)) + A1*(U(I+1,J+1,2)
     :          - U(I+1,J-1,2) - U(I-1,J+1,2) + U(I-1,J-1,2))
425       CONTINUE
c
c Satisfy centerline boundary conditions
c
          U(1,J,3)= 0.0
          W(1,J,3)= (4*W(2,J,3) - W(3,J,3))/3
        ENDIF
450   CONTINUE
```

```
      T= DT*(K-1)
c
c Solve axial displacements at specimen top and bottom
c
      IF (MUP .EQ. 1) THEN
        DO 475 I=1,IMAX+1
           W(I,1,3)= 193.032*A*T**2
           W(I,J6,3)= 0.0
475     CONTINUE
      ELSEIF (MUP .EQ. 2) THEN
        DO 500 I=1,IMAX+1
           W(I,1,3)= V*T
           W(I,J6,3)= 0.0
500     CONTINUE
      ELSE
        DO 525 I=1,IMAX+1
           W(I,1,3)= VO*(T-TO*DLOG(1+T/TO))
           W(I,J6,3)= 0.0
525     CONTINUE
      ENDIF
c
c Solve radial displacements at specimen top and bottom
c
      IF (NRS .EQ. 1) THEN
        DO 550 I=1,IMAX
           U(I,1,3)= (4*U(I,2,3) - U(I,3,3))/3
           U(I,J6,3)= (4*U(I,J5,3) - U(I,J4,3))/3
550     CONTINUE
      ELSE
        DO 575 I=1,IMAX+1
           U(I,1,3)= 0.0
           U(I,J6,3)= 0.0
575     CONTINUE
      ENDIF
c
c Satisfy boundary conditions at outer edge of specimen
c
      DO 600 J=2,KM-1
         U(IMAX+1,J,3)= U(IMAX,J,3) + A4*(U(IMAX,J,3)/(IMAX-1)
     :       + .5*(W(IMAX,J+1,3) - W(IMAX,J-1,3)))
         W(IMAX+1,J,3)= W(IMAX,J,3) + .5*(U(IMAX,J-1,3) - U(IMAX,J+1,3))
600   CONTINUE
      IF (NRS .EQ. 2) GOTO 625
      U(IMAX+1,1,3)= (4*U(IMAX+1,2,3) - U(IMAX+1,3,3))/3
      IF (K .LE. J7) THEN
        U(IMAX+1,J6,3)= 0.0
      ELSE
        U(IMAX+1,J6,3)= (4*U(IMAX+1,J5,3) - U(IMAX+1,J4,3))/3
      ENDIF
c
c Calculation of strains and stresses performed at certain time
```

```
c intervals
c
625   IF (L .EQ. NT) THEN
          DO 675 J=1,3
          DO 675 I=1,IMAX+1
             IF (J .EQ. 1) THEN
               JC= 1
               E3(I,J)= (-3*W(I,1,3) + 4*W(I,2,3) - W(I,3,3))/(2*DZ)
             ELSEIF (J .EQ. 2) THEN
               JC= J2
               E3(I,J)= (W(I,J3,3) - W(I,J1,3))/(2*DZ)
             ELSE
               JC= J6
               E3(I,J)= (3*W(I,J6,3) - 4*W(I,J5,3) + W(I,J4,3))/(2*DZ)
             ENDIF
             IF (I .EQ. 1) THEN
               E1(I,J)= (-3*U(I,JC,3) + 4*U(I+1,JC,3) -
     :           U(I+2,JC,3))/(2*DZ)
               E2(I,J)= E1(I,J)
             ELSE
               E2(I,J)= U(I,JC,3)/((I-1)*DZ)
               IF (I .EQ. IMAX+1) THEN
                 E1(I,J)= (U(I-2,JC,3) - 4*U(I-1,JC,3) +
     :             3*U(I,JC,3))/(2*DZ)
               ELSE
                 E1(I,J)= (U(I+1,JC,3) - U(I-1,JC,3))/(2*DZ)
               ENDIF
             ENDIF
675       CONTINUE
c
c Axial stress calculation
c
        DO 750 J=1,3
           S2T(I4,J,K)= 0.0
           DO 700 I=1,IMAX+1
             S2(I,J)= G/4632.768*((C1S-2*C2S)*(E1(I,J) + E2(I,J))
     :         + C1S*E3(I,J))
700        CONTINUE
           DO 725 I=1,IMAX
              S2T(I4,J,K)= S2T(I4,J,K) + A6*((3*I-2)*S2(I,J) +
     :          (3*I-1)*S2(I+1,J))
725        CONTINUE
750     CONTINUE
        L=0
      ENDIF
c
c If the initial wavefront hasn't arrived yet, set stresses equal to
c zero
c
      IF (K .LE. J6) THEN
        S2T(I4,2,K)= 0.0
```

```
        S2T(I4,3,K)= 0.0
      ELSEIF (K .LE. J7) THEN
        S2T(I4,3,K)= 0.0
      ENDIF
      IF (K .EQ. KMAX+1) GOTO 840
c
c Renumber the second and third passes of displacements as the first
c and second passes.
c
      DO 825 K1=1,2
      DO 825 J=1,JMAX+1
      DO 825 I=1,IMAX+1
         U(I,J,K1)= U(I,J,K1+1)
         W(I,J,K1)= W(I,J,K1+1)
825   CONTINUE
840   CONTINUE
c
c     **** ONE DIMENSIONAL ANALYSIS ****
c
900   WRITE(*,925)
925   FORMAT(/1X,'ONE DIMENSIONAL ANALYSIS IN PROGRESS')
      DT=DZ/(C3*12)
      C3S= C3**2
c
c Set displacements equal to zero on ficticious first two passes of
c finite difference algorithm
c
      DO 950 K=1,2
      DO 950 J=1,JMAX+1
         W(1,J,K)= 0.0
950   CONTINUE
c
c Begin stepping through time increments; find displacements and then
c stresses.  Finally, displacements are renumbered in preparation for
c the next calculation of displacements.
c
      DO 1900 K=2,KMAX3+1
         L= L+1
         IF (K .LE. JMAX) THEN
           KM= K
         ELSE
           KM= JMAX+1
         ENDIF
         T= DT*(K-1)
c
c Solve displacements at top and bottom of specimen
c
         IF (MUP .EQ. 1) THEN
           W(1,1,3)= 193.032*A*T**2
         ELSEIF (MUP .EQ. 2) THEN
           W(1,1,3)= V*T
```

```
          ELSE
            W(1,1,3)= VO*(T-TO*DLOG(1+T/TO))
          ENDIF
          W(1,JMAX+1,3)= 0.0
c
c Solve for displacements at other points in the specimen.
c Displacements equal zero before the initial wavefront arrives, and the
c wave equation solves for displacements after the initial wavefront
c arrives.
c
          DO 1000 J=2,JMAX
             IF (J .GE. KM) THEN
               W(1,J,3)= 0.0
             ELSE
               W(1,J,3)= -W(1,J,1) + W(1,J-1,2) + W(1,J+1,2)
             ENDIF
1000      CONTINUE
c
c Stresses are calculated at the top, middle, and bottom of the
c specimen only at certain time increments.
c
          IF (L .EQ. NT/2) THEN
            S2T(I4,1,K)= G/4632.768*C3S*(-3*W(1,1,3) + 4*W(1,2,3) -
     :        W(1,3,3))/(2*DZ)
            S2T(I4,2,K)= G/4632.768*C3S*(W(1,J3,3) - W(1,J1,3))/(2*DZ)
            S2T(I4,3,K)= G/4632.768*C3S*(3*W(1,J6,3) - 4*W(1,J5,3) +
     :        W(1,J4,3))/(2*DZ)
            L=0
          ENDIF
c
c If the initial wavefront hasn't arrived, set stresses equal to zero
c
          IF (K .LE. J2) THEN
            S2T(I4,2,K)= 0.0
            S2T(I4,3,K)= 0.0
          ELSEIF (K .LE. J6) THEN
            S2T(I4,3,K)= 0.0
          ENDIF
          IF (K .EQ. KMAX3+1) GOTO 1920
c
c Renumber the first and second passes of displacements as the
c first and second passes
c
       DO 1900 K1=1,2
       DO 1900 J=1,JMAX+1
          W(1,J,K1)= W(1,J,K1+1)
1900   CONTINUE
c
c      **** END OF ONE DIMENSIONAL ANALYSIS ****
c
c End of major loop.  Upon completing the displacement, strain, and
```

```
c stress calculations, output many of the input variables.
c
1920  WRITE(9,1925) H, HDR, C1, C2, C3, G, IMAX, JMAX, KMAX, NT
1925  FORMAT(/6X,'H = ',F4.2,6X,'HDR = ',F4.2,6X,'C1 = ',F5.0,
     :6X,'C2 = ',F5.0,6X,'C3 = ',F5.0/6X,'G = ',F4.0,6X,'IMAX = '
     :,I3,5X,'JMAX = ',I3,6X,'KMAX = ',I4,6X,'NT = ',I4)
      IF (MUP .EQ. 1) THEN
        WRITE(9,1950) A
      ELSEIF (MUP .EQ. 2) THEN
        WRITE(9,1975) V
      ELSE
        WRITE(9,2000) V0, A0
      ENDIF
1950  FORMAT(6X,'A = ',F4.0)
1975  FORMAT(6X,'V = ',F4.0)
2000  FORMAT(5X,'V0 = ',F4.0,6X,'A0 = ',F9.0)
c
c Output averave axial stresses as a function of dimensionless time
c
      WRITE(9,2025)
2025  FORMAT(/////34X,'AXIAL STRESS'/34X,'DISTRIBUTION'///
     :3X,'AXIAL',64X,'DIM'/2X,'POSITION',5X,'1-D',12X,'2-D',9X,'%',
     :9X,'2-D',9X,'%',7X,'TIME'/3X,'(z/H)',21X,'NRS=2',7X,'DIFF',6X,
     :'NRS=1',7X,'DIFF',3X,'(C1T/H)'/)
      DO 2100 J=1,3
         IF (J .EQ. 1) THEN
           DJ=0.0
         ELSEIF (J .EQ. 2) THEN
           DJ=0.5
         ELSE
           DJ=1.0
         ENDIF
         WRITE(9,2050) DJ
2050     FORMAT(//4X,F3.1)
      DO 2100 K=1,KMAX+1,NT
         K3= (K-1)/2+1
         TD= .5*(K-1)/JMAX
         IF (S2T(3,J,K3) .EQ. 0.0) THEN
           S2T(4,J,K)= 0.0
           S2T(5,J,K)= 0.0
         ELSE
           S2T(4,J,K)= (S2T(3,J,K3)/S2T(2,J,K)-1)*100
           S2T(5,J,K)= (S2T(3,J,K3)/S2T(1,J,K)-1)*100
         ENDIF
         WRITE(9,2075) S2T(3,J,K3), S2T(2,J,K), S2T(4,J,K), S2T(1,J,K),
     :     S2T(5,J,K), TD
2075     FORMAT(11X,2(E12.5,3X),F5.1,2X,E12.5,2X,F5.1,4X,F5.2)
2100  CONTINUE
      CLOSE(9,STATUS='KEEP')
      STOP
      END
```

APPENDIX C

SAMPLE OUTPUT OF PROGRAMS 'WAVES' AND 'COMPARE'

PROGRAM 'WAVES' OUTPUT

TWO DIMENSIONAL WAVE ANALYSIS

H = 2.00 HDR = 2.00 C1 = 1000. C2 = 600.
G = 120. IMAX = 10 JMAX = 40 KMAX = 160 NT = 16
A = 400.

FULL LATERAL RESTRAINT AT SPECIMEN TOP AND BOTTOM

STRESSES

	TOP		MIDDLE		BOTTOM		
DIM TIME	RADIAL	SHEAR	RADIAL	SHEAR	RADIAL	SHEAR	r/R
.5							
	-.7145E+01	.0000E+00	.0000E+00	.0000E+00	.0000E+00	.0000E+00	.00
	-.7134E+01	.4962E+00	.0000E+00	.0000E+00	.0000E+00	.0000E+00	.10
	-.7103E+01	.9877E+00	.0000E+00	.0000E+00	.0000E+00	.0000E+00	.20
	-.7061E+01	.1491E+01	.0000E+00	.0000E+00	.0000E+00	.0000E+00	.30
	-.7012E+01	.2025E+01	.0000E+00	.0000E+00	.0000E+00	.0000E+00	.40
	-.6962E+01	.2605E+01	.0000E+00	.0000E+00	.0000E+00	.0000E+00	.50
	-.6932E+01	.3260E+01	.0000E+00	.0000E+00	.0000E+00	.0000E+00	.60
	-.6986E+01	.4052E+01	.0000E+00	.0000E+00	.0000E+00	.0000E+00	.70
	-.7331E+01	.5145E+01	.0000E+00	.0000E+00	.0000E+00	.0000E+00	.80
	-.8848E+01	.7032E+01	.0000E+00	.0000E+00	.0000E+00	.0000E+00	.90
	-.1609E+02	.1130E+02	.0000E+00	.0000E+00	.0000E+00	.0000E+00	1.00
1.0							
	-.1351E+02	.0000E+00	.1176E+01	.0000E+00	.0000E+00	.0000E+00	.00
	-.1351E+02	.8100E+00	.1083E+01	-.1630E-01	.0000E+00	.0000E+00	.10
	-.1352E+02	.1646E+01	.9732E+00	-.4423E-01	.0000E+00	.0000E+00	.20
	-.1353E+02	.2537E+01	.8218E+00	-.8219E-01	.0000E+00	.0000E+00	.30
	-.1355E+02	.3516E+01	.6479E+00	-.1057E+00	.0000E+00	.0000E+00	.40
	-.1359E+02	.4631E+01	.4381E+00	-.1104E+00	.0000E+00	.0000E+00	.50
	-.1369E+02	.5949E+01	.2024E+00	-.1145E+00	.0000E+00	.0000E+00	.60
	-.1395E+02	.7608E+01	-.1415E-01	-.1261E+00	.0000E+00	.0000E+00	.70
	-.1480E+02	.9947E+01	-.1460E+00	-.1319E+00	.0000E+00	.0000E+00	.80
	-.1795E+02	.1397E+02	-.1049E+00	-.9735E-01	.0000E+00	.0000E+00	.90
	-.3244E+02	.2284E+02	-.8225E-02	.2157E-01	.0000E+00	.0000E+00	1.00

AXIAL STRESS DISTRIBUTION

AXIAL POSITION (z/H)	RADIAL POSITION (r/R) .0	.5	1.0	AVERAGE AXIAL STRESS	DIM TIME ($C_d T/H$)
.0					
	.00000E+00	.00000E+00	.00000E+00	.00000E+00	.00
	-.11159E+02	-.11005E+02	-.17297E+02	-.11597E+02	.20
	-.21048E+02	-.20540E+02	-.43788E+02	-.23579E+02	.40
	-.29613E+02	-.29217E+02	-.70181E+02	-.35331E+02	.60
	-.38281E+02	-.38539E+02	-.93256E+02	-.46936E+02	.80
	-.48239E+02	-.48524E+02	-.11586E+03	-.58714E+02	1.00
	-.58182E+02	-.58117E+02	-.14098E+03	-.70624E+02	1.20
	-.66962E+02	-.67135E+02	-.16649E+03	-.82378E+02	1.40
	-.75808E+02	-.76455E+02	-.18998E+03	-.94016E+02	1.60
	-.85651E+02	-.86279E+02	-.21318E+03	-.10580E+03	1.80
	-.95676E+02	-.96072E+02	-.23840E+03	-.11791E+03	2.00
.5					
	.00000E+00	.00000E+00	.00000E+00	.00000E+00	.00
	.00000E+00	.00000E+00	.00000E+00	.00000E+00	.20
	.00000E+00	.00000E+00	.00000E+00	.00000E+00	.40
	-.48231E+01	-.44410E+01	-.53170E+01	-.46844E+01	.60
	-.11317E+02	-.13359E+02	-.14799E+02	-.13812E+02	.80
	-.25487E+02	-.24473E+02	-.23807E+02	-.24066E+02	1.00
	-.36388E+02	-.35941E+02	-.34020E+02	-.35315E+02	1.20
	-.45119E+02	-.45571E+02	-.47048E+02	-.46020E+02	1.40
	-.57952E+02	-.58108E+02	-.59722E+02	-.58598E+02	1.60
	-.75718E+02	-.76656E+02	-.76551E+02	-.76543E+02	1.80
	-.98300E+02	-.97468E+02	-.96731E+02	-.97012E+02	2.00
1.0					
	.00000E+00	.00000E+00	.00000E+00	.00000E+00	.00
	.00000E+00	.00000E+00	.00000E+00	.00000E+00	.20
	.00000E+00	.00000E+00	.00000E+00	.00000E+00	.40
	.00000E+00	.00000E+00	.00000E+00	.00000E+00	.60
	.00000E+00	.00000E+00	.00000E+00	.00000E+00	.80
	.00000E+00	.00000E+00	.00000E+00	.00000E+00	1.00
	-.13232E+02	-.13105E+02	-.31433E+02	-.16297E+02	1.20
	-.32203E+02	-.29461E+02	-.77098E+02	-.37350E+02	1.40
	-.48235E+02	-.49375E+02	-.13205E+03	-.62780E+02	1.60
	-.73903E+02	-.72787E+02	-.18278E+03	-.89681E+02	1.80
	-.86839E+02	-.89000E+02	-.23161E+03	-.11142E+03	2.00

PROGRAM 'COMPARE' OUTPUT

AXIAL STRESS DISTRIBUTION

AXIAL POSITION (z/H)	1-D	2-D NRS=2	% DIFF	2-D NRS=1	% DIFF	DIM TIME (CT/H)
.0						
	.00000E+00	.00000E+00	.0	.00000E+00	.0	.00
	-.11111E+02	-.11597E+02	-4.2	-.10667E+02	4.2	.20
	-.22222E+02	-.23579E+02	-5.8	-.20640E+02	7.7	.40
	-.33333E+02	-.35331E+02	-5.7	-.30710E+02	8.5	.60
	-.44444E+02	-.46936E+02	-5.3	-.41649E+02	6.7	.80
	-.55556E+02	-.58714E+02	-5.4	-.52582E+02	5.7	1.00
	-.66667E+02	-.70624E+02	-5.6	-.62557E+02	6.6	1.20
	-.77778E+02	-.82378E+02	-5.6	-.72474E+02	7.3	1.40
	-.88889E+02	-.94016E+02	-5.5	-.83420E+02	6.6	1.60
	-.10000E+03	-.10580E+03	-5.5	-.94440E+02	5.9	1.80
	-.11111E+03	-.11791E+03	-5.8	-.10460E+03	6.2	2.00
.5						
	.00000E+00	.00000E+00	.0	.00000E+00	.0	.00
	.00000E+00	.00000E+00	.0	.00000E+00	.0	.20
	.00000E+00	.00000E+00	.0	.00000E+00	.0	.40
	-.55556E+01	-.46844E+01	18.6	-.46283E+01	20.0	.60
	-.16667E+02	-.13812E+02	20.7	-.13474E+02	23.7	.80
	-.27778E+02	-.24066E+02	15.4	-.23423E+02	18.6	1.00
	-.38889E+02	-.35315E+02	10.1	-.34876E+02	11.5	1.20
	-.50000E+02	-.46020E+02	8.6	-.45941E+02	8.8	1.40
	-.66667E+02	-.58598E+02	13.8	-.58252E+02	14.4	1.60
	-.88889E+02	-.76543E+02	16.1	-.75125E+02	18.3	1.80
	-.11111E+03	-.97012E+02	14.5	-.94964E+02	17.0	2.00
1.0						
	.00000E+00	.00000E+00	.0	.00000E+00	.0	.00
	.00000E+00	.00000E+00	.0	.00000E+00	.0	.20
	.00000E+00	.00000E+00	.0	.00000E+00	.0	.40
	.00000E+00	.00000E+00	.0	.00000E+00	.0	.60
	.00000E+00	.00000E+00	.0	.00000E+00	.0	.80
	.00000E+00	.00000E+00	.0	.00000E+00	.0	1.00
	-.22222E+02	-.16297E+02	36.4	-.14307E+02	55.3	1.20
	-.44444E+02	-.37350E+02	19.0	-.31520E+02	41.0	1.40
	-.66667E+02	-.62780E+02	6.2	-.52808E+02	26.2	1.60
	-.88889E+02	-.89681E+02	-.9	-.78616E+02	13.1	1.80
	-.11111E+03	-.11142E+03	-.3	-.98073E+02	13.3	2.00

REFERENCES

1. Kolsky, H. 1963. Stress waves in solids. Chapters 2, 3. New York: Dover Publications.

2. Carroll, W. F. 1988. Fast triaxial shear device evaluation. Vicksburg, MS: U.S. Army Corps of Engineers Waterways Experiment Station, Technical Report SL-88-2.

3. Timoshenko, S., and J. N. Goodier. 1969. Theory of elasticity. 3rd ed., Chapter 14. New York: McGraw-Hill Book Company.

4. Love, A. E. H. 1927. Mathematical theory of elasticity. Chapter 9. New York: Dover Publications.

5. Wasley, R. J. 1973. Stress wave propagation in solids, an introduction. pp 48-57, 144. New York: Marcel Dekker, Inc.

6. Bertholf, L. D. 1966. Longitudinal elastic wave propagation in finite cylindrical bars. Ph.D. diss., Washington State University.

7. Habberstad, J. L. 1969. Axisymmetric elastic wave propagation in bars containing a discontinuity. Ph.D. diss., Washington State University.

8. Boresi, A. P., and P. P. Lynn. 1974. Elasticity in engineering mechanics, pp 415, 416. Englewood Cliffs, NJ: Prentice-Hall, Inc.

9. Crandall, S. H., N. C. Dahl, and T. J. Lardner. 1978. An introduction to the mechanics of solids, pp 261, 284. New York: McGraw-Hill Book Company.

10. Segel, L. A. 1977. Mathematics applied to continuum mechanics. Chapters 6, 9. New York: Macmillan Publishing Company, Inc.

11. Dennemeyer, R. 1968. Introduction to partial differential equations and boundary value problems. Chapter 4. New York: McGraw-Hill Book Company.

12. James, M. L., G. M. Smith, and J. C. Wolford. 1967. Applied numerical methods for digital computation with fortran, pp 294, 295. Scranton, PA: International Textbook Company.

13. Davis, J. L. 1986. Finite difference methods in dynamics of continuous media. Chapter 3. New York: Macmillan Publishing Company.